AN ABSTRACT OF THE DISSERTATION OF

Elizabeth B. Ruedig for the degree of Doctor of Philosophy in Radiation Health Physics presented on June 14, 2013.

Title: Dose-Effects Relationships In Non-Human Biota: Development of Field Sampling, Dosimetric and Analytic Techniques Through a Case Study of the Aquatic Snail *Campeloma decisum* at Chalk River Laboratories

Abstract approved: _____

Kathryn A. Higley

In the last decade regulatory bodies have begun to implement standards to protect populations of non-human biota (NHB) from the consequences of radiation exposure. This is a departure from previous regulatory frameworks which were concerned only with protecting man. The implementation of these new standards has started an ongoing discussion concerning appropriate dose-rate limits for NHB. For the most part, the data utilized for estimating appropriately protective dose-rate limits has come from data collected via the irradiation of NHB in a laboratory setting. While some dose-effects studies have been performed under field conditions, such experiments represent a minority of the available data. This deficit in the literature has resulted in challenges to the established paradigm, with researchers reporting increased radiosensitivity in NHB under field conditions. However, many such studies overlook critical components of dose-effects analysis: lacking either robust ecological technique or dosimetric rigor. This study serves as a template for future in-depth study of the relationship between radiation dose and ecological health. It utilizes sound field, dosimetric, analytic and statistical techniques to study dose-effects relationships in the aquatic snail, *Campeloma decisum*, at Chalk River Laboratories in Ontario, Canada. Multiple benchmarks (number of snails, mass of individuals, etc) were employed as proxies for snail population health, which was assessed after accounting for two dozen environmental variables. Dose-rates were calculated via a novel voxelized model, developed for this study to estimate internal dose rates for the species of interest. A linear model was employed to tease out the relationship between individual snails, their environment, and radiation dose rate. There was no evidence that snail population health was influenced by radiation exposure ($p=0.70$) at the observed dose rates. Of the environmental variables tested, water concentration of Ca was well correlated with snail mass size ($p<0.001$), while water concentration of P was well correlated with the number of snails lured to a trap ($p<0.001$). The protocols and procedures developed as a part of this study represent novel, robust techniques for evaluating the relationship between radiation dose and population effects in NHB.

Dose-effects Relationships in Non-Human Biota: Development of Field Sampling, Dosimetric and Analytic Techniques Through a Case Study of the Aquatic Snail *Campeloma decisum* at Chalk River Laboratories

by
Elizabeth B. Ruedig

A DISSERTATION

submitted to

Oregon State University

in partial fulfillment of
the requirements of the
degree of

Doctor of Philosophy

Presented June 14, 2013

Commencement June 2014

Doctor of Philosophy dissertation of Elizabeth B. Ruedig presented on June 14, 2013.

APPROVED:

Major Professor, representing Radiation Health Physics

Head of the Department of Nuclear Engineering & Radiation Health Physics

---

Dean of the Graduate School

I understand that my dissertation will become part of the permanent collection of Oregon State University libraries. My signature below authorizes release of my dissertation to any reader upon request.

Elizabeth B. Ruedig, Author

ACKNOWLEDGEMENTS

I am grateful to Chalk River Laboratories, and particularly David Rowan, for the opportunity to perform field work at their site. It is unique in the world, and I was truly privileged to be a guest researcher there. Many staff at CRL were critical to this work, including Jamie Carr, Craig Cochrane, and Stephanie Walsh, who assisted with field work. Xin Dai and Sheila Kramer-Tremblay provided countless hours of assistance with radiochemical purification and counting, while Sang Bog Kim provided valuable assistance with tritium counting.

At Oregon State University, I would be remiss not to thank all of our support staff, including Scott Menn and Jim Darrough, who spent countless hours helping me operate the Radiation Center's equipment. My thanks also go to all of the department's administrative staff, including Janet Knudson, Heidi Braly, Casey Mills, Shaun Bromagem, Chris Thompson, and Joan Stueve. Many of my fellow students, both undergraduate and graduate, provided moral and technical support: thank you so much for your time, assistance and all the laughs. I am also grateful to my committee members, David Hamby, Alena Paulenova, Sue Carozza, and Kate Lajtha, whose hours of guidance and assistance have made this study immeasurably more robust.

My adviser, Kathy Higley, has provided me with excellent guidance these past three years, as well as numerous opportunities for professional development and networking. I can only aspire to one day be as outstanding a mentor as she has been for me.

I would like to express my gratitude to my whole family, who have done so much to support my over the years, but particularly my parents, Peter and Dianne Houser. Finally, my husband, Nick Ruedig, has spent hours helping me pour over my data and this thesis, and hours more providing moral support throughout this difficult process. Thank you to all.

Ἄξιόν σε ἐν πᾶσι καιροῖς ὑμνεῖσθαι φωναῖς α σίαις, Υἱὲ Θεοῦ, ζωὴν ὁ διδούς· διὸ ὁ κόσμος σὲ δοξάζει.

TABLE OF CONTENTS

		Page
1	**Introduction**	**1**
1.1	Motivation for Work	3
1.2	Previous Work	5
2	**Chalk River Laboratory Site**	**12**
2.1	Facilities at the Chalk River Site	12
2.2	Environmental Radionuclide Contamination	15
2.2.1	"Waste Management Area"s (WMAs)	15
2.2.2	NRX Accident & Discharge	18
2.3	Environment - Abiotic	18
2.4	Environment - Biotic	21
2.4.1	Flora	21
2.4.2	Fauna	22
2.5	Previous Radioecological Work On-Site	23
2.5.1	Aquatic Radionuclide Monitoring	23
2.5.2	Terrestrial Radionuclide Monitoring	23
2.5.3	Modeling	24
2.5.4	Effects Monitoring	30
3	**Experimental Design**	**31**
3.1	Description of Species Under Investigation	31
3.2	Drought as a Stressor	33
3.3	Description of Sampled Sites	34
3.4	Sample Collection	36
3.4.1	Water	36
3.4.2	Snails	37
3.4.3	Sediments	39
3.4.4	Predation	39
4	**Methods**	**41**
4.1	Sample Preparation	41
4.1.1	Water	41
4.1.2	Sediments	42
4.1.3	Snails	42
4.2	Radiochemistry / ^{90}Sr Purification	44
4.3	Sample Analysis	45
4.3.1	Counting Techniques	45
4.3.2	Other Analytic Techniques	48
4.4	Derivation of Absorbed Fractions	48
4.5	Dosimetry	52
5	**Data**	**56**
5.1	Limnological Data	56
5.1.1	Cation analysis by mass spectrometry	56
5.1.2	*In situ* measured variables	59
5.2	Snail Data	62
5.2.1	Biological data	62

TABLE OF CONTENTS (CONTINUED)

Page

5.2.2 Cation analysis of snails by mass spectrometry . . . 65
5.3 Radiological Data . . . 70
5.3.1 Generalized minimum detectable activity information . . . 70
5.3.2 Beta emitters . . . 71
5.3.3 Gamma emitters . . . 73
5.4 Dosimetric Results . . . 76
5.4.1 MCNP Results . . . 76
5.4.2 Range of Calculated Dose Rates . . . 84
5.4.3 Estimation of Natural Background from ^{40}K . . . 86

6 Analysis **87**
6.1 Data parsing for regression analysis . . . 87
6.2 Multiple Linear Regression: Mass as a Response Variable . . . 89
6.2.1 Elimination of collinear variables . . . 89
6.2.2 Models run . . . 90
6.2.3 Final variables . . . 92
6.2.4 Residual Plots . . . 95
6.3 Speculation concerning unexplained variation in snail mass . . . 97
6.4 Multiple Linear Regression: Number of Lured Snails as a Response Variable . . . 98
6.4.1 Data parsing for regression analysis . . . 99
6.4.2 Elimination of collinear variables . . . 99
6.4.3 Models run . . . 99
6.4.4 Final variables . . . 100
6.4.5 Residual Plot . . . 102
6.5 Derivation of environmental concentration ratios . . . 103
6.5.1 (^{90}Sr) Water concentration as an indicator of shell-tissue concentration . . . 104
6.6 Environmental factors influencing ^{90}Sr concentration ratio . . . 108
6.6.1 Data parsing for regression analysis . . . 109
6.6.2 Elimination of collinear variables . . . 109
6.6.3 Models run . . . 110
6.6.4 Final variables . . . 110
6.6.5 Residual Plot . . . 112
6.6.6 Improving R^2 by use of additional explanatory variables . . . 113
6.7 Importance of Substrate . . . 114

7 Discussion **115**
7.1 Comparison of voxelized Monte Carlo results with previous dosimetric modeling . . . 115
7.1.1 Blaylock 1993 . . . 116
7.1.2 Voxel vs Simplified Modeling . . . 119
7.2 Comparison with studies at Chernobyl . . . 120
7.3 ANOVA Results . . . 120

8 Conclusion **122**

TABLE OF CONTENTS (CONTINUED)

Page

A Technical Theory **124**
A.1 Gamma Spectroscopy . . . 124
A.2 Liquid Scintillation Counting (LSC) . . . 125
A.3 Inductively Coupled Plasma Mass Spectrometry (ICP-MS) . . . 126
A.4 Inductively Coupled Plasma Atomic Emission Spectrometry (ICP-AES) . . . 128
A.5 Column Chromatography . . . 128
A.6 Monte Carlo Modeling . . . 129
A.7 Least-Squares Regression Modeling . . . 130
A.8 Assumptions underlying least squares regression . . . 131
A.9 Analysis of Variance and the F-test . . . 133

B Protocols and Procedures **135**
B.1 Snail lure placement . . . 135
B.2 Snail lure retrieval . . . 137
B.3 Snail preparation . . . 138
B.4 Water sample processing (AES) . . . 139
B.5 Water sample processing (^{90}Sr analysis) . . . 140
B.6 Snail shell digestion . . . 141
B.7 Snail body digestion . . . 142
B.8 Sediment Density Fractionation . . . 143
B.9 Sediment leeching . . . 149
B.10 Column chromatography . . . 150
B.10.1 Assembling the Box . . . 150
B.10.2 Column Conditioning . . . 150
B.10.3 Separation of Sr . . . 151
B.10.4 ICP-MS Analysis . . . 152
B.11 Sample MCNP card . . . 153

References **156**

LIST OF FIGURES

Figure		Page
1	Characterizing UNSCEAR 96 references - studies by type of irradiation.	6
2	Characterizing UNSCEAR 96 references - studies by experiment condition.	7
3	Characterizing UNSCEAR 96 references - studies by site location.	8
4	Radiosensitivity of NHB	10
5	Spatial distribution of Ontario's forests	19
6	Map of CRL water bodies.	20
7	Spatial distribution of Ontario's soils	21
8	Eastern wolf food web after Hart and McKee	28
9	Snail species observed at CRL	32
10	Map of locations sampled as a part of this study.	36
11	Snail lure ready for placing	37
12	Snail lure ten days after placement	38
13	Substrate sampling device	39
14	Photo of ^{90}Sr purification apparatus	45
15	β-spectra for the initial (t=0) count of four samples, distinguished by separate colors.	47
16	Sagittal view of the whole snail CT image.	49
17	Contouring a snail in 3D Doctor.	50
18	CT image of snail shell (left) and 3D rendering of snail (right) illustrating body and shell segments.	51
19	LSC spectra of ^{90}Sr in four samples. Vertical lines indicate the theoretical (blue) and observed (green) average particle energy.	54
20	Water calcium as measured by mass spectrometry.	57
21	Water potassium as measured by mass spectrometry.	57
22	Water magnesium as measured by mass spectrometry.	58
23	Water sodium as measured by mass spectrometry.	58
24	Distribution of electroconductivities measured, sorted by location.	59
25	Distribution of pH measured, sorted by location.	60
26	Distribution of total dissolved solids measured, sorted by location.	60
27	Distribution of water temperature measured, sorted by location.	61
28	Distribution of incident light (at surface) on snail lure measured, sorted by location.	61
29	Distribution snail lengths, sorted by location.	62
30	Distribution of snail mass, sorted by location.	63
31	Relationship between snail mass and length, coded by location.	64
32	Fraction of wet mass that is snail shell, coded by location.	65
33	Snail shell calcium as measured by mass spectrometry	66
34	Snail shell potassium as measured by mass spectrometry	66
35	Snail shell magnesium as measured by mass spectrometry	67
36	Snail shell sodium as measured by mass spectrometry	67
37	Snail shell phosphorus as measured by mass spectrometry	68
38	Snail shell strontium as measured by mass spectrometry	69
39	Strontium-90 concentrations in snail shells ordered by location.	72
40	Absorbed fraction of electron energy for source located in the body.	78
41	Absorbed fraction of electron energy for source located in the shell.	79
42	Absorbed fraction of photon energy for source located in the body.	81
43	Absorbed fraction of photon energy for source located in the shell.	82
44	Snail shell dose rate for individual snails, by location.	85

LIST OF FIGURES (CONTINUED)

Figure		Page
45	Jittered residual plot for mass~water_ca	96
46	Jittered residual plot for mass~light	97
47	Jittered residual plot for num_snails~water_p	103
48	Regression relating the ratio [^{90}Sr] to [^{nat}Sr] in tissues to the same ratio in environmental (water) samples. Grey area represents the 95% CI.	105
49	Regression relating tissue concentrations of ^{90}Sr to environmental concentrations (water) of the same species. Grey area represents the 95% CI.	106
50	Regression relating the ratio [^{90}Sr] to [^{nat}Ca] in tissues to the same ratio in environmental (water) samples. Grey area represents the 95% CI.	107
51	Shell:water concentration ratio (^{90}Sr/Ca) as a function of mass. Grey area represents the 95% CI.	108
52	Jittered residual plot for snail_conc_sr~water_conc_sr	113
53	Comparison of segment-specific electron absorbed fractions for (a) source in shell and (b) source in body with whole-body absorbed fractions from Blaylock[12].	117
54	Comparison of segment-specific photon absorbed fractions for (a) source in shell and (b) source in body with whole-body absorbed fractions from Blaylock[12].	118
55	Snail mass as a function of snail shell dose rate.	121
56	Gamma spectrum, without energy calibration	124
57	Conceptual diagram depicting each step of an ICP mass spectrometer.	127
58	Density fractionation diagram.	145
59	Test tube after centrifugation.	146
60	Vacuum filtration apparatus.	147
61	Sediment fractions and filter paper masses, ready for drying.	148

LIST OF TABLES

Table		Page
1	Dose Rates to NHB at South Swamp	10
2	Summary of Radioactive Groundwater Plumes at the CRL Supervised and Controlled Areas	17
3	CRL Ecosystem model definitions	25
4	CRL dosimetry model definitions	29
5	Sampling locations at CRL. Doses as estimated by Hart and McKee[38].	35
6	Microwave digestion protocol	44
7	Explanation of variables used in dosimetry.	53
8	Explanation of variables used in dosimetry.	55
9	Major ion concentrations as determined by ICP-AES	56
10	Limnological characteristics measured *in situ*.	59
11	Snails collected from CRL water bodies	62
12	Average cation content of snail shell.	65
13	Average cation content of snail body.	69
14	Blank sample data from gamma spectroscopy.	70
15	Blank sample data from liquid scintillation counting performed at CRL.	70
16	Blank sample data from ^{90}Sr liquid scintillation counting performed at OSU.	71
17	Tritium concentrations in water.	71
18	Strontium-90 concentrations in water.	71
19	Strontium-90 concentrations in snail shells.	72
20	Strontium-90 concentrations in snail bodies.	73
21	Gross beta concentrations in sediment samples.	73
22	^{137}Cs concentrations in water.	73
23	^{60}Co concentrations in water.	74
24	Cobalt-60 concentrations in snail shells.	74
25	Cesium-137 concentrations in snail shells.	74
26	Cobalt-60 concentrations in snail bodies.	75
27	Cesium-137 concentrations in snail bodies.	75
28	Cesium-137 concentrations in sediment samples.	75
29	Cobalt-60 concentrations in sediment samples.	76
30	Absorbed fraction of electron energy.	77
31	Absorbed fractions of photon energy.	80
32	Strontium-90 DCFs	84
33	Yttrium-90 DCFs	84
34	Hydrogen-3 DCFs	84
35	Mean shell dose rates for *C. decisum* at CRL, by location	85
36	^{40}K DCFs in units of μGy-kg (Bq-d)$^{-1}$ for snail tissues.	86
37	Dose to snail shell from^{40}K located in shell.	86
38	Snail mass and replicates for entire data set, grouped by location. ANOVA showed convincing evidence of variation in shell mass by location ($p<<0.001$).	87
39	Snail shell mass and replicates for subgroup analyzed for ^{90}Sr content, grouped by location. ANOVA showed no evidence of variation in shell mass by location ($p=0.31$).	88
40	Shell dose rate and replicates for subgroup analyzed for ^{90}Sr content, grouped by location.	88
41	Regression model variable descriptions.	90
42	ANOVA table for first regression model.	91

LIST OF TABLES (CONTINUED)

Table		Page
43	VIF table for first regression model.	91
44	ANOVA table for a model that showed a high degree of covariance.	92
45	VIF table for a model that showed a high degree of covariance.	92
46	Collinearity of regression model variables for snail mass model.	93
47	ANOVA table for model inclusive of all linearly-independent factors.	93
48	VIF table for model inclusive of all linearly-independent factors.	94
49	ANOVA table for the simplified model.	94
50	VIF table for the simplified model.	94
51	ANOVA table for first regression model.	100
52	VIF table for first regression model.	100
53	Collinearity of regression model variables for number of snails model.	101
54	ANOVA table for model inclusive of all linearly-independent factors.	101
55	VIF table for model inclusive of all linearly-independent factors.	101
56	ANOVA table for the simplified model.	102
57	CR regression model variable descriptions.	109
58	Collinearity of regression model variables for number of snails model.	110
59	ANOVA table for model inclusive of all linearly-independent factors.	111
60	VIF table for model inclusive of all linearly-independent factors.	111
61	ANOVA table for the simplified model.	112
62	Change in R^2 due to inclusion of additional explanatory variables in regression model.	114
63	DCFs (μGy kg $Bq^{-1}d^{-1}$) for Strontium-90 (including Yttrium-90) for the simplified and voxelized models.	116
64	Microwave digestion protocol	142
65	Mixing table for SPT solutions (makes 1L).	144

1 Introduction

The concept of environmental protection is a modern one. Historically, and especially in the United States, protestant dominion theology, combined with the manifest destiny movement of the nineteenth century has resulted widespread exploitation of natural resources with little eye toward sustainability. In the latter-half of the twentieth century, when the human impact of industrialization could no longer be denied, public opinion on the subject began to shift. The result was the passage of landmark legislation such as the Clean Air Act (1963), the National Environmental Policy Act (1969), Safe Drinking Water Act (1974) and many others. The principle motivation behind these early environmental movements was the protection of man: acid rain was causing visible damage in cities; the miasma in Los Angeles was giving rise to increased incidence of asthma. This attitude continues today: global climate change has been mostly ignored or denied by the American public, and it has been well-documented that weather events with personal impact (e.g., drought, fires, hurricanes) are better at swaying public opinion than hard data about the rate of e.g., Arctic ice loss[76, 84]. Quite simply, the American public often chooses not to worry about environmental issues until they have a direct, individual impact upon quality of life. Despite this, protective legislation has moved past merely regulating those environmental hazards with a direct impact upon the anthroposphere. Today, there exists legislation at both the federal and state levels whose focus is not only the protection of man, but also the protection and maintenance of the environment itself. This recognition of the inherent value of the environment is perhaps one of the most important macro-scale philosophical changes to arise out of the last century of environmentalism[63, 16].

The establishment of protection standards requires understanding the interaction between ecosystem (including humans) and hazard. For example, to regulate runoff from copper mines, we must understand how both heavy metals and low-pH impact an ecosystem. Once risk and consequences are understood, it is possible to construct an appropriate system of benefit analysis and incentivize (or penalize) certain behaviors. And so, in the case of radiation protection, we must ask the question: how much radiation is too much?

Like all such questions, the answer is complicated. After a century of research into the subject we are beginning to understand this issue as it applies to humans. While there is still much discus-

sion and debate on the subject of the exact calculation of risk, we have certainly minimized the number of radiation-related impacts on society at large. We have adopted the ALARA (as low as reasonably achievable) paradigm and used the principles of justification, optimization, and limitation to ensure that there is some benefit commensurate with risk each time a human is exposed to radiation. Decades of research have given us some limited insight into the effects of ionizing radiation exposure in humans, and we use this data to construct responsible and conservative dose limits.

When it comes to the environment, the answer to this fundamental question is less clear. The hallmark of human society is our macro-scale shaping of the environment: we accept and even encourage environmental manipulation, often damaging in some way the non-human residents of that environment. To humans, the consequences of environmental change or damage may be acceptable. We weigh the risks and benefits environmental change: how does the impact of a shopping mall compare to the impact of a superfund site? Even when the science is clear, this question is challenging to answer in a democratic society where multiple stakeholders with conflicting interests will influence every decision to be made. Even if science could definitively produce a numerical answer - a highly unlikely prospect - political and social pressures ensure that the subject of environmental damage cannot be reduced to a single metric.

Yet we must establish both a limit of environmental effect that is acceptable and a metric by which to assess that effect. But what metric should be applied? How do we distill the complexity of an entire ecosystem into a single metric? Or even a handful of metrics? Finally, how should we choose an appropriate screening value for our hypothetical metric, above which site remediation is compulsory?

This dissertation has focused on collecting data to inform the scientific and policy decisions described above. Some previously collected data regarding non-human biota (NHB) dose-effects exists; most of it collected under laboratory conditions that are far removed from the environments that an organism encounters in its natural habitat. The work of a few prolific authors has recently called attention to this dearth of data and have begun to dominate the protection narrative. In this environment, additional study is very much called for.

1.1 Motivation for Work

The earliest guidance issued by the International Commission on Radiological Protection (ICRP) asserted that the protection of man would ensure appropriate protection of non-human biota due to the especially strict standards employed in the protection of man. This paradigm is still dominant in the United States, and states that:

> Although the principal object of radiation protection is the achievement and maintenance of appropriately safe conditions for activities involving human exposure, the level of safety required for the protection of all human individuals is thought likely to be adequate to protect other species, although not necessarily individual members of these species. The Commission therefore believes that if man is adequately protected then other living things are also likely to be sufficiently protected. [77]

Succinctly, the ICRP has concluded that the protection of NHB in terms of ecosystem function, is assured as long as man is protected. This seems intuitively correct: man resides at the top of the food chain and thus his exposure is likely to be high due to bioaccumulative effects. Additionally, the ICRP notes that man, and particularly children, tend to be protected very strictly, so limitations on environmental contamination ought to be be sufficiently severe to prohibit any deleterious effects in NHB. However, this concept has limitations: if man is absent from the contaminated ecosystem (as would likely occur following any large scale release of environmental radioactivity), then it is possible for man to be protected while NHB receive hefty radiation doses.

To address this disconnect, a number of methodologies have recently been proposed with the intent of preventing radiation impacts upon an ecosystem where man is absent. Still, in this recent guidance the ICRP acknowledges that "no simple or single universal definition of environmental protection is applied internationally and that the concept of environmental protection differs from country to country and from one circumstance to another"[43]. Regardless of this lack of standardization, the ICRP notes that the goal of most NHB protection legislation is to "safeguard the environment by

preventing or reducing the frequency of effects likely to cause early mortality or reduced reproductive success in individual fauna and flora to a level where they would have a negligible impact on conservation of species, maintenance of biodiversity, or the health and status of natural habitats or communities"[82]. In other words, to adequately protect an ecosystem we must ensure that all species are conserved, biodiversity is maintained, and health impacts prevented. It should be acknowledged that the above statements by the ICRP still affirm that NHB protection should *not* be approached from the perspective of protecting individuals (as we approach the protection of man), but instead that *populations* and *ecosystem function* should be preserved. This approach essentially neglects an acutely fatal dose as long as it is not widespread enough to impact an entire population or ecosystem. Commensurate with the ICRP's guidance, national governments have been slowly adopting regulatory frameworks that address the protection of NHB, particularly in the case of deep geologic repositories (DGRs). Of particular note are the recommendations of the international working group BIOPROTA[73], who have proposed a tiered approach to consequence-evaluation: dose-rates exceeding a broad-scoped "no effects" screening limit would require additional justification demonstrating both the utility of the site and site-specific protective measures related to any populations that exceed screening limits.

The key to any kind of NHB-protective paradigm is determining what magnitude of radiation dose will cause an ecosystem to exceed those limits outlined by the ICRP in 2003. A simple lethal-dose study may prove a starting point for evaluating the radio-sensitivity of a single species, but does nothing to address the challenges inherent in the assessment of the health of an entire population or ecosystem. There are multiple mechanisms of impact: a continuous, non-lethal dose may weaken individuals of a particular species, making them more vulnerable to predation or a given dose might also reduce reproductive success. Both of these outcomes may result in a gradual decline of population size, a more subtle effect than death of individuals via an acutely lethal dose. If we wish to develop meaningful metrics capable of reflecting the multitude of interactions occurring throughout an ecosystem, bench-top irradiation experiments will be insufficient to determine protective standards.

1.2 Previous Work

There are a number of canned codes for modeling dose rates in NHB. Among the most-utilized are the ERICA tool[17] and RESRAD BIOTA[1]. These tools provide an estimate of radiation dose rates to a subset of organisms, usually ICRP's reference animals and plants (RAPs). However, models may provide a false sense of security inasmuch as the environmental transfer data they are based on may not be reliable[39]. Further, the scientific literature lacks a strong understanding of NHB dose-effects within the framework of an entire ecosystem. Several authors have studied this question and tried to offer succinct wisdom, for example UNSCEAR[3], and others[8, 9, 20, 44, 67]. However, these publications frequently rely on data that is collected under laboratory conditions; whether this data can responsibly be applied to RAPs in a field setting is questionable.

To assess the status of NHB dose-effects research, references from UNSCEAR 96[3] were used as a litmus test. Most current studies and regulatory guidance (for example [17, 10, 18, 82, 73, 43] et cetera) utilize UNSCEAR 96's results in some manner, so it is not improper to suggest that UNSCEAR's results have framed the discussion surrounding NHB dose-effects in a unique and important way.

The references from UNSCEAR 96 were evaluated, and two hundred and sixty five of the references from the report were determined to be relevant to the question of radiation dose-effects in NHB. Of these, 223 were locatable (available, in English, etc). These were scored according to the type of radiation used to induce an effect in some representative NHB; the results are depicted in Figure 1.

[1] http://web.ead.anl.gov/resrad/home2/biota.cfm

Figure 1: Characterizing UNSCEAR 96 references - studies by type of irradiation.

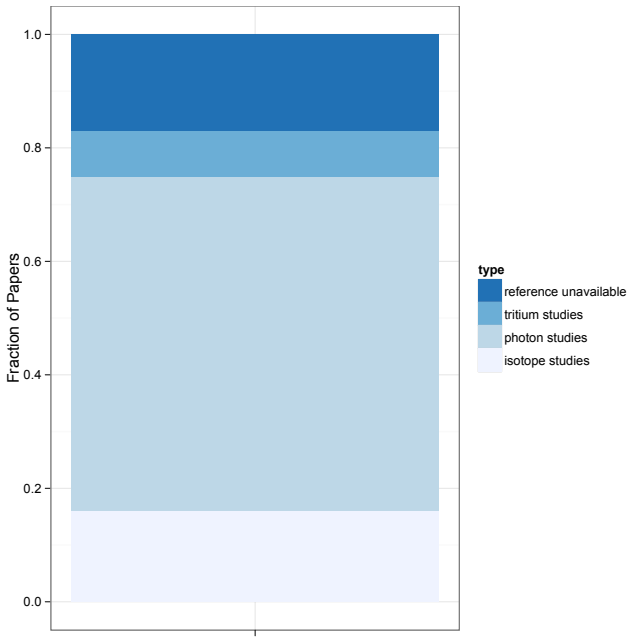

Tritium was the isotope under investigation in 18 of the studies, and photons from an irradiator were the radiation source in 146 of the studies cited. Tritium was separated out as the low-energy beta emitted by this isotope is considered by some to have a unique biological effect[23]. The remaining 39 studies from UNSCEAR 96 referencing NHB dose-effects were non-Tritium isotope studies, and were scored as being either a laboratory or a field study. Studies were classified as being "laboratory" (nine studies) if they were conducted under conditions where natural stressors such as predation were absent, while "field" data (thirty studies) were collected in such a way that the subject under investigation was present, or nearly present, in its normal ecological niche. These results are depicted in Figure 2.

Figure 2: Characterizing UNSCEAR 96 references - studies by experiment condition.

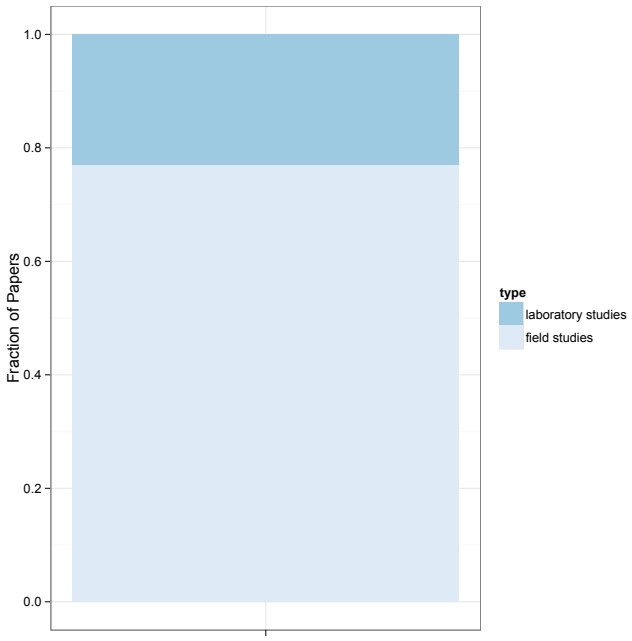

Finally, to determine what sites isotope studies were conducted at, the isotope and field studies (thirty studies) were scored by location. Unsurprisingly, the majority of data are from the area around the Chernobyl nuclear power plant (eighteen studies), with a few from the Ural Mountains (six studies) and elsewhere (six studies). These results are depicted in Figure 3.

Figure 3: Characterizing UNSCEAR 96 references - studies by site location.

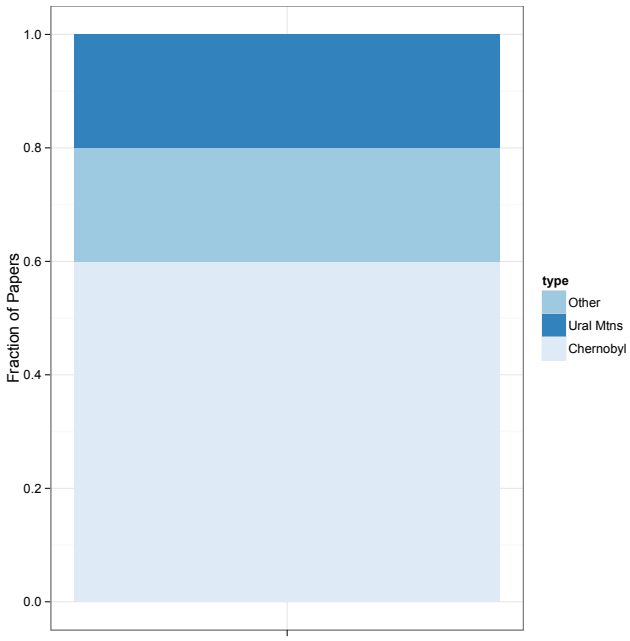

It is worth noting that most previous work has concluded that relatively high dose limits are of no concern for the health of an ecosystem. UNSCEAR's 96 publication states that in terrestrial plants and aquatic animals, dose rates of up to 400 μGy h^{-1} are permissible. In terrestrial animals, reproductive effects are observable at dose rates of 40-100 μGy h^{-1}, while population effects are not observed until 400 μGy h^{-1}. Recent publications have called UNSCEAR 96 into question. Of particular note is the work of Møller and Mousseau[55, 54, 57, 56, 58], which seeks to establish, independent of UNSCEAR or any other recommending body's guidance, dose-effects relationship in wildlife around the Chernobyl exclusion zone. Their work is deeply lacking in a number of ways: for example, dosimetrically, their work considered only the external component of dose rate as determined by a hand-held geiger counter. Additionally, the work is lacking ecologically: studies are conducted by two scientists and study periods are usually only a few days. Because of this, their studies lack the rigor of those conducted over an entire season, or multiple years. Finally, these studies also lack any sort of double-blind protection. Establishing a robust standard of study for these types of radioecological investigations, as is the goal of this dissertation, is paramount at a

time when collected data may influence the standards just now being set by regulatory bodies that limit environmental radiation exposure.

The fact remains that there is very little data available to refute or support claims that the dose-effects threshold ought to be lower than previously believed. Garnier-Laplace[32] et al have recently raised these same issues in the literature, with the dominant criticism being the applicability of laboratory-collected data to field conditions. UNSCEAR included only thirty studies in their 1996 publication that meet the criteria for field conditions and utilized a biogeochemically cycling radioactive source. Most other data comes from laboratory studies (e.g., bench-top irradiations with lethality as the endpoint), or field studies using only external radiation sources (e.g., a source placed in a field and left for days to years to irradiate local biota). Both of these experimental designs have flaws that call into question the applicability of their data for use evaluating a contaminated ecosystem. In the case of a laboratory study, effects that only weaken an individual, as opposed to outright killing it, may not be observable, while in the field this weakening may lead to predation, starvation or other cause of death. In the case of irradiators left in an ecosystem, it is difficult to quantify dose rates received by mobile biota: while these studies may work well for estimating dose-sensitivity in plants, they are unable to establish dose-effect relationships in mobile forms of life. Thus, additional data derived from the comprehensive review of an ecosystem using a biogeochemical paradigm, in conjunction with systemic ecological monitoring to assess dose effects would augment scientific understanding and provide valuable data for the determination of the safety and suitability of deep geologic repositories. The aquatic snail was selected for study due to modeling results which suggest that these organisms are subject to the highest dose rates of any species on the CRL site[38], mostly due to accumulated ^{90}Sr in the shell. Models indicate that NHB located at CRL's South Swamp experience dose rates high enough to cause population-level effects (see Table 1, below, for estimated dose rates to NHB in south swamp[38]), so it was selected as an upper-limit along the dose-rate gradient investigated in this study. Several other locations on-site have lower dose rates, providing a gradient useful for the creation of a dose-response curve.

Table 1: Dose Rates to NHB at South Swamp

Organism	Mean Dose Rate uGy h^{-1}	Max Dose Rate uGy h^{-1}
Green Frog	178	1,637
Snail	5,469	50,530
Aquatic Plant	387	3,575
Riparian Plant	212	1,953
Water Shrew	486	4,489
Great Blue Heron	7.7	65.9

There are benefits and drawbacks to using snails as the species of interest for this study. One of the major drawbacks is that snails are radio-resistant, so even at dose rates approaching 50,000 uGy h^{-1}, we do not anticipate observing acute lethality[68]. Figure 4, reproduced from data compiled by Sparrow et al[74], illustrates the relative insensitivity of snails (mollusks):

Figure 4: Radiosensitivity of NHB

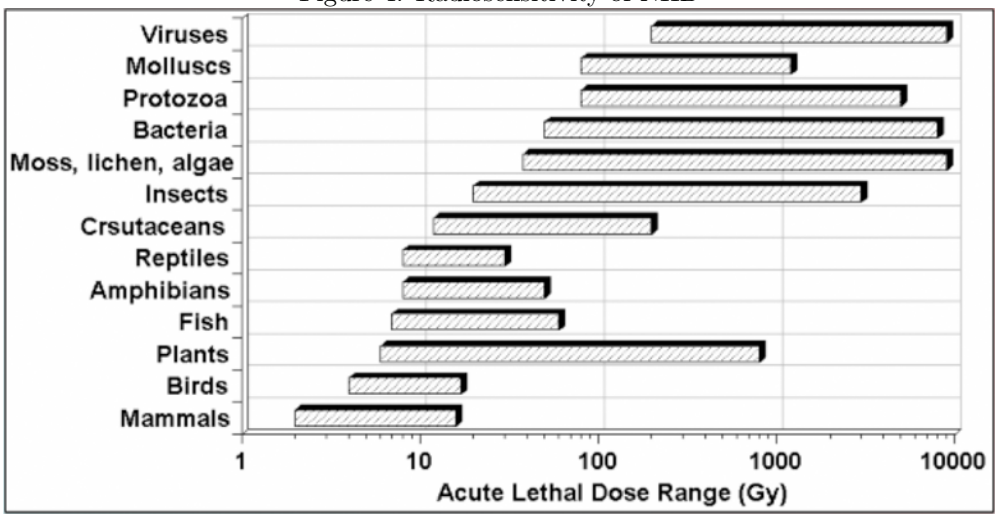

Previous work [65, 69] has established the acutely lethal dose to snails as a few hundred Gray, with impaired reproduction at tens of Gray. Maximum dose rates in South Swamp exceed 1 Gy d^{-1} and are high at other areas of CRL, so the potential for impaired populations is very real.

It should be noted that water shrews appear to also be receiving receive chronically high (relative to the acutely lethal dose) dose rates at South Swamp. Future study of dose-effects in water shrews

could provide interesting results using a mammalian model. However the time, cost, and population effects of sampling sufficient numbers of water shrews to obtain statistically significant results have made it impossible to focus on this species for the present study.

There are numerous benefits to using snails as the focal species for a study of this kind. The most obvious of these is the ease of sampling and analyzing snails. The use of snails as a benchmark species for heavy metal contamination has previously been well established in the ecological sciences[52, 11, 14, 36]. Snails are useful indicators of heavy-metal contamination in an ecosystem as their shells tend to accumulate heavy metals. Additionally, snails manifest changes in shell morphology and mass that can be useful indicators of detrimental effect from a precisely known amount of contamination. The ability to assess not just population dynamics but also individual fitness makes snails an excellent candidate for study.

2 Chalk River Laboratory Site

The laboratories at Chalk River, Ontario, Canada were established in 1944 under the authority of the National Research Council (NRC) of Canada. In 1945, the first nuclear reactor to go critical outside of the United States, Canada's Zero Energy Experimental Pile (ZEEP) went critical at the facility. Early work at Chalk River focused nearly exclusively on the development of reactor technology for commercial power production; in furtherance of this goal Atomic Energy of Canada Limited (AECL) was founded at Chalk River in December of 1952 with a mandate to develop the peaceful uses of nuclear energy.

2.1 Facilities at the Chalk River Site

Since the 1950s, Chalk River have been mostly devoted to R&D related to commercial power production and waste treatment issues, somewhat similar to work carried out in the United States at the Hanford site. A partial list and description of larger facilities of interest, as detailed by Hart & McKee[38], is given here:

1. Reactor Facilities

   (a) **NRU Reactor** (1957-) is a heavy water reactor that operates up to a power of 135 MW(Th.). Principle uses are engineering experiments and the production of medical isotopes.

   (b) **MAPLE1 and MAPLE2 reactors** (2000-) are light-water pool reactors that are used exclusively to produce medical isotopes. These reactors, together with the New Processing Facility (NPF) are owned by MDS-Nordion and operated by AECL.

   (c) **ZED-2 Reactor** is a zero energy (<200W), heavy water facility used mainly for reactor physics experiments.

   (d) **NRX Reactor** (1947-1995) was a heavy water moderated reactor that was used as a back-up for the NRU reactor for a number of years. Its rod bay was used for storage until 1995 and had been discharging tritium and ^{90}Sr into the groundwater since 1959.

(e) **Pool Test Reactor** (closed 1990) was a zero energy (100W) reactor used for physics research.

2. Fuel Fabrication & Hot Cell Facilities

(a) **Universal Cells** are shielded facilities that are used for remote manipulation, testing, and examination of large quantities of radioactive materials.

(b) **Fuels and Materials Cells** are shielded facilities similar to the Universal Cells, but used for metallurgical testing and examination with reactor fuels and components.

(c) **Nuclear Fuel Fabrication Facilities** are used to fabricate fuel assemblies and Mo-99 targets for the NRU and MAPLE1 reactors.

3. Waste Facilities

(a) **Waste Treatment Centre (WTC)** (1997-) is a site for processing radioactive wastes, both those generated on-site and those received from off-site generators. Solid and liquid wastes are accepted.

(b) **Recycle Fuel Fabrication Laboratories (RFFL)** (1970s-) consists of several laboratories dedicated to the fabrication of alpha-active ceramic fuels (e.g., uranium-plutonium, thorium-plutonium, and thorium-^{233}uranium).

(c) **Waste Management Areas - CRL** consists of several waste areas used for disposal of radioactive materials. Each area has different contaminants, most of which have spread contamination into the surrounding ecosystem. They will be discussed in detail in section 2.5.

(d) **Plutonium Recovery Laboratory** (1949-1957) was used to extract plutonium from enriched fuels.

(e) **Waste Water Evaporator** (closed 1971) was part of the fuel processing and uranium recovery facilities at CRL.

(f) **Plutonium Tower** (1948-1954) was a joint project of AECL and UKAEA whose research goal was to develop aqueous extraction schemes for the separation of plutonium from dissolved irradiated-uranium solutions.

4. Other Facilities

(a) **Molybdenum-99 Production Facility** (2005-) is a chemistry laboratory where ^{99}Mo is extracted from an irradiated uranium-based target. CRL is the world's largest supplier of ^{99}Mo, an important medical isotope.

(b) **New Processing Facility (NPF)** is a facility for processing uranium targets from the MAPLE 1 and 2 reactors for the generation of medical isotopes (specifically ^{99}Mo).

(c) **Tritium Laboratory** is a laboratory dedicated for work with tritium, specifically meeting research and development needs concerning heavy-water management and tritium control in the CANDU reactors.

(d) **Heavy Water Upgrading Plant** (closed 1999) was used to clean and upgrade heavy water to reactor-use quality.

(e) **Health Physics Neutron Generator** (1961-) is a high voltage accelerator that can accelerate up to 1mA of D^+ to produce 14 or 2.7 MeV neutrons through the D(T,n)^{4}He or D(D,n)^{3}He reactions.

(f) **Combined Electrolysis Catalytic & Exchange Upgrading Detritiation (CECEUD) Test Facility** (closed 2001) was a proof-of-concept facility for detritiation and heavy-water upgrading.

Many of the currently operational facilities have airborne releases that are filtered and monitored. Previous effluent releases - both gaseous and liquid - have occurred at several facilities, and will be

discussed in greater detail in section 2.5.

2.2 Environmental Radionuclide Contamination

Dolinar et al[26] and Hart & McKee[38] describe in detail the various waste management challenges at CRL; these areas constitute the principle sources of environmental contamination at the CRL site and are summarized here.

2.2.1 "Waste Management Area"s (WMAs)

1. **WMA-A** was a soil trench used for disposal of solid and liquid radioactive waste between 1946 and 1955. A particularly large amount of liquid waste was disposed here after the 1952 NRX reactor incident.

2. **WMA-B** includes both unlined soil trenches (used 1953-1963) and asphalt lined/capped trenches (used 1950s) as well as concrete bunkers (until 1979) that were used for solid waste management.

3. **WMA-C** was excavated in 1963 to hold low-level wastes that will be hazardous for less than 150 years. These wastes are stored in covered soil trenches that use soil backfill. There are waste drums and sections of the NRX stack stored on the surface of this area.

4. **WMA-D / Bulk Storage** area is an area established in 1976 and used to store old equipment parts known or suspected to be contaminated. The Bulk Storage Area was closed in 1973, but before this date was used store large equipment that has residual low-level contamination. These materials are all stored above ground.

5. **WMA-E** is near the Waste Tank Farm and was operated between 1977 and 1984 to store slightly contaminated soil and building material. The total volume of waste here is small.

6. **WMA-F** was used between 1976 and 1979 to store contaminated soils containing ^{226}Ra, arsenic, and uranium that were taken from Port Hope, Albion Hills, and Ottawa.

7. **WMA-G** is an above-ground dry storage facility established in 1989. Concrete canisters hold irradiated fuel from the Rolphton NPD power reactor. Additionally, canisters containing high level ^{99}Mo production waste have been stored here in recent years.

8. **WMA-H** is a newly constructed (2001) site designed for modular, above-ground storage of low-level radioactive waste.

9. **Liquid Dispersal Area (LDA)** received liquid waste from 1953-2000 via pipeline. It includes two reactor pits containing wastes from the NRU and NRX reactors which in recent years have been treated at the WTC facility, as well as a chemical pit that received radioactive chemical waste from local laboratories, and a laundry pit, which was used in 1956 to disperse waste water from an active decontamination center.

10. **Waste Tank Farm** has been used since 1961 to store high and intermediate level waste from CRL. The waste is stored in tanks, some of which are housed inside concrete bunkers lined with stainless steel. These wastes are recoverable.

11. **Acid, Chemical, Solvent (ACS) Pits** were used between 1982 and 1987 to disperse inactive acids, chemicals, and organic solvents.

12. **Glass Block Sites** have been established as test sites for the study of dispersement from vitrified waste.

13. **Thorium Pit** was used between 1955 and 1960 to receive wastes from CRL's ^{233}U extraction facility. Wastes contain ^{233}U, Th, and small amounts of fission products.

14. **Nitrate Plant** was used to decompose ammonium nitrate in reprocessing waste solutions. The plant shut down in 1954, after an accident resulted in the discharge of untreated waste to an infiltration pit not designed for this purpose. Subsequent to this event, some equipment and the buildings associated with the plant were buried in situ.

The CRL property features several contaminated groundwater plumes, principally arising from the waste management areas and from the plant site itself, on the shoreline of the Ottawa River. Table 2 is a summary of these plumes, as taken from the research of Dolinar et al[26] and Eyvindson[48].

Table 2: Summary of Radioactive Groundwater Plumes at the CRL Supervised and Controlled Areas

Drainage Basin	Area	Source of Contamination	Main Contaminants
Perch Lake	WMA-A	Sand Trench, reprocessing solutions	^{90}Sr,^{137}Cs extent: 38,000 m^2
	LDA	Chemical Pit, active drain discharges	^{90}Sr, ^{60}Co extent: 8,000m^2
		Reactor Pit #1	^{90}Sr extent: 9,000m^2
		Reactor Pit #2, rod bay water discharges	^{3}H, extent: 200,000m^2 ^{90}Sr, extent: 18,000m^2
	WMA-B	Sand Trench	^{3}H
		Sand and/or asphalt trenches	^{90}Sr extent:8,500m^2
	Glass Block Experiment	Blocks of vitrified waste placed to test leaching	^{90}Sr extent:3,000m^2
Maskinonge Lake	WMA-C	Mixed low-level wastes	^{3}H, ^{14}C extent:38,000m^2
	Nitrate Plant	Reprocessing wastes, process upsets	^{90}Sr,^{137}Cs extent:16,000m^2
	Thorium Plant	Reprocessing waste direct-to-ground discharge	90Sr extent: 6,000m^2
Ottawa River	Plant Site, Controlled Area 2	NRX rod bay leak, Bldg. 204, most (0%) reports to river via 04 Storm Sewer	^{3}H, ^{90}Sr extent: 28,000m^2
		NRU Building, from rod bay or pipeline from NRU to Liquid Dispersal Area	^{3}H extent: 24,000m^2
		Leaks from old active drain system, including Tank 240	^{3}H &/or ^{90}Sr: plumes merge with NRX/NRU plumes

Plumes at CRL are monitored frequently; interception and plume manipulation systems have been installed at a number of sites to prevent or slow transport of radionuclides through the groundwater.

2.2.2 NRX Accident & Discharge

The NRX reactor was a an early experimental reactor that went online at Chalk River in July 1947. It was a vertically oriented, heavy water moderated reactor with boron carbide control rods, and at the time of the accident was the world's most powerful research reactor, as well as the most expensive science experiment in Canada[1].

In December of 1952, during low power testing, a supervisor noticed that an operator was pulling control rods from the core. The operator corrected this error, but not all of the control rods fully re-entered the core; a communication error at this point led to the withdrawal of four safeguard control rods, after which the operators noticed power levels exponentially increasing. The reactor scrammed, but three of the scram rods did not enter the reactor and the fourth took about 90 seconds to be inserted. The increasing power boiled the coolant water and ruptured cooling piping. Reactor power peaked at 80MW, approximately double the normal operating power before a single functional scram rod finally brought the reaction back under control.

The coolant system, kept running to remove decay heat, leaked contaminated coolant to the floor of the NRX building. About 400 TBq of radioactive material was discharged to the basement, dissolved in about 4000 m^3 of water. The reactor was ultimately repaired and brought online about two years later; operations continued for forty years thereafter. The NRX accident itself, however, is the source of much of the radiological contamination at CRL[38].

2.3 Environment - Abiotic

Chalk River is a rural community located in Renfrew County, Ontario, Canada, approximately approximately 180 km northwest of Ottawa. The site is part of the Great Lakes-St. Lawrence forest biome; figure 5 is a map of the biomes of Ontario, after a map available from the Ontario Ministry

of Natural Resources[2]. The Great Lakes-St. Lawrence region is bordered to the south by deciduous forest and to the north by boreal forest. Chalk River resides in the Ottawa River Valley, and is characterized by the Ottawa River itself and gently rolling hills interspersed with many small lakes. The site is located on a former island in the Ottawa River; the surrounding terrain was carved out at the end of the last glaciation period[31, 35, 38].

Figure 5: Spatial distribution of Ontario's forests

Chalk River itself resides on the Ottawa River, which marks the eastern border of Ontario (shared with Quebec). Ontario experiences a continental climate, with harsh winters and humid summers; the mean annual temperature in Chalk River is 4.1^{o}C. July is the warmest month with a mean temperature of 19.6^{o}C; January is the coldest, with a mean temperature of -12.8^{o}C. The minimum number of frost free days is 100, although this is uncharacteristically short; the average growing

[2]http://www.mnr.gov.on.ca/

season is 136 days. Annually, mean precipitation is about 80cm of which 19cm are in the form of snow[64]. Hare[37] estimates 50cm of potential evapotranspiration per annum in Chalk River and places the moisture index at 80, characteristic of a humid climate. The site is characterized by numerous small ponds and swamps; the majority of drainage in the area ends in the Ottawa River. Figure 6 is a map[45] of the water features on CRL's property.

Figure 6: Map of CRL water bodies.

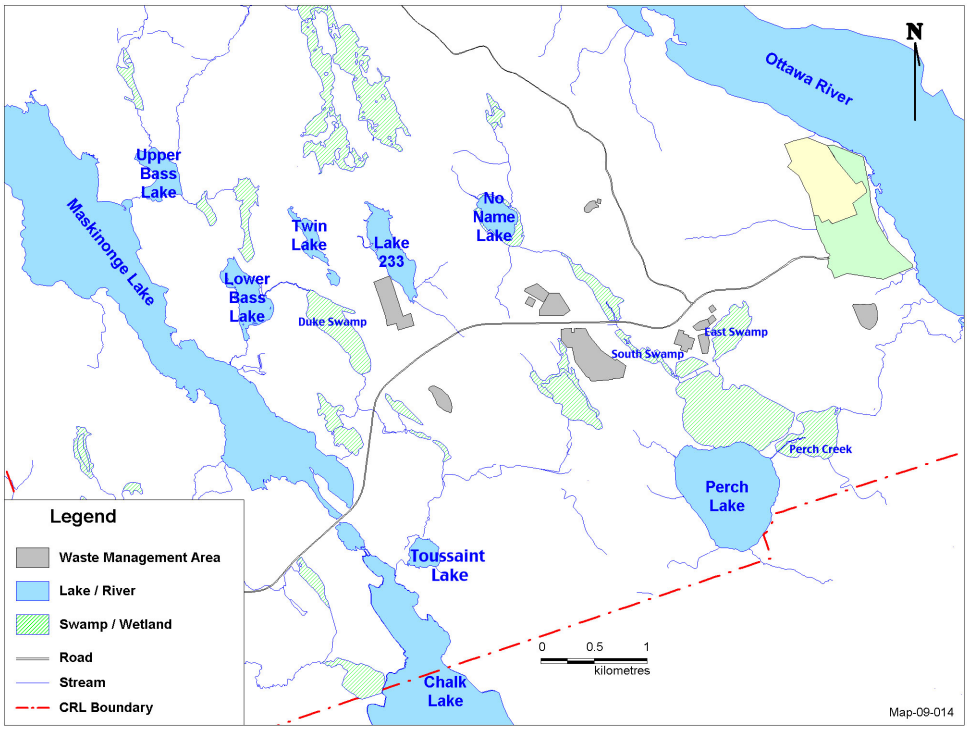

The locations of different soils in Ontario correlates well with the forest region. Thus, Chalk River, which resides in the Great Lakes St. Lawrence forest is covered with a brown podsolic soil[42]. A detailed map with soil subtypes is available from Perera[64] which provides not only spatial data, but a summary of the character of each of the soil types found in Ontario and is included as Figure 7. That podsols are the primary soil in the Chalk River area is not surprising, given their association with glacial tills and outwash.

Figure 7: Spatial distribution of Ontario's soils

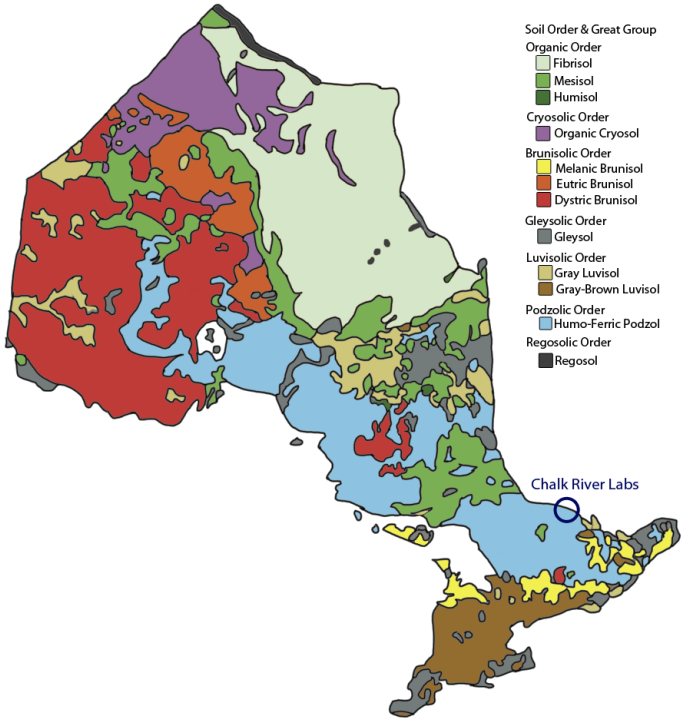

2.4 Environment - Biotic

The biotic environment at the CRL site is typical of the Great Lakes-St. Lawrence biome, with a mostly forested landscape interspersed with freshwater aquatic habitats in the form of lakes or rivers. Individual plant and animal species are fairly typical for this biome.

2.4.1 Flora

The Chalk River site is largely forested, with White Pine (*Pinus strobus*), Hemlock (*Tsuga canadensis*), Sugar Maple (*Acer rubrum*), Yellow Birch (*Betula lutea*), and Beech (*Fagus grandifolia*) dominating. Less frequently, one encounters Quaking Aspen (*Populus tremuloides*), Large-tooth Aspen

(*Populus grandidentata*), White Birch (*Betula payrifera*), Red Pine (*Pinus resinosa*) and Jack Pine (*Pinus banksiana*)[83]. Much of the area was cleared for farming in the early parts of the twentieth century, so wooded uplands range from 40-80 years old, and wooded wetlands appear to be relatively young[34].

Hart and McKee[38] describe the wetland communities as either a swamp-type or marsh-type, stating that: "deciduous swamp communities comprised of speckled alder shrubs and trees or black ash and silver maple are more abundant than coniferous swamp communities [which are] typically dominated by black spruce or less commonly by white cedar". This contrasts with the marsh-type wetland community, which is described as being "dominated by shrubs or herbaceous and graminoid (grass-like) species because of the relatively permanent moisture regime... Permanently flooded areas, generally associated with lake shores and the shore of the Ottawa River, support a range of robust emergents and aquatic floating-leaved plants".

The CRL property also contains a few unforested areas. Bare rock is rare within the property area, and where it is found the plant communities consist mostly of lichens, mosses, grasses, and shrubs. Somewhat more common is open shoreline and sand dunes, which are found along the Ottawa River at Point au Baptême. This sand dune vegetation is considered significant in Ontario, and these communities are home to most of the "rare" classified species that are found on site.

2.4.2 Fauna

The CRL property features terrestrial wildlife that is typical for the boreal region in Ontario and includes breeding birds (106 species), mammals (23 species), reptiles (10 species), and amphibians (12 species)[34]. The site hosts one threatened species, the common Musk Turtle (*Sternotherus odoratus*), as well as four species - Wood Turtle (*Glyptemys insculpta*), Red-shouldered hawk (*Buteo lineatus*), Red-headed Woodpecker (*Melanerpes erythrocephalus*), Eastern Wolf (*Canis lycaon*) - that have been designated as of special concern by the Committee on the Status of Endangered Wildlife in Canada.

Chalk River Laboratories also encompasses extensive aquatic habitats, and forty-four species of fish have been encountered on-site and in the adjacent Ottawa River. Two species - Lake Sturgeon (*Acipenser fulvascens*) and Rosyface Shiner (*Nortropis rubellus*) - from the Ottawa River are "of interest" to the Committed on the Status of Endangered Wildlife in Canada. Additionally, Black Bullhead (*Ameiurus melas*), caught in the Perch Lake wetlands[34] have been identified as rare to uncommon on Ontario. Perch Lake has been significantly impacted in recent decades by the introduction of northern pike in the late 1980s[87] which has decimated the local populations of perch, chubs, minnows, and pearl dance. Benthic invertebrates are widespread throughout the site.

Macro-invertebrates found on the CRL site include diving beetles, dragonflies, waterboatmen, giant water bugs, and other nymphs and flies. Several kinds of crustaceans are also present, including four species of aquatic snail, fingernail clams, worms, leeches, and freshwater mussels[38].

2.5 Previous Radioecological Work On-Site

Chalk River Laboratories maintains an environmental science division that has performed exhaustive radioecological research on the site. Over the past sixty years ongoing work has catalogued the concentrations of contaminant radionuclides in many of the flora and fauna.

2.5.1 Aquatic Radionuclide Monitoring

Concentrations of radionuclides in water and sediment are regularly monitored at most of the aquatic sites at CRL, and in some cases have been monitored for decades[86, 38, 60, 19, 81, 62, 47, 27, 41, 6, 48]. Aquatic biota have also been monitored at most of the aquatic sites, and concentration data are available for a limited number of sites[87]; more frequently, concentrations in biota are calculated from models using radionuclide concentrations from nearby water sources[38].

2.5.2 Terrestrial Radionuclide Monitoring

Soil and air concentrations of radionuclides have been monitored in a number of locations at the Chalk River Laboratory site, particularly near the waste management areas[50, 22, 27, 28]. Gamma dose rate contour maps have are also available[50, 48]. A few studies have directly investigated concentrations of radionuclides in NHB but it is easier to locate concentrations for plant tissues,

which are well documented for some areas[22, 48]. Limited large animal data are available from opportunistic harvesting of animal tissues[60, 61]; there are also concentration data available for woodchucks after studies addressed concerns that these mammals were inhabiting, and burrowing in, WMA-F[51]. For the most part, concentrations in fauna have been estimated from computational models based upon soil and plant tissue concentrations[38].

Very little monitoring work, either aquatic or terrestrial, has followed the same site and species over a period of years to establish time-dependent trends in radionuclide concentrations. Indirect indicators are followed through the frequent monitoring of effluent streams, and used to computationally derive concentrations of radionuclides in NHB. Measurements of radionuclide concentrations in plant species have occasionally been repeated, although not expressly for the purpose of monitoring the time-dependence of concentrations[21, 22].

2.5.3 Modeling

Extensive radiation dose modeling has previously been undertaken for each of the contaminated areas at CRL[38]. At aquatic sites, doses to biota were estimated using measured values of concentration and function (e.g., K_D values) for water, sediment, plant and animal tissues (where available) and, where of concern due to contamination of groundwater, effluent or up-gradient surface water. At terrestrial sites - typically the WMAs - data for concentrations in air, soil, and where available, plant and animal tissues were considered.

Table 3 defines those variables that are applicable to the ecosystem model discussed:

Table 3: CRL Ecosystem model definitions

Symbol	Explanation	Symbol	Explanation
$C_{s(fw)}$	concentration in sediment (Bq kg^{-1} FW)	$C_{s(dw)}$	concentration in sediment (Bq kg^{-1}DW)
C_w	concentration in water (Bq L^{-1})	ρ_w	density of water (1 kg L^{-1})
θ	sediment porosity (unit-less)	K_d	distribution coefficient (L kg^{-1})
ρ_s	density of solids (kg L^{-1})	f_{dw}	dry weight fraction of sediment (unit-less)
$C_{s(pw)}$	concentration in soil porewater (Bq L^{-1})	C_a	concentration in air (Bq m^{-3})
RF_{pw}	ratio of HTO in porewater:air (0.3)	H_a	atmospheric absolute humidity (0.0066L m^{-3})
$C_{s(pw)_C}$	concentration of C in soil porewater (1.2 g m^{-3})	C_{a-C}	concentration of C in air (0.2 g m^{-3})
C_{f-C}	concentration of C in fish (121.8 g kg^{-1} FW)	C_{w-C}	concentration of C in water (g L^{-1})
DW_p	dry weight fraction for plant (0.25)	C_{p-C}	concentration of C in plant (125 g kg^{-1} FW)
TF	ingestion rate transfer factor (d kg^{-1})	C_x	concentration in the ingested item (Bq kg^{-1})
I_x	ingestion rate of item x (kg d^{-1})		

Perch Lake data were used to estimate distribution coefficients[86]. The default value of 0.6 was used for soil porosity throughout the site; at Perch Lake this value was changed to 0.7, although soil porosity ranges from 0.5 to 0.9 at this location[86, 48]. The following equations were used to estimate water:sediment partitioning:

$$C_{s(fw)} = \frac{\theta C_w \rho_w + (1-\theta) C_w K_d \rho_s}{\theta \rho_w + (1-\theta)\rho_s} \tag{2.1}$$

$$C_{s(dw)} = \frac{C_s(fw)}{f_{dw}} \tag{2.2}$$

$$f_{dw} = \frac{(1-\theta)\rho_s}{\theta\rho_w + (1-\theta)\rho_s} \tag{2.3}$$

The exchange of airborne particulate radionuclides such as ^{131}I onto the soil column must be accounted for in our model. Partitioning coefficients were estimated using OPG[4]default values for soil accumulation via the atmospheric deposition pathway. According to Hart and McKee[38] "These values are calculated from dry+wet deposition velocities, and losses from soil due to erosion, leaching, radioactive decay and volatilization over a 40-year period". This model assumes a 20cm soil mixing depth.

Partitioning of air and soil for HTO and $^{14}CO_2$ use the following specific activity models:

$$C_{s(pw)-HTO} = \frac{RF_{pw}}{H_a} C_{a-HTO} \tag{2.4}$$

$$C_{s(pw)-14C} = \frac{C_{s(pw)-c}}{C_{a-C}} C_{a-14C} \tag{2.5}$$

$$C_{s(fw)} = \frac{C_{s(pw)}}{f_{pw}} \tag{2.6}$$

$$f_{pw} = \frac{\theta\rho_w}{\theta\rho_w + (1-\theta)\rho_s} \tag{2.7}$$

For ^{14}C, concentration ratio data collected at other swamps on site was assumed to be applicable. Terrestrial plant data not available from the IAEA were estimated according to the method of Travis and Arms[80]. HTO and ^{14}C were assumed to be taken into terrestrial ecosystems principally through the air and were estimated according to the OPG model[4] respectively as:

$$C_{p-HTO} = \frac{1.1(1-DW_p)}{H_a} C_{a-HTO} \tag{2.8}$$

and

$$C_{p-14C} = \frac{C_{p-C}}{C_{a-C}} C_{a-14C} \tag{2.9}$$

Perch Lake data were used to estimate aquatic bioaccumulation factors (BAFs) for key radionuclides (^{90}Sr, ^{60}Co, ^{137}Cs) using measured tissue data in fish, frogs, snails, and aquatic plants[87]. A BAF of unity was assumed for HTO, while an activity model for ^{14}C in fish was used:

$$BAF_{14C} = \frac{C_{f-C}}{C_{w-C}} \tag{2.10}$$

This model has been used in previous literature[4]as a reasonable estimate of the BAF for aquatic biota; for snails the BAF was doubled to account for additional carbon in the shell.
Aquatic BAFs for other nuclides were taken primarily from IAEA publications[2].

Sample et al[29] provide BAFs for particulate radionuclides in terrestrial invertebrates, while estimates for HTO and 14C BAFs in terrestrial invertebrates were calculated by the same means as in plants, above. Transfer factors were estimated allometrically as[51]:

$$TF = aW^{-0.7} \tag{2.11}$$

Where a is an experimental parameter and W is the body mass of the animal in question in kilograms.

Food webs were constructed for each of the benchmark species. An example food web is depicted as Figure 8, after the work of Hart and McKee[38] for the Eastern Wolf. Solid yellow lines show pathways of atmospheric/terrestrial exposure, solid green lines indicate aquatic, and dashed lines indicate a relationship that was omitted from the model.

Figure 8: Eastern wolf food web after Hart and McKee

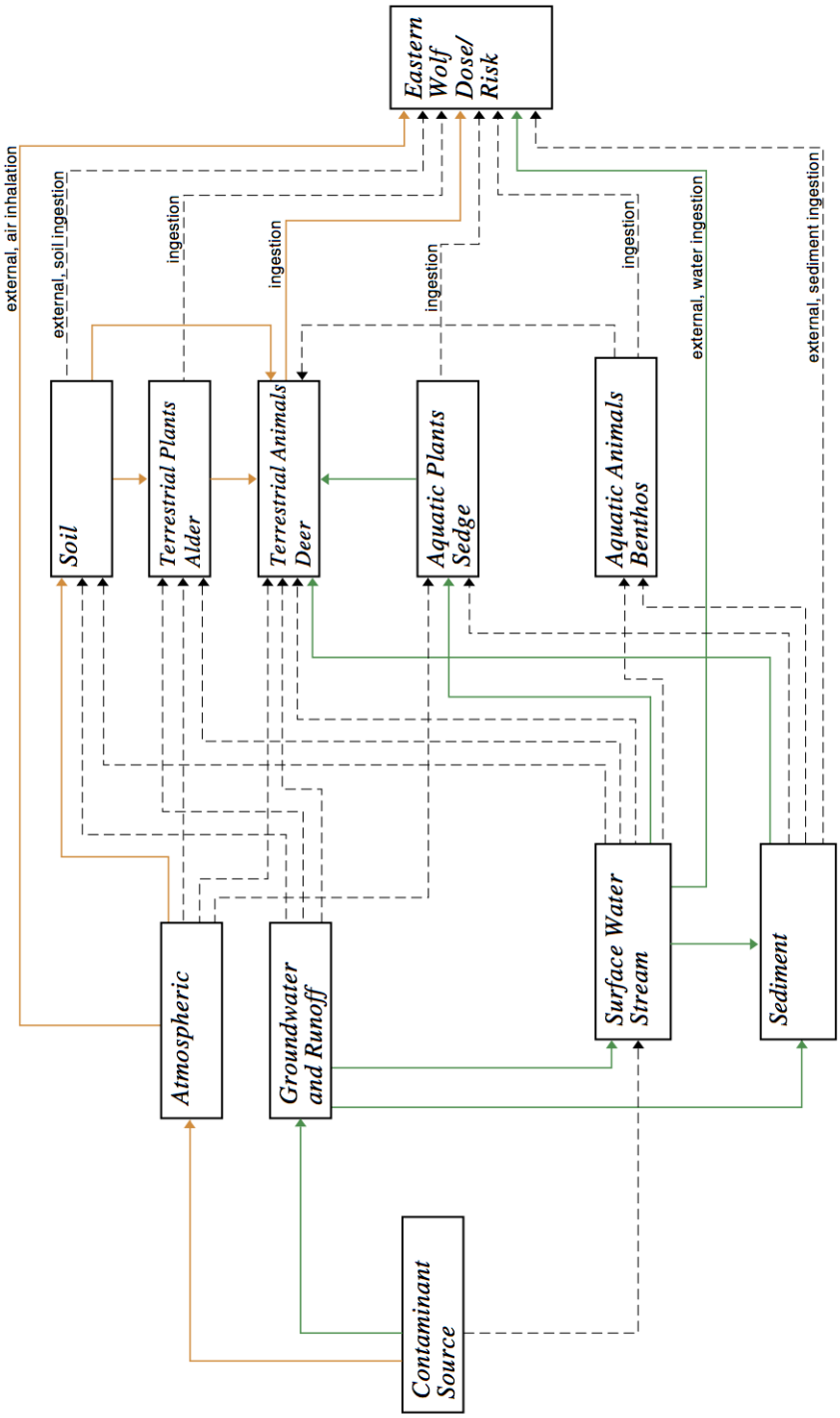

Such models are employed to mathematically estimate the concentrations of radionuclides in an organism of interest as

$$C_t = \sum C_x I_x TF \tag{2.12}$$

which tabulates the total concentration in an organism, by nuclide, according to the concentration in that organism's food sources.

Calculations were performed to translate the concentration information yielded through food web modeling into a radiation dose rate that combined both internal and external components; variables are defined in Table 4.

Table 4: CRL dosimetry model definitions

Symbol	Explanation	Symbol	Explanation
$5.76x10^{-4}$	MeV nt^{-1} to uGy h^{-1} conversion factor	$\bar{E}_x$	average energy per nt for emission x (MeV nt^{-1})
n_x	proportion of transitions producing energy E_x	AF_x	fraction of internally emitted radiation absorbed
C_t	whole body tissue concentration (Bq kg^{-1} FW)		

Concentrations are converted into doses according to the methods of Blaylock et al[12] by summing the total energy emitted from all disintegrations and their short-lived daughters.

$$D_{int} = \left(5.76x10^{-4}\right)\left(\sum E_x n_x AF_x\right) C_t \tag{2.13}$$

$$D_{ext,w} = \left(5.76x10^{-4}\right)\left(\sum E_x n_x \left(1 - AF_x\right)\right) C_w \tag{2.14}$$

$$D_{ext,s} = \left(2.88x10^{-4}\right)\left(\sum E_x n_x \left(1 - AF_x\right)\right) C_s \tag{2.15}$$

This produced the final dose rate estimates reported in Hart and McKee[38].

2.5.4 Effects Monitoring

Limited monitoring has been done at the CRL site to detect any radiation-dose related effects in NHB. Specifically, monitoring has been performed on fish at Perch Lake, measuring growth and the occurrence of parasites, tumors and deformities in Brown Bullhead and Northern Pike[70]. In 2003, Pumpkinseed from Perch Lake were compared to those in Perch Creek and local reference lakes[87]. Neither of these studies demonstrated any adverse effects to biota. Studies have also been conducted to monitor the survival and reproduction of *Chironomus tentans* (Midge Fly) in Ottawa River sediment versus laboratory control sediment. These studies also failed to detect adverse outcomes in the organisms under investigation.

3 Experimental Design

3.1 Description of Species Under Investigation

The Brown Mystery Snail (*Campeloma decisum*) is ubiquitous at the Chalk River site. Of the dozen sites tested for the presence of this species, only those areas most severely stressed by drought condition yielded no individuals. Also present on site in limited number and range are types of Turret Snails (*Valvata*), as well as species of *Physella* and *Helisoma*. Because of their ubiquity and ease of capture, this study focused on *C. decisum*, excluding *Valvata*, *Physella*, and *Helisoma* snails (although the presence of these snails at sampling sites was also noted); photographs of each species are depicted in Figure 9.

Figure 9: Snail species observed at CRL

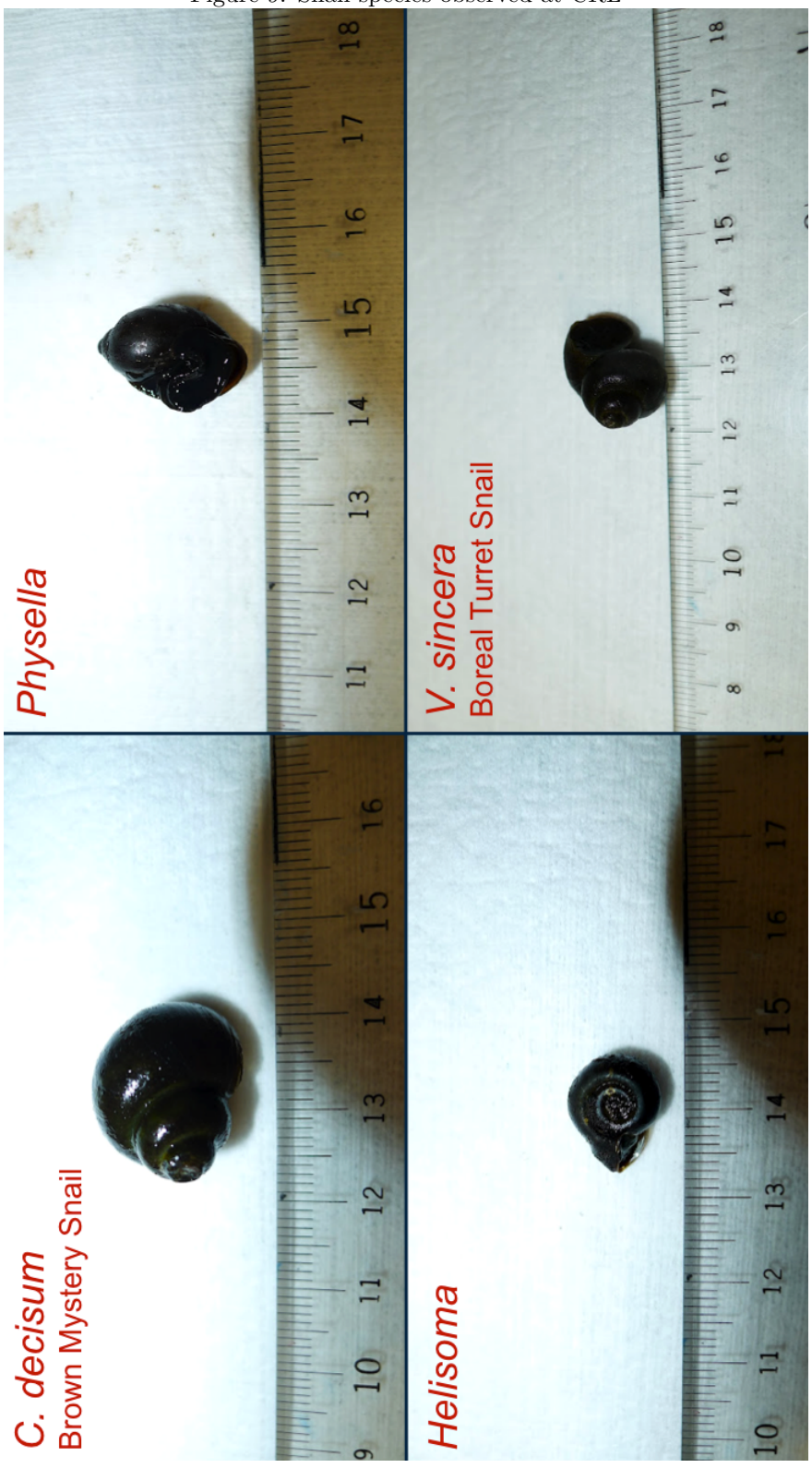

C. decisum is an oviviparous snail widely distributed throughout the freshwater bodies of North America[46]. Bovbjerg[13] has written about the ecological preferences of the species and demonstrated that this snail prefers a soft, muddy substrate and cannot function properly on a bare, hard surface. Additionally, Allison[7] was able to trap snails using fish or cloth packets of dog, cat, chicken, ferret or muskrat dung, concluding that this species is a detritovore. Arthur et al.[46] note that *C. decisum* is an important species in both the fish and diving duck food chains. *C. decisum* survives for multiple years, even in relatively harsh climates, with the maximum age of snails grown in favorable laboratory conditions of about four years[46].

These behavioral characteristics make *C. decisum* a good candidate for radioecological study. The long lifespan means years for radiostrontium to accumulate in each individual's shell, while Allison's method of baiting snails provides an estimate of species activity, an indicator of both population size and health status.

3.2 Drought as a Stressor

Severe drought in Eastern Ontario limited the number of sites available for sampling over the course of this study. Figure 3.2 shows the temperature variation during the summer of 2012 compared to the average; 2012 is clearly well above historic values. Additionally, there was a six week period during the summer that was completely without rain (during the summer months rainfall is typically in excess of 40cm). In the absence of rainfall, the most contaminated areas on site dried out completely, making it impossible to conduct research in these locations. Furthermore, even in those areas that retained some amount of water, it seemed unlikely that any decrease in populations would be due to radiation exposure during a time of such extreme environmental stress. Fortunately, water levels at the five sites chosen for study remained sufficiently high throughout the summer, even if water levels remained below typical levels. As this study was not tracking changes in population between years, the drought of 2012 is considered to have little influence on our outcome.

3.3 Description of Sampled Sites

Initially, collection of snails was attempted at eleven locations on the Chalk River site and one off-site lake. Table 5 is a brief description of each site sampled; a map of sampling locations is included as Figure 10.

Table 5: Sampling locations at CRL. Doses as estimated by Hart and McKee[38].

Location	Description	Status
Toussaint Lake	*Size*: 4ha *Dose Rate (snails,est)*:not estimated Adjacent to Maskinonge drainage.	Included in study.
Upper Bass Lake	*Size*: 6ha *Dose Rate (snails,est)*:not estimated North of Duke Swamp and east of Maskinonge.	Included in study.
Lower Bass Lake	*Size*: 10ha *Dose Rate (snails,est)*:0.66μGy h^{-1} South of Duke Swamp and east of Maskinonge	Included in study.
Maskinonge Lake	*Size*: 160ha *Dose Rate (snails,est)*:0.18μGy h^{-1} Largest lake on site, very rocky basin, very few *C. decisum* present.	Excluded; dominant species *V. sincera*
Nearshore Ottawa River	*Size*: n/a *Dose Rate (snails,est)*:0.40μGy h^{-1} Very deep and very wide; more like a lake but highly variable water level making it difficult to estimate snail populations.	Excluded due to drought.
Perch Lake Inlet	*Size*: n/a *Dose Rate (snails,est)*:53μGy h^{-1} Totally dry in severe drought year.	Excluded due to drought.
Perch Lake	*Size*: 28ha *Dose Rate (snails,est)*:8.8μGy h^{-1} Lake fed by east swamp drainage, many macrophytes, silty basin.	Included in study.
Perch Creek (Perch Lake Outlet)	*Size*: n/a *Dose Rate (snails,est)*:6.9μGy h^{-1} Pools above Perch Creek Weir; ponded environment; weir formed an effective barrier to snails further downstream.	Included in study.
Duke Swamp	*Size*: 5ha *Dose Rate (snails,est)*:0.31μGy h^{-1} Located between bass lakes, fed by ^{90}Sr and T contaminated groundwater discharge (cold water may interfere with snail populations)	Excluded; no snails present.
East Swamp	*Size*: 8ha *Dose Rate (snails,est)*:480μGy h^{-1} Swamp adjacent to waste storage C. Totally dry in severe drought year.	Excluded due to drought.
South Swamp	*Size*: 6ha *Dose Rate (snails,est)*:5500μGy h^{-1} Swamp adjacent to waste storage C. Totally dry in severe drought year.	Excluded due to drought.
Jack's Lake	*Size*: 16ha *Dose Rate (snails,est)*:not estimated Off-site control; snail shells present on site, but lures failed to capture any live snails.	Excluded; no snails present.

Sites were selected to have certain characteristics in common: notably, an absence of water current and a silty bottom. As *C. decisum* is a burrowing snail that cannot survive on a hard substrate, sites with rocky bottoms were not sampled.

3.4 Sample Collection

Samples were collected from several water bodies at Chalk River Laboratories across a gradient of contaminant concentrations. Generally, three types of samples were collected: live snails were collected from a series of baited lures, then sediments and water samples were collected from the areas immediately adjacent to these lures. Thus, each lure location became associated with several types of data: water, sediment, and biotic components were all tied to a single location. Site-selection occurred semi-randomly: lures were placed every 10m as practicable, either in terms of site-access or substrate conducive to snail survival.

Figure 10: Map of locations sampled as a part of this study.
*generated via google maps (http://maps.google.com)

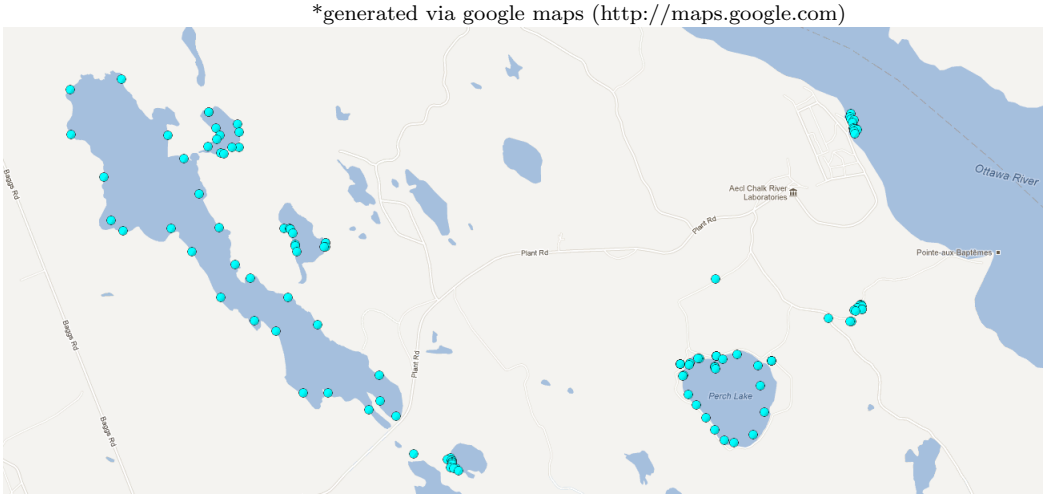

3.4.1 Water

Water samples were collected from an assortment of locations at each sample site. Samples for limnological analysis (e.g., AES for major ions) were collected from each sample point as three

250mL aliquots, then combined in the laboratory,. For ^{90}Sr analysis, 3x1L bottles were collected from each water body.

Certain water characteristics were also measured in situ, these were: temperature (°C, measured with an HM digital COM-100 EC/TDS/TEMP probe), pH (estimated using pH paper), total dissolved solids (ppm, measured with an HM digital COM-100 EC/TDS/TEMP probe), light incident on lure site (lux, measured with a Mastech digital illuminance meter), and electroconductivity (mS or µS, measured with an HM digital COM-100 EC/TDS/TEMP probe).

3.4.2 Snails

Snails were collected using baited lures, according to the method of Allison[7]. In this method, a small amount of dried chicken dung was placed inside a piece of double-layered cheesecloth (Figure 11). The cloth was tied to a stake and partially covered in littoral sediments. After approximately ten days, the lures were collected and snails either adhering to the lure itself or within 0.1m^2 of the lure were collected (Figure 12).

Figure 11: Snail lure ready for placing

Figure 12: Snail lure ten days after placement

Additionally, substrate sampling was performed for three locations (Perch Lake, Maskinonge Lake, and Perch Creek). Substrate samplers consisted of tile, rough side facing out, fastened with epoxy resin to a set area of chicken wire (Figure 13) and placed on the floor of a water body for two months to allow for colonization. Without exception, snails preferred natural substrate to the tile colonizers. We were completely unable to sample population size using this method.

Figure 13: Substrate sampling device

Mark-and-release sampling was attempted at Toussaint and Lower Bass Lakes. No individuals were recaptured, indicating either large snail populations or limited distance traveled per individual. Allison[7] reports marked snail recapture at up to 20 ft distant to the position of release (the greatest distance tested in his study) with no preference for movement up or downstream in moving currents. Lures in this study were placed further apart than Allison's, so it is difficult to determine whether size of snail populations or limited range most influenced snail recapture rate in this study.

3.4.3 Sediments

A minimum of 400g of wet sediment was collected in each location adjacent to a snail lure (while the lure as being retrieved).These samples were placed in plastic, zip-top baggies and frozen for several weeks. At the end of the summer, they were thawed and dried at 60^{o}C for 48h, then shipped back to Oregon State University.

3.4.4 Predation

Crayfish traps baited with dog food were used to sample fish species present in water bodies. Traps were checked daily for one week, and the species found within recorded. This in turn is useful as an

indicator of predation stress on *C. decisum.*

4 Methods

Following is a description of methodology employed as a part of this study. Detailed step-wise protocols follow in Appendix A.

4.1 Sample Preparation

Sample preparation is the process of preparing biological samples for laboratory analysis.

4.1.1 Water

Samples of water sent for atomic emission spectrometry (AES) to quantify major ion concentrations were filtered through a Whatman 0.45 μm cellulose nitrate membrane filter (catalog no. 7184-004) and diluted in plastic centrifuge tubes at a ratio of 1:50 in 1% high purity nitric acid. Samples were then sent for AES.

To analyze the dilute quantities of ^{90}Sr present in water samples, a modified version of Dai's co-precipitation procedure[24] was used. Analysis began with 1L of water collected from the location of interest and stored in a nalgene bottle. The water was acidified to approximately 1% nitric acid shortly after collection to inhibit biologic activity and aid in digestion of any particulate matter. Next, samples were filtered through a Whatman 0.45 μm cellulose nitrate membrane filter (catalog no. 7184-004) to remove any remaining particulate matter.

Under continuous stirring, 10mL of concentrated nitric acid was added to each sample. Then, 2 mL of 40mg Ca^{2+} mL^{-1} calcium nitrate solution, 1mL of Sr standard solution (1mg mL^{-1} in 3% nitric acid) and 1mL of concentrated phosphoric acid are added. Of this, 1 mL is removed and diluted in 50mL of water, then sent for ICP-MS so that recovery of cold Sr can be monitored. Next, the pH is adjusted using concentrated ammonium hydroxide, until the solution is >9. This causes white

calcium [strontium] phosphate precipitate to form.

500mL of this solution is placed into a centrifuge tube and centrifuged at 3500rpm for 3 minutes. The supernatant is decanted and discarded, and an additional aliquot of sample solution is added, followed by another period of centrifugation. Again, the supernatant is discarded, and the final aliquot of sample, plus three rinses of the sample jar, is centrifuged. Again, the supernatant is discarded and deionized water is added to the centrifuge tube; the tube is agitated to wash the precipitate and then centrifuged a final time.

The water is decanted and discarded; additional water is added to the tube so that there are 10mL of water in the tube, then 10mL of concentrated nitric acid is added to dissolve the precipitate. This mixture is transferred to a plastic centrifuge tube to await radiochemical purification.

4.1.2 Sediments

Density fractionation was performed to separate out the mineral and organic components of the sediment matrix. A single cut was made with 2.0 g mL^{-1} sodium polytungstate, according to the procedure outlined in Appendix B.8. The light fraction of the sediment was taken as a proxy for snail nutriment, a reasonable assumption for the detritivorous *C. decisum*. Fractionated samples were digested in nitric acid prior to gross-β counting.

4.1.3 Snails

Snails were frozen individually at the time of collection and thawed at the end of the summer. A wet mass for the whole animal was recorded. After thawing, bodies were mechanically separated from shells and placed in an oven at 60^{o}C for 48h. Dry weights of the shell and body were recorded separately.

8mL of 16M high purity nitric acid was used to digest a shell that had been placed in a plastic centrifuge tube. The samples were allowed to sit overnight in the fume hood. The following morning, 2mL of hydrogen peroxide was added to assist in the digestion of the organic components and the tube is again allowed to sit overnight. Next, 1mL of Sr standard (1mg mL^{-1}in 3% nitric acid) was added, followed by 6mL of 1MΩ distilled, deionized water. 1mL of this solution is diluted in 50mL of 1% high purity nitric acid and sent for ICP-MS. The remainder is used for radiochemical purification.

nb: The ^{90}Sr purification requires that the sample be in 4-8N nitric acid. Because the snail shells are principally calcium carbonate, there was a significant neutralization during the digestion process. The effect of this neutralization on the molarity of the final solution was estimated conservatively by assuming that the mass of the largest shell (3.183g) was entirely calcium carbonate. As equation 3.3 illustrates, even the most extreme change in molarity due to this neutralization still produces a solution that meets the acidity requirements for the subsequent radiochemical purification.

$$3.183\text{g}\mathrm{CaCO_3}\left(\frac{1\text{mol}\mathrm{CaCO_3}}{100.0869\text{g}\mathrm{CaCO_3}}\right)\left(\frac{2\text{mol}\mathrm{HNO_3}}{1\text{mol}\mathrm{CaCO_3}}\right) = 0.06362\text{mol}\mathrm{HNO_3}\text{consumed} \tag{4.1}$$

$$8\frac{\text{mol}}{\text{L}}\left(\frac{1\text{L}}{1000\text{mL}}\right)(15\text{mL}) = 0.12\text{mol}\mathrm{HNO_3}\text{added} \tag{4.2}$$

$$(0.12\text{mol} - 0.06362\text{mol}) = 0.57\text{mol}\mathrm{HNO_3}\left(\frac{1}{15\text{mL}}\right)\left(\frac{1000\text{mL}}{1\text{L}}\right) = 3.8\text{N}\mathrm{HNO_3} \tag{4.3}$$

Dried snail bodies were digested using a Milestone MLS 1200-mega microwave digestion system. Before and between samples, vials used for digestion were washed by microwaving 6 mL of high purity nitric acid at 500W for 10 minutes. The acid wash was discarded and vial components are rinsed twice with 1MΩ distilled, deionized water, which is also discarded.

Samples were massed into the digestion vial. For safety, digestions were limited to 500mg; all samples were sufficiently small to be digested whole. Bodies were digested in 6mL of high purity 67% nitric

acid and 1mL of high purity 30% hydrogen peroxide. The protocol used for digestion was as follows:

Table 6: Microwave digestion protocol

Time (min)	Power (watt)
1	250
1	0
5	250
5	400
5	650

Samples were cooled for 1h before being removed from the microwave and poured into a plastic centrifuge tube. Two rinses with 1mL of 1MΩ distilled, deionized water were added to the digestate. An additional 4mL of 1MΩ distilled, deionized water is added to each tube to adjust the concentration of acid to that required by the radiochemical purification protocol (8N).

4.2 Radiochemistry / ^{90}Sr Purification

Strontium-90 purification was performed by the method of Dai et al[24]; the purification set up is depicted in Figure 14. This method uses Eichrom's Sr-resin in pre-packed cartridges under vacuum pressure to quickly separate ^{90}Sr from its daughter ^{90}Y. Each column is prepared by washing with 10mL of 1MΩ distilled, deionized water at a flow rate of ca. 3mL min^{-1}. Next, 10mL of 8N nitric acid is used to condition the column at a flow rate again ca. 3mL min^{-1}. After the acid has passed through the column, the sample solution is placed on the column and passed through at a flow rate no greater than 1 mL min^{-1}. The sample container is rinsed twice with 3-5mL of 8N nitric acid which is added to the column as the column reservoir drains. After the sample passes through, the column is again washed with 10mL of 8N nitric acid; after this drains the time is noted as the time of separation - this is important for radioactive decay calculations. Finally, the column was eluted with 6mL of 1MΩ distilled, deionized water, passed through no faster than 1 mL min^{-1}. 100µL of the eluate was removed and diluted in 50mL of 1% nitric acid then sent for ICP-MS. To the remaining eluate we added 14mL of Perkin Elmer's Ultima Gold AB liquid scintillation cocktail; this is capped, shaken, and sent for liquid scintillation counting. The acid washes are retained in a plastic centrifuge

tube and sent for gamma spectroscopy.

Figure 14: Photo of ^{90}Sr purification apparatus

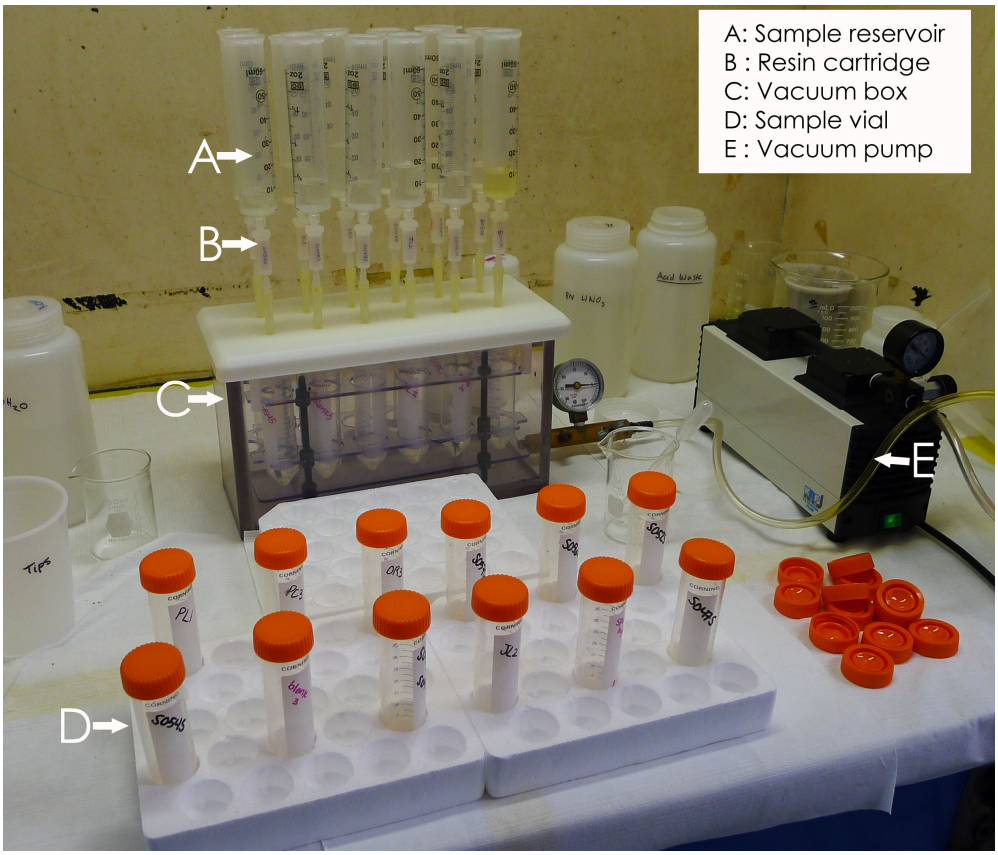

4.3 Sample Analysis

Sample analysis was accomplished through a variety of radiological and chemical techniques. The theory of these techniques is outlined in appendix A; given here is a brief outline of the parameters used for analysis as well as their success and contributions to the final product.

4.3.1 Counting Techniques

The following are radiological counting techniques employed as a part of this dissertation.

Gamma spectroscopy was performed on Oregon State University's High Purity Germanium (HPGe) detector systems. Solid and liquid samples were placed in replicate cups to ensure consistent geometry. All samples were counted for twelve hours. Detector energies were calibrated using a mixed-source standard at a minimum of twice weekly.

Tritium counting was performed for water samples taken from each site by mixing 8mL of filtered sample water with 12mL of Perkin Elmer Ultima Gold XR liquid scintillation cocktail. Each vial was counted for 100 minutes on a Beckman 6500 liquid scintillation counter; analysis was performed using counts from the low-energy (Tritium-specific) window. Each sample was analyzed as two replicates to improve statistical considerations.

Strontium-90 counting at CRL was performed on a Hidex 300SL (super low level liquid scintillation counter). Samples were counted for thirty minutes each immediately after separation, then counted again one week later so that ^{90}Y ingrowth could be used to assess the amount of ^{90}Sr present. Analysis of the β-spectrum for each individual sample informed the decision about the energy window used to assess ^{90}Sr concentrations. This was helpful and necessary as samples counted later in a batch displayed some ^{90}Y ingrowth as visible in the spectrum depicted in Figure 15:

Figure 15: β-spectra for the initial (t=0) count of four samples, distinguished by separate colors.

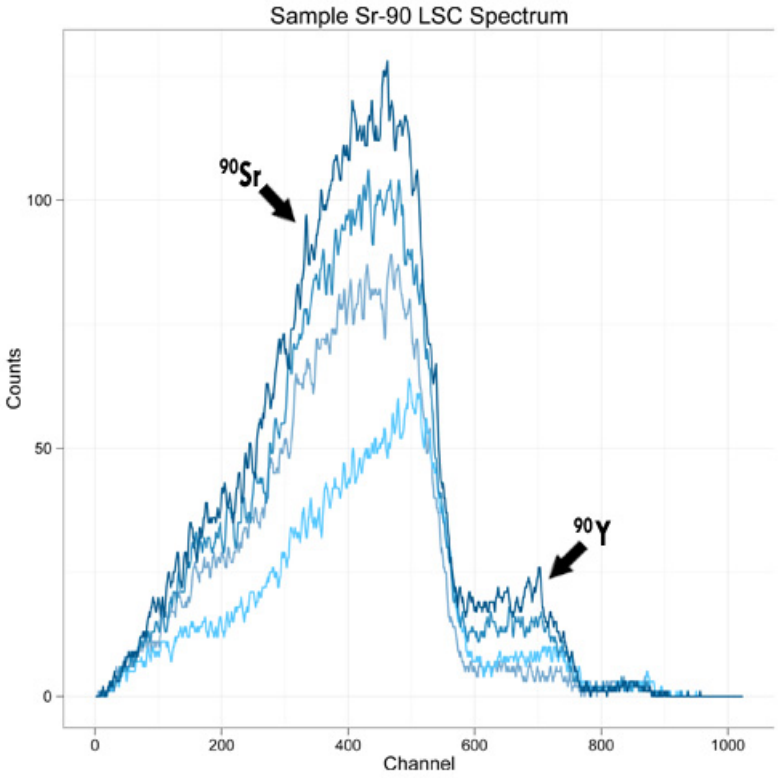

Calculation of MDA Minimum detectable activity (MDA) was calculated according to the Currie equation[49]:

$$N_D = 4.653\sigma_{N_B} + 2.706 \tag{4.4}$$

Where N_D is the minimum detectable number of counts, and σ_{N_D} is the square root of the number of counts registered in the region of interest during a blank count. The Currie equation gives the critical level where no larger than 5% of detected counts are false positives.

Based upon six blank-counts given in Table 13, the average MDA for ^{137}Cs detected via gamma spectroscopy was 0.42 Bq. For ^{60}Co the MDA was 0.46Bq. The average MDA for ^{90}Sr detected via

LSC was 0.09247Bq based upon blank-count data given in Table 14.

4.3.2 Other Analytic Techniques

Following are miscellaneous techniques employed as a part of this dissertation.

Single Photon Emission Computed Tomography (SPECT) SPECT (gamma camera) imaging was performed on the chance that the low-probability gamma rays that result from ^{90}Y's decay (either characteristic or annihilation gammas) would be sufficient the obtain an image of the distribution of radionuclides within the snails' shell. Unfortunately, the concentration of radionuclides within the snail shell was too low for an image to be created using SPECT imaging.

Inductively Coupled Plasma Mass Spectrometry (ICP-MS) Inductively coupled plasma mass spectrometry was used to determine the fraction of cold strontium in samples (both that naturally present and that introduced as a carrier). This in turn was used to monitor the fraction of Sr recovered after the chemical purification step. ICP-MS was also used to determine Ca content in snail shells (since the sample was already being sent for ICP-MS to assess Sr, and it made sense analyze for Ca as well, rather than send a second sample for ICP-AES to observe only Ca). ICP-MS analysis was performed by CRL's analytical chemistry branch.

Inductively Coupled Plasma Atomic Emission Spectrometry (ICP-AES) Inductively coupled plasma atomic emission spectrometry was principally used to assess major ion (Ca, K, Mg, Na, P) concentrations in water samples. ICP-AES analysis was performed by CRL's analytical chemistry branch.

4.4 Derivation of Absorbed Fractions

A voxelized model of the snail was created for the purpose of determining absorbed fractions and

calculating total body dose to the snails from radionuclide concentration data. The was a three-step process, detailed here.

Imaging of Snail

Two snails were imaged utilizing a Toshiba Aquilion 64 slice CT scanner at Oregon State University's College of Veterinary Medicine diagnostic radiology facilities. The images were acquired at 80 kVp and 50mA; a sample slice from one of the tomographic images is Figure 16. The first image consisted of only the snail's shell, while the second was a whole snail (shell + body), preserved for approximately three months in 10% ethyl alcohol. The empty shell was imaged on the chance that the shell would cause too much radiation scatter to effectively image the snail body as well. However, the snail shell with the body intact was easily imaged and so was selected for the creation of the dosimetric phantom.

Figure 16: Sagittal view of the whole snail CT image.

Contouring Volumes and MCNP Input File

Images obtained via medical imaging devices can be translated into a three dimensional model of the original object via a fairly straightforward procedure. 3D Doctor[3], produced by the Able Software Company, is a piece of software intended to assist with the creation of such a three-dimensional

[3]Able Software Corp. 5 Appletree Lane, Lexington MA 02420. http://www. ablesw.com/3d-doctor/index.html

model. Originally developed to aid in the visualization of medical images produced by CT and MRI devices, it contains advanced rendering, processing, and analysis software.
Within 3D Doctor, the user is able to specify (or "segment") regions of interest on each slice of a CT or MRI scan. 3D Doctor then builds the three dimensional structure of each region that has been segmented. Autosegementation based on density of tissues is available; however, it was not reliably able to segment regions of interest for the snail, and thus was not used for this study. After the segmentation has been performed, 3D Doctor can reliably and easily calculate volume parameters such as surface area, distance, and volume, all useful tools for the detailed analysis of medical images.

For the purposes of contouring the snail, we created two regions of interest: the soft body and the hard shell; contouring is depicted in Figure 17. There was insufficient difference in density to distinguish the internal organs of the snail from each other and from the surrounding tissues, and since snail concentration data were only available for the whole body and snail shell, this approximation did not impact the outcome of the dosimetric calculation.

Figure 17: Contouring a snail in 3D Doctor.

For the purposes of the contouring, red represents snail body, the green area the snail shell, and the blue boundary represents an "outside world" volume, to be filled with void space in the MCNP input file.

Figure 18: CT image of snail shell (left) and 3D rendering of snail (right) illustrating body and shell segments.

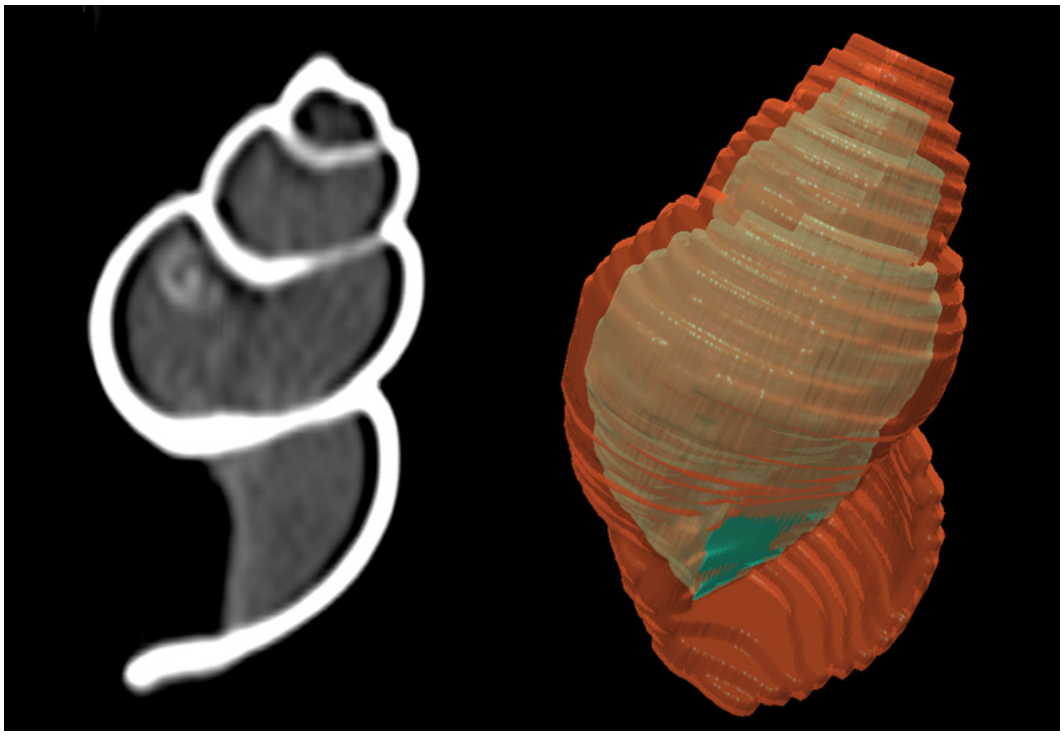

The snail shell slices were rendered into a 3D image (Figure 18) through 3D Doctor's volume rendering feature. Shown above is the body (blue), shell (yellow), and "outside world" (grey cylinder). A short video of the rendering is available on the web[4].

After the creation of the 3D boundary file via 3D Doctor, Voxelizer[5] (Kevin Capello and Erick Cardenas-Mendez of the Human Monitoring Laboratory, Canada)[33] was utilized to create a repeated-structure format image description of the typed used by MCNP. Voxelizer takes input in the form of 3D Doctor objects and correlates them with Monte Carlo universes. It is a user-friendly interface that relies upon Python to output an ASCII file of the geometry under investigation that is understandable to Monte Carlo tools. Voxelizer is free for public use.

[4]Rendering available at: http://youtu.be/mpi8DIR95n4

[5]Human Monitoring Laboratory, National Internal Radiation Assessment Section, Radiation Protection Bureau, 775 Brookfield Road PL6302D, Ottawa, Ontario K1A 1C1, Canada

MCNP

A generic MCNP card was tailored to include the voxelized geometry of the rendered snail. Densities for the shell and body were chosen according to experimentally derived values from field-collected snails. It has been reported[85] that calcium carbonate comprises between 97.0% and 98.8% of dry-weight mass in fresh-water snail shells, suggesting that this is a reasonable approximation of this relatively high effective-Z material. Snail body was composed according to a standard ratio of elements in soft organic tissues: $C_{14}H_{62}O_{21}N_1$ with smaller amounts of the macro and micronutrients P, S, Na, K, Cl, Mg, Si, Fe, and Zn. The density of this material was adjusted to mimic the fresh-weight density of captured snail tissues.

Three source geometries were modeled: sources were located in the snail shell, in the snail body, and in the outside world. 500,000,000 particles were run for photon simulations and 10,000,000 for electron simulations. An order of magnitude more particles were run for sources located in the outside world. Despite this, coefficients of variance remained between 50 and 1000% for the outside word source, and so absorbed fraction data have not been reported for an external source. Large numbers of particles were necessary as many of the sources modeled were effectively penetrating radiations due to the small size of *C. decisum*; source size was also constrained by available computing time. The *f8 (average energy deposited per particle, in MeV)[78, 71] tally was utilized to calculate absorbed fractions for the snail shell and body.

4.5 Dosimetry

The ICRP[43] utilizes nuclide-specific dose conversion factors as a convenient way to determine dose rate from tissue concentration. First, dose rate is calculated as:

$$\dot{D} = C \times Y \times B_r \times E \times AF \times e \times t \tag{4.5}$$

Where variables are defined and have units as given in Table 7:

Table 7: Explanation of variables used in dosimetry.

Symbol	Explanation	Symbol	Explanation
$\dot{D}$	Dose rate $[\frac{\mu Gy}{d}]$	E	Decay energy [keV]
C	Concentration of radionuclide $[\frac{Bq}{kg}]$	AF	Absorbed fraction[6] [unitless]
Y	Nuclear yield [unitless]	e	Conversion keV→μJ $[1.602 \times 10^{-10} \frac{\mu J}{keV}]$
B_r	Branching ratio [unitless]	t	Conversion sec→d $[86400 \frac{sec}{d}]$

[1]Absorbed fractions were generated per the procedure in section 4.5 and are presented in section 5.4.

Data on energy, branching ratio, and yield were taken from the Chart of Nuclides. Absorbed fractions were calculated using the MCNP protocol described above. The nuclides under investigation as a part of this study (^{90}Y, ^{90}Sr, ^{3}H) all decay by the emission of a beta particle. Since beta decay is a three-body process (the daughter nuclide, beta particle, and anti-neutrino all retain a portion of the available decay energy), the energy of the beta particle exists on a spectrum. A good rule of thumb for the average energy of a spectrum of beta particles is that $\mathsf{E}_\beta^{\mathsf{avg}} = \frac{1}{3}\mathsf{E}_\beta^{\mathsf{max}}$. It was not possible to experimentally derive the average beta energy due to a lack of channel-to-energy calibration for the Hidex liquid scintillation counter used for this experiment. Additionally, it was not possible to efficiency-correct the energy spectrum, leading to fewer counts observed at lower channels. While this did not interfere with determination of ^{90}Sr activity for those samples counted using a known standard, it prevented the derivation of activity from a spectrum alone. This is can be demonstrated by looking at the spectrum in Figure 19. Here it is clear that the average beta energy predicted by theory (in channel 196) is far lower than the average energy calculated from the spectrum (in channel 375). This type of skewing may arise due to the any or several of processes that produce spectral shift, including the energy dependence of efficiency, color quench, and chemical quench.

Figure 19: LSC spectra of ^{90}Sr in four samples. Vertical lines indicate the theoretical (blue) and observed (green) average particle energy.

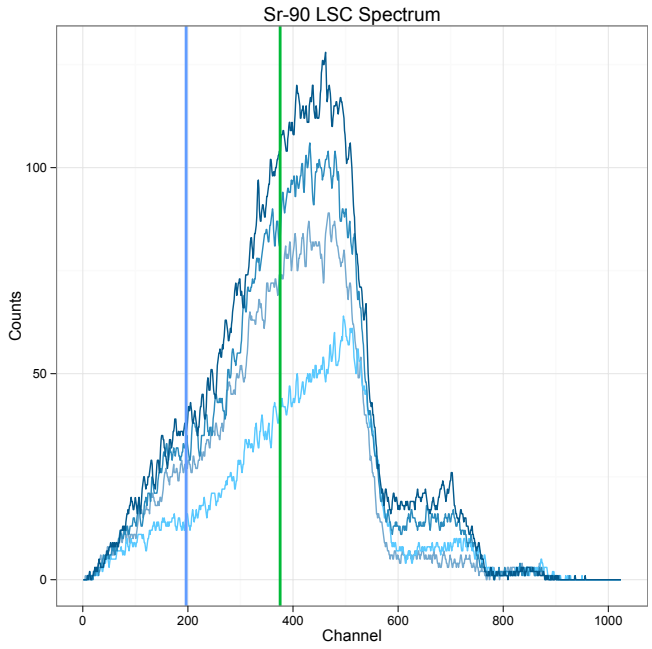

Dose rate, when normalized to a nuclide concentration of 1 Bq kg^{-1}, is what ICRP[43] refers to as a dose-conversion factor (DCF). ICRP utilizes DCFs to quickly estimate total dose rate to a target from one or more sources based upon tissue concentrations of radionuclides. Because no tissue weighting factors exist for snails, dose rates were estimated separately for shell and body. Calculations (excluding external dose rate) were made according to the following summations:

$$D_B = C_{T,B}DCF_{T,B\quad B} + C_{T,S}\dot{D}CF_{T,B\quad S} + C_{Sr,B}DCF_{Sr,B\quad B} \tag{4.6}$$

$$+C_{Sr,S}DCF_{Sr,B\quad S} + C_{Y,B}DCF_{Y,B\quad B} + C_{Y,S}DCF_{Y,B\quad S}$$

$$D_S = C_{T,S}DCF_{T,S\quad S} + C_{T,B}\dot{D}CF_{T,S\quad B} + C_{Sr,B}DCF_{Sr,S\quad B} \tag{4.7}$$

$$+C_{Sr,S}DCF_{Sr,S\quad S} + C_{Y,B}DCF_{Y,S\quad B} + C_{Y,S}DCF_{Y,S\quad S}$$

With variables defined as in Table 8:

Table 8: Explanation of variables used in dosimetry.

Symbol	Explanation	Symbol	Explanation
$\dot{D}_S$ $\dot{D}_B$	Dose rate to shell and body, respectively	$DCF_{T,W\ X}$, $DCF_{Y,W\ X}$ $DCF_{Sr,W\ X}$	Dose conversion factor for T, Y, and Sr from tissue X to tissue W.
$C_{T,X}$, $C_{Y,X}$ $C_{Sr,X}$	Concentration of T, Y and Sr in tissue X	$DCF_{X,B\ B}$ $DCF_{X,S\ S}$ $DCF_{X,B\ S}$ $DCF_{X,S\ B}$	Dose conversion factors for isotope X, body to body, shell to shell, shell to body, and body to shell.
$C_{X,B}$ $C_{X,S}$	Concentration of radionuclide X in body or shell		

Dose conversion factors for nuclide-specific source:target configurations are presented in chapter 5.

5 Data

This chapter presents average values of data obtained as a part of this study in tabular form. Where applicable, all data available have been reported graphically to illustrate the distribution of values.

5.1 Limnological Data

Several analysis were performed on lake waters, measured both *in situ* and in the laboratory. Table 9 tabulates this data, while Figures 20-23 depict it graphically.

5.1.1 Cation analysis by mass spectrometry

Table 9: Major ion concentrations as determined by ICP-AES

Location	$[\bar{Ca}]$ mg L^{-1}	2σ	$[\bar{K}]$ mg L^{-1}	2σ	$[\bar{Mg}]$ mg L^{-1}	2σ
Upper Bass	5.8	0.2	0.78	0.08	2.4	0.07
Lower Bass	6.1	0.2	1.0	0.08	2.3	0.06
Perch Creek	12.6	0.3	1.4	0.08	4.5	0.1
Perch Lake	10.9	0.3	1.5	0.08	3.5	0.1
Toussaint	6.1	0.2	0.82	0.08	2.4	0.06
Ottawa River	13.9	0.40	1.1	0.08	3.3	0.1
Duke Swamp	12.1	0.7	1.69	0.2	3.7	0.2
Location	$[\bar{Na}]$ mg L^{-1}	2σ	$[\bar{P}]$ mg L^{-1}	2σ	$[\bar{Sr}]$ µg L^{-1}	2σ
Upper Bass	1.8	0.05	<0.07	-	1.31	0.08
Lower Bass	9.5	0.3	<0.07	-	1.50	0.08
Perch Creek	5.0	0.1	<0.07	-	1.61	0.07
Perch Lake	11.1	0.3	<0.07	-	1.29	0.06
Toussaint	2.2	0.06	<0.07	-	1.15	0.06
Ottawa River	15.9	0.7	0.29	0.7	3.54	0.2
Duke Swamp	24.4	1.5	0.08	0.1	-	-

Figure 20: Water calcium as measured by mass spectrometry.

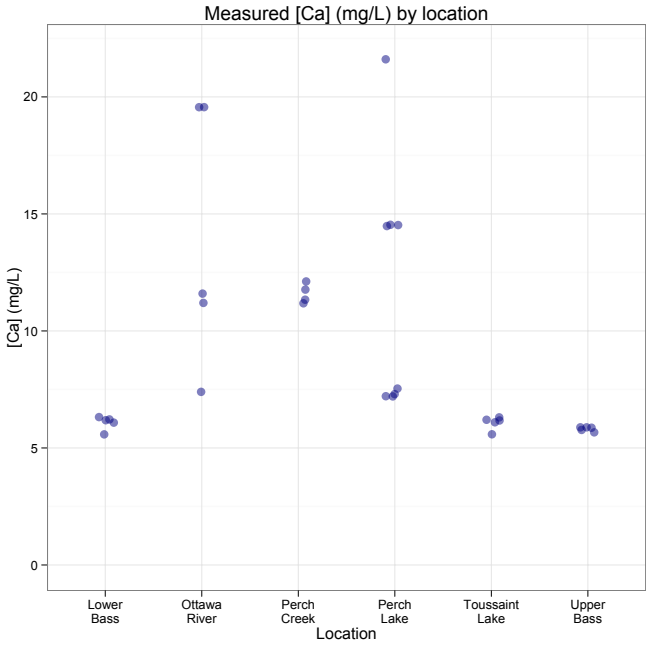

Figure 21: Water potassium as measured by mass spectrometry.

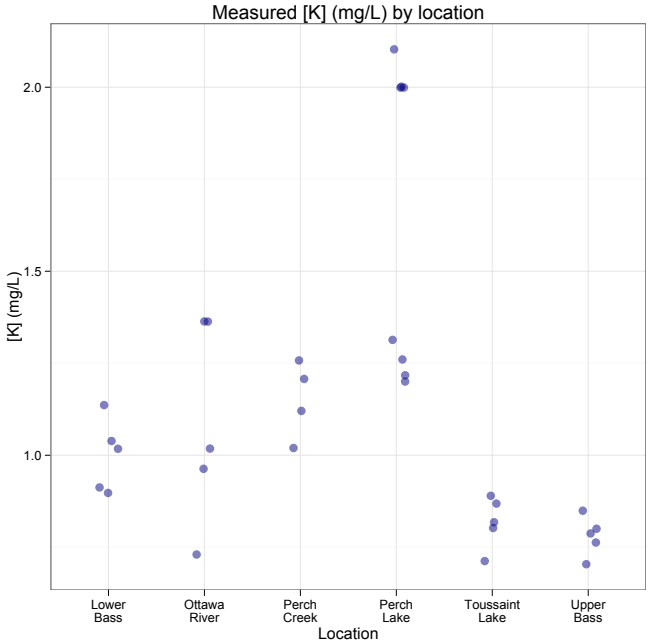

Figure 22: Water magnesium as measured by mass spectrometry.

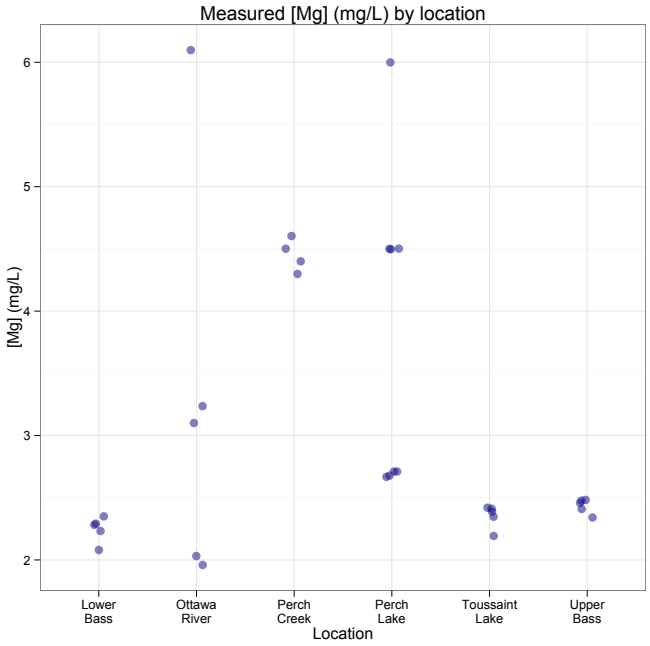

Figure 23: Water sodium as measured by mass spectrometry.

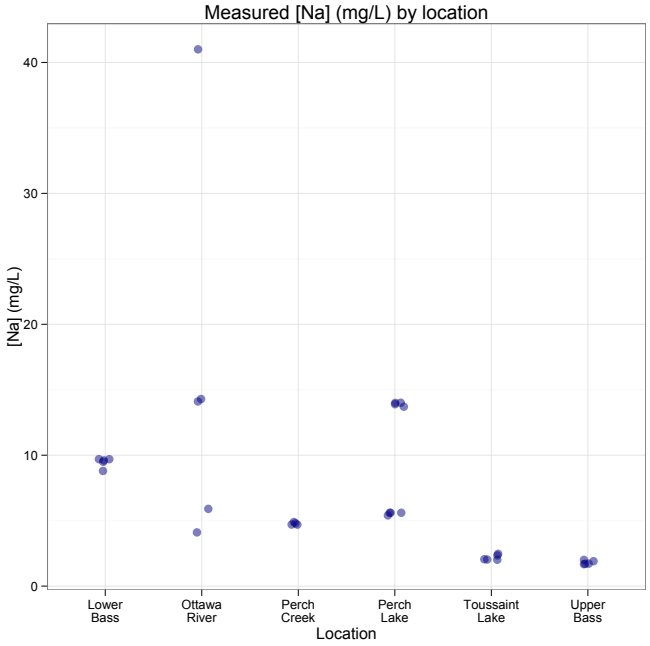

5.1.2 *In situ* measured variables

Certain environmental variables were measured *in situ*. These are tabulated in Table 10 and depicted graphically in Figures 24-28.

Table 10: Limnological characteristics measured *in situ*.

Location	Water Temp ºC	pH	TDS ppm	light lux	EC µS
Upper Bass	21.8	6.4	29.7	45640	59
Lower Bass	25.3	6.4	53.3	45370	105
Perch Creek	22.0	7.2	67.1	32015	131
Perch Lake	25.2	7.0	78.9	55330	154
Toussaint	23.6	6.8	30.5	23430	61
Ottawa River	22.9	7.0	257	39733	520

Figure 24: Distribution of electroconductivities measured, sorted by location.

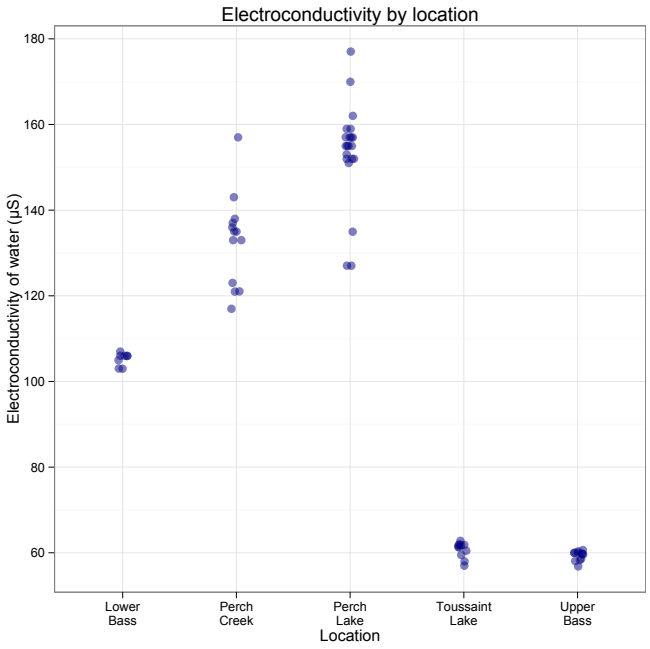

Figure 25: Distribution of pH measured, sorted by location.

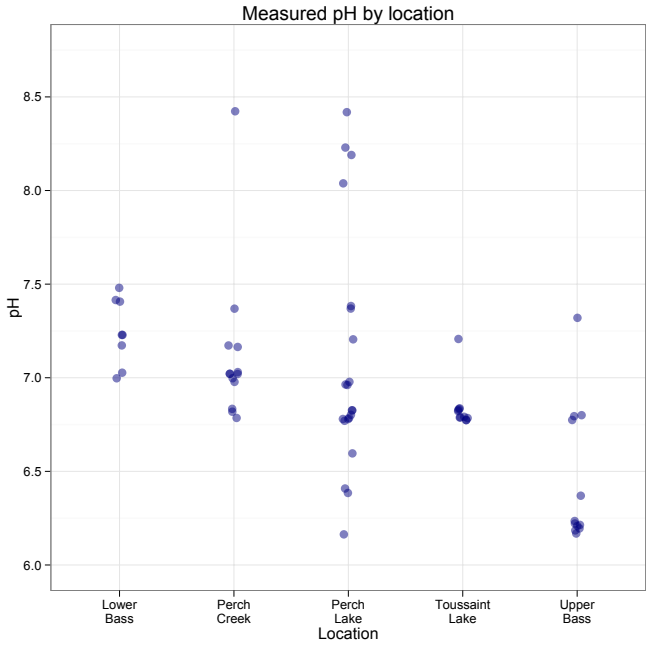

Figure 26: Distribution of total dissolved solids measured, sorted by location.

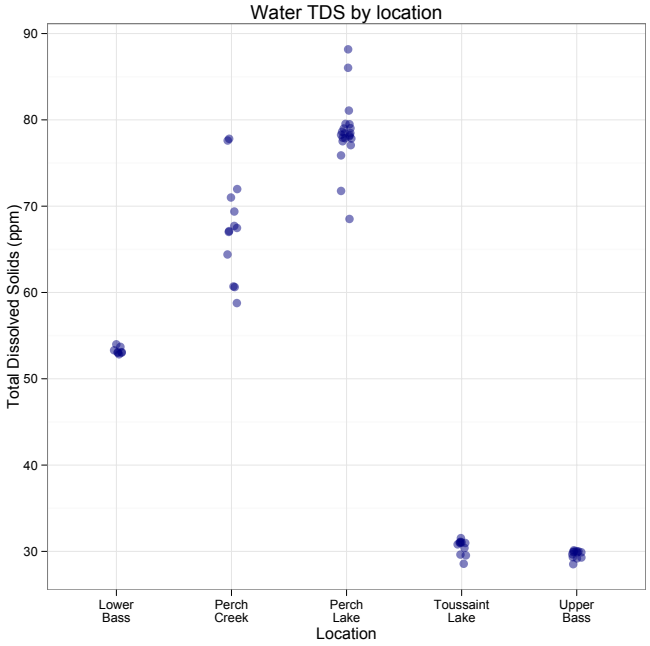

Figure 27: Distribution of water temperature measured, sorted by location.

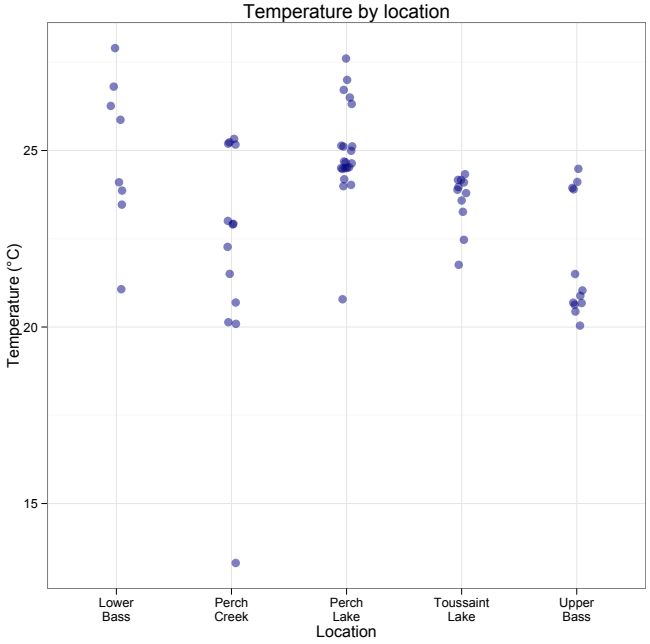

Figure 28: Distribution of incident light (at surface) on snail lure measured, sorted by location.

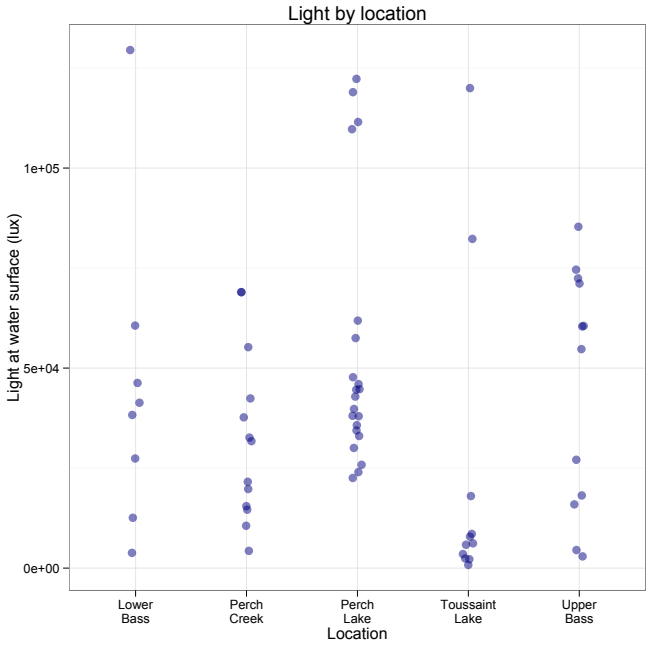

5.2 Snail Data

Similarly to water data, snails were measured *in situ* and then removed to the laboratory for further analysis; these are tabulated in Table 11 and depicted graphically as Figures 29-32.

5.2.1 Biological data

Table 11: Snails collected from CRL water bodies

Location	# Lures Placed	# Snails Collected	Median Mass (mg)	Median length (mm)	# 'active' lures	# of luring periods
Upper Bass	12	29	1467	19.73	3	2
Lower Bass	11	23	1166	18.13	4	2
Perch Creek	13	48	2206	22.68	8	2
Perch Lake	20	21	1142	16.61	6	2
Toussaint	11	92	1117	18.09	8	2

Figure 29: Distribution snail lengths, sorted by location.

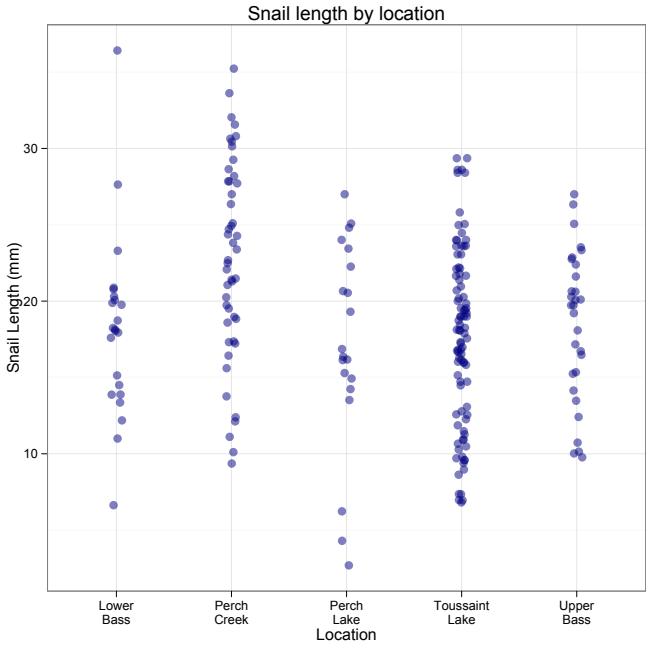

Figure 30: Distribution of snail mass, sorted by location.

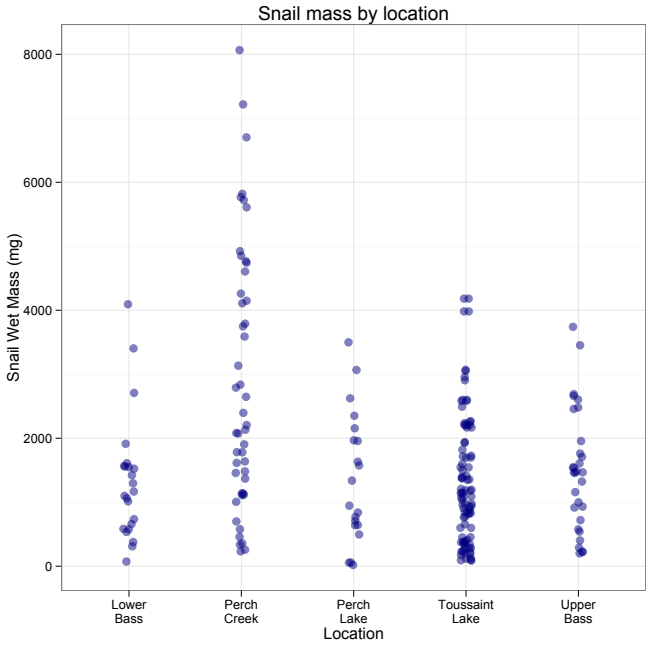

Figure 31: Relationship between snail mass and length, coded by location.

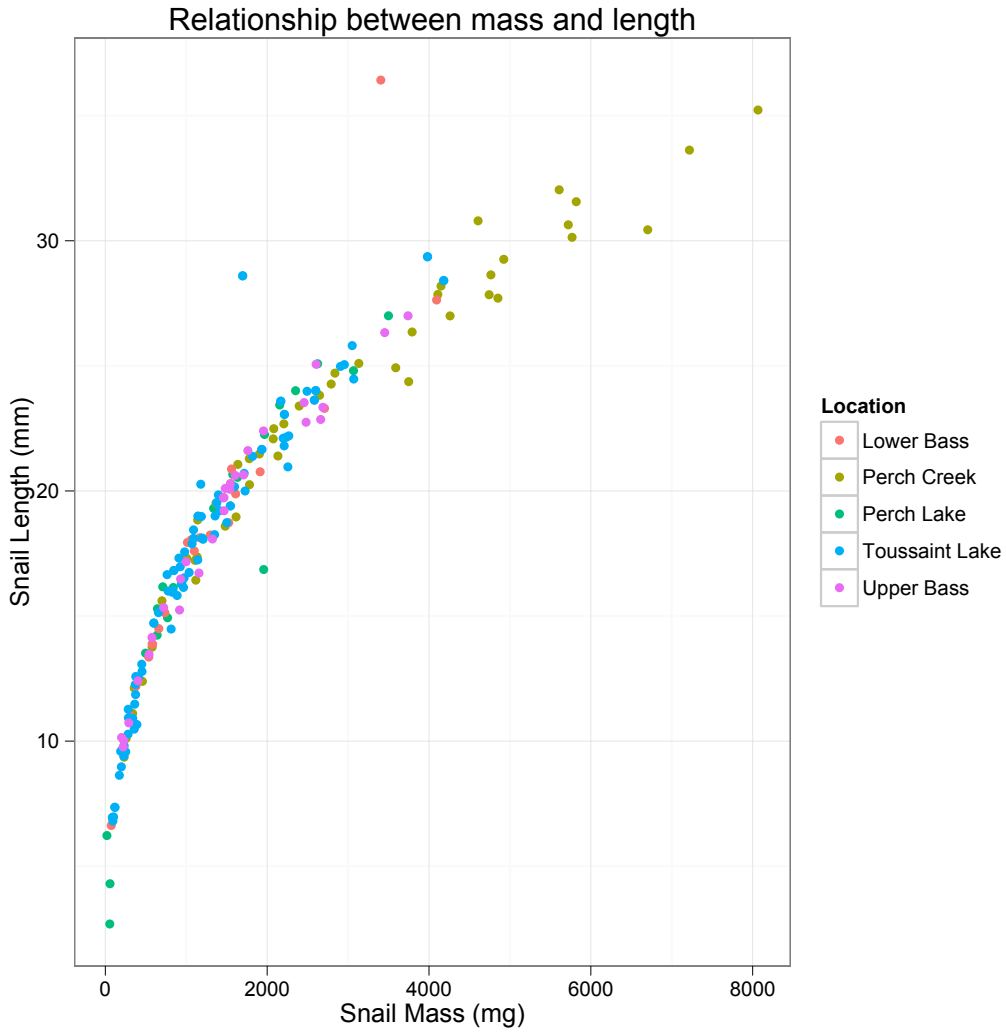

Figure 32: Fraction of wet mass that is snail shell, coded by location.

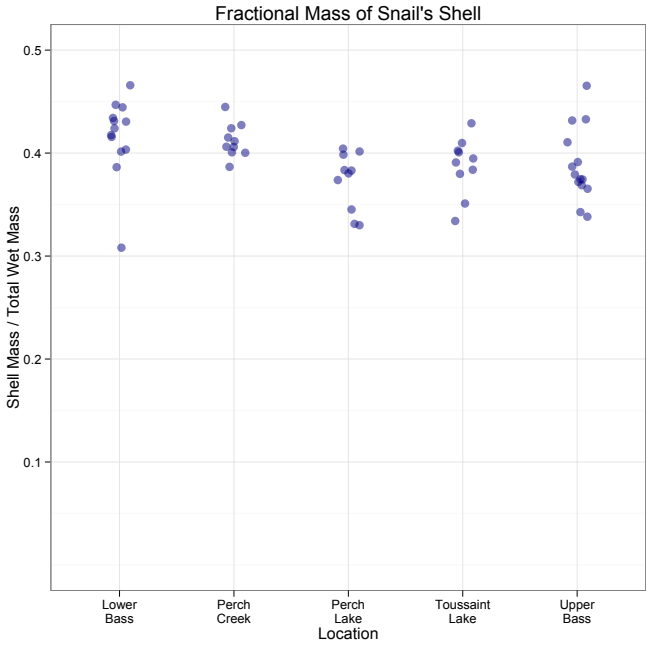

5.2.2 Cation analysis of snails by mass spectrometry

Concentrations of certain macronutrients were measured by mass spectrometry. These are tabulated in Tables 12 and 13 and depicted graphically as Figures 33-38.

Table 12: Average cation content of snail shell.

Location	$[\bar{Ca}]$ mg L^{-1}	2σ	$[\bar{K}]$ mg L^{-1}	2σ	$[\bar{Mg}]$ mg L^{-1}	2σ
Upper Bass	407.8	25.6	0.3	0.4	0.07	0.01
Lower Bass	881.2	52.3	0.6	0.8	0.10	0.01
Perch Creek	289.3	17.4	0.5	0.6	0.07	0.01
Perch Lake	299.8	19.1	0.5	0.6	0.08	0.01
Toussaint	385.3	23.7	0.3	0.3	0.08	0.01

Location	$[\bar{Na}]$ mg L^{-1}	2σ	$[\bar{P}]$ mg L^{-1}	2σ	$[\bar{Sr}]$ mg L^{-1}	2σ
Upper Bass	1.4	0.1	2.5	0.3	2.4	0.1
Lower Bass	2.9	0.2	8.0	0.6	4.9	0.3
Perch Creek	1.3	0.1	6.3	0.5	3.7	0.2
Perch Lake	1.3	0.1	6.9	0.5	3.2	0.2
Toussaint	1.3	0.1	1.1	0.2	2.5	0.1

Figure 33: Snail shell calcium as measured by mass spectrometry

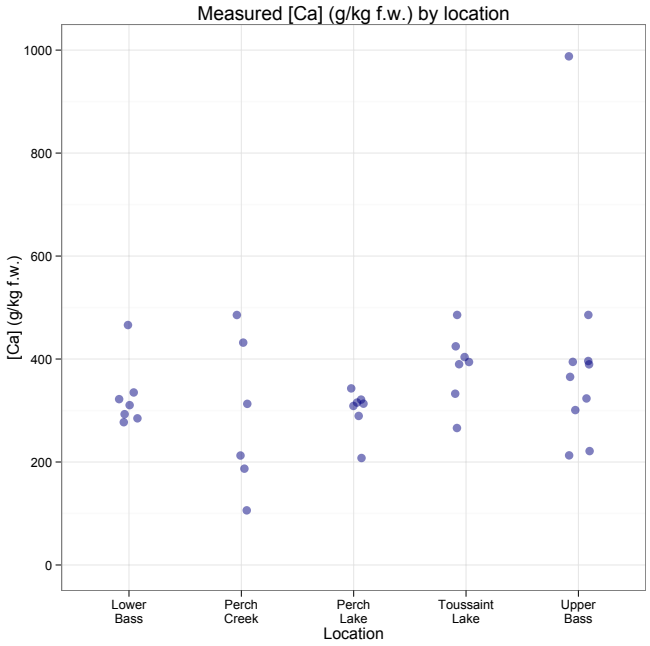

Figure 34: Snail shell potassium as measured by mass spectrometry

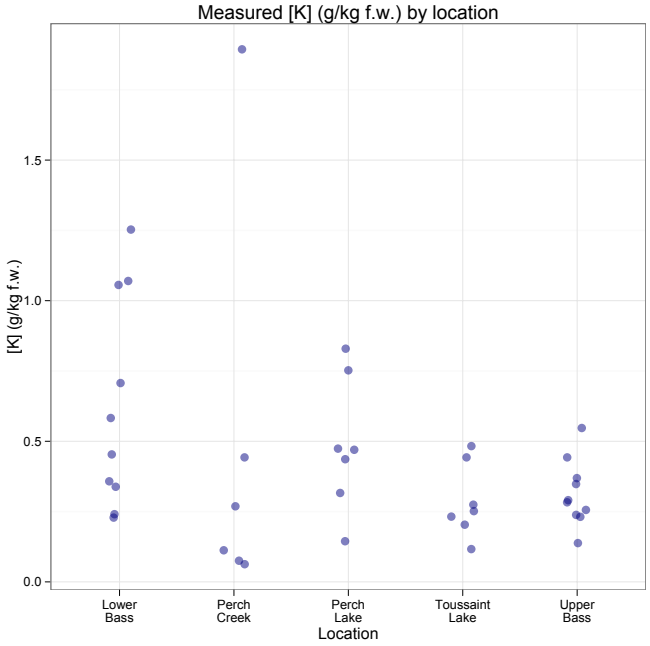

Figure 35: Snail shell magnesium as measured by mass spectrometry

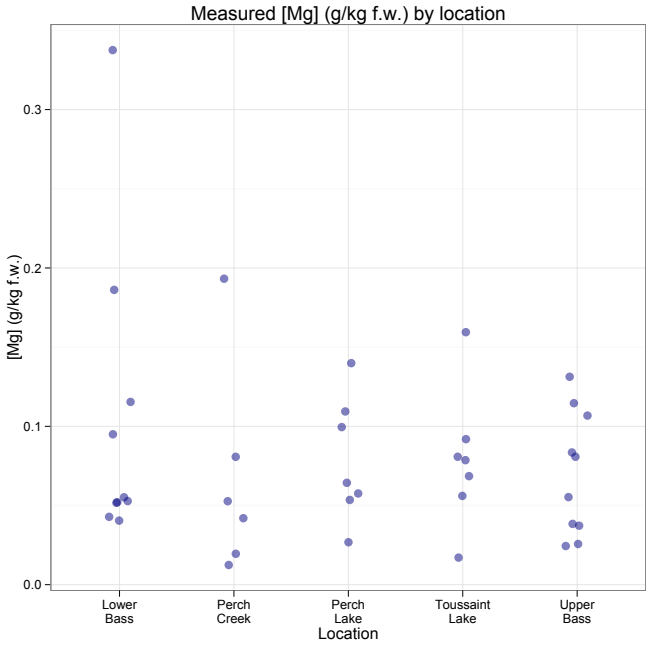

Figure 36: Snail shell sodium as measured by mass spectrometry

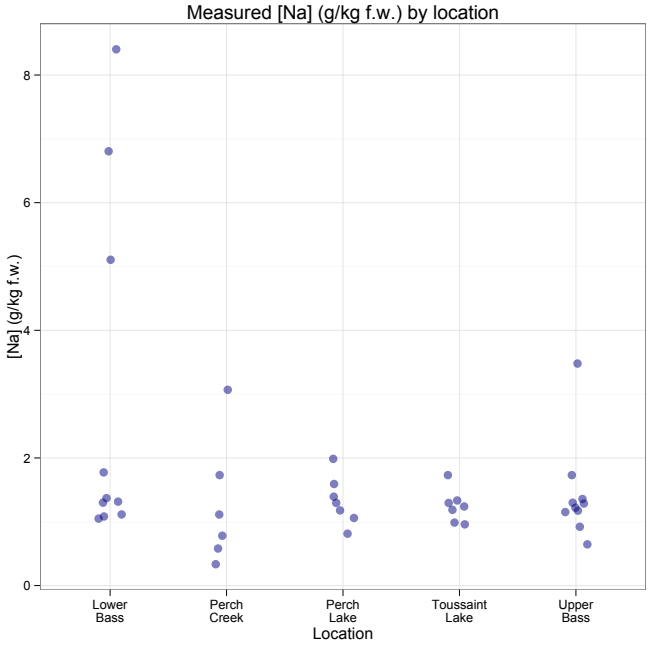

Figure 37: Snail shell phosphorus as measured by mass spectrometry

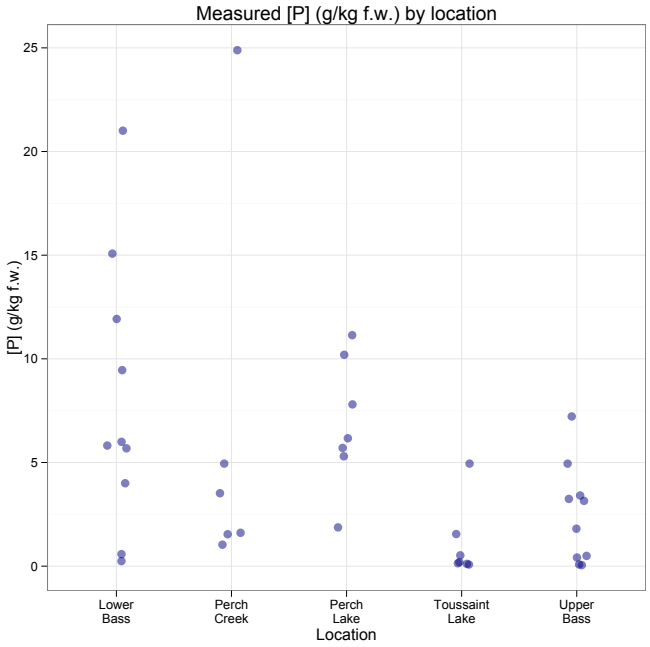

Figure 38: Snail shell strontium as measured by mass spectrometry

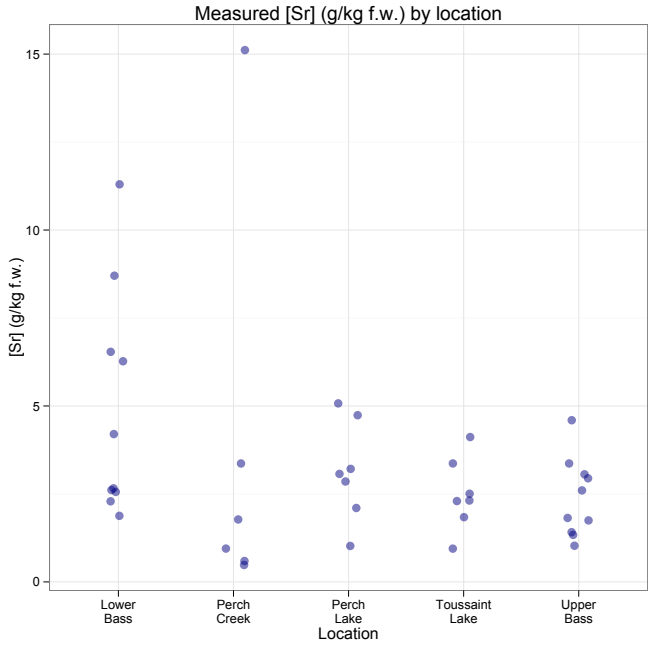

Table 13: Average cation content of snail body.

Location	$[\bar{Ca}]$ g kg^{-1} f.w.	2σ	$[\bar{K}]$ g kg^{-1} f.w.	2σ	$[\bar{Mg}]$ g kg^{-1} f.w.	2σ
Upper Bass	55.1	3.3	3.2	0.9	4.8	0.3
Lower Bass	99.4	6.0	5.7	1.2	99.1	0.6
Perch Creek	63.2	3.5	4.4	0.4	6.5	0.4
Perch Lake	200.0	12.1	5.3	1.2	12.4	0.7
Toussaint	61.6	3.6	4.7	1.0	8.9	0.5

Location	$[\bar{Na}]$ g kg^{-1} f.w.	2σ	$[\bar{P}]$ g kg^{-1} f.w.	2σ	$[\bar{Sr}]$ g kg^{-1} f.w.	2σ
Upper Bass	33.3	2.2	8.1	0.7	6.9	0.3
Lower Bass	74.4	4.9	10.9	0.9	10.7	0.5
Perch Creek	43.0	2.9	7.6	0.5	3.3	0.2
Perch Lake	90.0	5.5	10.3	1.0	9.8	0.5
Toussaint	61.0	3.8	10.8	0.9	7.8	0.4

5.3 Radiological Data

Radiological analysis was conducted both at CRL and at OSU. Minimum detectable activities are presented below in Tables 14-16. Beta emitters are tabulated in Tables 17-21, and concentrations of ^{90}Sr are graphically presented in Table 39. Tables 22-29 present concentrations of gamma emitters in environmental samples.

5.3.1 Generalized minimum detectable activity information

Table 14: Blank sample data from gamma spectroscopy.

*MDC will vary with digested sediment mass, thus only MDA is presented.

Nuclide	Counts	MDA* (Bq)
^{137}Cs	10	0.42
	8	0.39
	9	0.40
	5	0.24
	15	0.52
	11	0.44
MEAN		0.42

Nuclide	Counts	MDA*(Bq)
^{60}Co	2	0.43
	4	0.47
	3	0.44
	3	0.44
	2	0.43
	3	0.44
MEAN		0.46

Table 15: Blank sample data from liquid scintillation counting performed at CRL.

Nuclide	Counts	MDA (Bq)
^{90}Sr	1105	0.087
	1321	0.095
	1250	0.092
	1266	0.094
	1168	0.090
	1329	0.096
MEAN		0.092

Table 16: Blank sample data from ^{90}Sr liquid scintillation counting performed at OSU.

Nuclide	Cpm	MDA (Bq)
^{90}Sr	8	0.04
	10	0.046
	10	0.046
	11	0.048
	8	0.04
	11	0.48
	10	0.046
MEAN		0.046

5.3.2 Beta emitters

Table 17: Tritium concentrations in water.

Location	Avg. Concentration (Bq L^{-1})	2σ (Bq L^{-1})	MDC (Bq L^{-1})
Upper Bass	57	4	14
Lower Bass	568	7	11
Perch Creek	3209	14	11
Perch Lake	1364	10	11
Toussaint	131	4	12
South Swamp	936	12	14
Ottawa River	1730	12	11

Table 18: Strontium-90 concentrations in water.

Location	Avg. Concentration (Bq L^{-1})	2σ (Bq L^{-1})	MDC (Bq L^{-1})
Upper Bass	<MDA	0.06	0.09
Lower Bass	1.04	0.09	0.09
Perch Creek	1.16	0.09	0.09
Perch Lake	7.45	0.2	0.09
Toussaint	<MDA	0.06	0.09

Table 19: Strontium-90 concentrations in snail shells.

Location	Avg. Concentration (Bq kg^{-1}f.w.)	2σ (Bq kg^{-1}f.w.)	MDA* (Bq)
Upper Bass	24	99	0.09
Lower Bass	16760	418	0.09
Perch Creek	28350	522	0.09
Perch Lake	59940	950	0.09
Toussaint	18380	335	0.09

*MDC will vary with snail shell mass, thus only MDA is presented.

Figure 39: Strontium-90 concentrations in snail shells ordered by location.

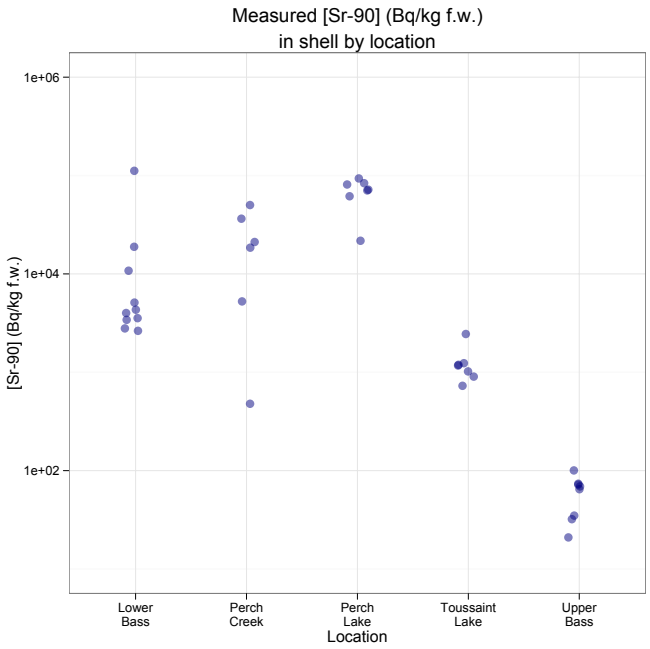

Table 20: Strontium-90 concentrations in snail bodies.

Location	Median. Concentration (Bq kg^{-1}f.w.)	2σ (Bq kg^{-1}f.w.)	MDA* (Bq)
Upper Bass	421	303	0.09
Lower Bass	1160	482	0.09
Perch Creek	4415	337	0.09
Perch Lake	14,440	541	0.09
Toussaint	226	399	0.09

*MDC will vary with snail body mass, thus only MDA is presented.

Table 21: Gross beta concentrations in sediment samples.

Location	Avg. Concentration (organic fraction) (Bq kg $d.w.^{-1}$)	Avg. Concentration (mineral fraction) (Bq kg $d.w.^{-1}$)	MDA* (Bq)
Upper Bass	<MDA	<MDA	0.046
Lower Bass	<MDA	<MDA	0.046
Perch Creek	<MDA	<MDA	0.046
Perch Lake	<MDA	<MDA	0.046
Toussaint	<MDA	<MDA	0.046
East Swamp	<MDA	180	0.046
Ottawa River	<MDA	<MDA	0.046

*MDC will vary with digested fraction of mass, thus only MDA is presented.

5.3.3 Gamma emitters

Table 22: ^{137}Cs concentrations in water.

Location	Avg. Concentration (Bq L^{-1})	MDC (Bq L^{-1})
Upper Bass	<MDC	0.42
Lower Bass	<MDC	0.42
Perch Creek	<MDC	0.42
Perch Lake	<MDC	0.42
Toussaint	<MDC	0.42

Table 23: ^{60}Co concentrations in water.

Location	Avg. Concentration (Bq L^{-1})	MDC (Bq L^{-1})
Upper Bass	<MDC	0.46
Lower Bass	<MDC	0.46
Perch Creek	<MDC	0.46
Perch Lake	<MDC	0.46
Toussaint	<MDC	0.46

Table 24: Cobalt-60 concentrations in snail shells.

Location	Avg. Concentration (Bq kg^{-1}f.w.)	MDA* (Bq)
Upper Bass	<MDA	0.46
Lower Bass	<MDA	0.46
Perch Creek	<MDA	0.46
Perch Lake	<MDA	0.46
Toussaint	<MDA	0.46

*MDC will vary with snail shell mass, thus only MDA is presented.

Table 25: Cesium-137 concentrations in snail shells.

Location	Avg. Concentration (Bq kg^{-1}f.w.)	MDA* (Bq)
Upper Bass	<MDA	0.42
Lower Bass	<MDA	0.42
Perch Creek	<MDA	0.42
Perch Lake	<MDA	0.42
Toussaint	<MDA	0.42

*MDC will vary with snail shell mass, thus only MDA is presented.

Table 26: Cobalt-60 concentrations in snail bodies.

Location	Avg. Concentration (Bq kg^{-1}f.w.)	MDA* (Bq)
Upper Bass	<MDA	0.46
Lower Bass	<MDA	0.46
Perch Creek	<MDA	0.46
Perch Lake	<MDA	0.46
Toussaint	<MDA	0.46

*MDC will vary with snail body mass, thus only MDA is presented.

Table 27: Cesium-137 concentrations in snail bodies.

Location	Avg. Concentration (Bq kg^{-1}f.w.)	MDA* (Bq)
Upper Bass	<MDA	0.42
Lower Bass	<MDA	0.42
Perch Creek	<MDA	0.42
Perch Lake	<MDA	0.42
Toussaint	<MDA	0.42

*MDC will vary with snail body mass, thus only MDA is presented.

Table 28: Cesium-137 concentrations in sediment samples.

Location	Avg. Concentration (Bq kg d.w.$^{-1}$)	MDA* (Bq)
Upper Bass	<MDA	0.46
Lower Bass	<MDA	0.46
Perch Creek	<MDA	0.46
Perch Lake	<MDA	0.46
Toussaint	<MDA	0.46

*MDC will vary with digested sediment mass, thus only MDA is presented.

Table 29: Cobalt-60 concentrations in sediment samples.

Location	Avg. Concentration (Bq kg d.w.$^{-1}$)	MDA* (Bq)
Upper Bass	<MDA	0.46
Lower Bass	<MDA	0.46
Perch Creek	<MDA	0.46
Perch Lake	<MDA	0.46
Toussaint	<MDA	0.46

*MDC will vary with digested sediment mass, thus only MDA is presented.

5.4 Dosimetric Results

5.4.1 MCNP Results

The following tables (Tables 30 and 31) and figures (Figures 40-43) present absorbed fraction data for photon and electron sources located in either the snail shell or snail body. Generally, the coefficient of variance (COV) was between 5% and 10%. When the COV exceeded 10%, a dash was entered into the table.

Table 30: Absorbed fraction of electron energy.

	Source located in shell																			
	Energy (MeV)																			
Target	0.100	0.1862	0.200	0.300	0.400	0.500	0.546	0.600	0.700	0.760	0.800	0.900	1.000	1.200	1.400	1.600	1.800	2.000	2.280	2.500
Shell	0.9680	0.9188	0.9065	0.8373	0.7638	0.6912	0.6584	0.6230	0.5619	0.5297	0.5104	0.4670	0.4316	0.3769	0.3381	0.2779	0.2561	0.2377	0.2153	0.1990
Body	-	-	-	0.0767	0.1091	0.1406	0.1546	0.1695	0.1944	0.2071	0.2148	0.2299	0.2409	0.2540	0.2571	0.2233	0.3368	0.1371	0.1079	0.0924

	Source located in body																			
	Energy (MeV)																			
Target	0.100	0.1862	0.200	0.300	0.400	0.500	0.546	0.600	0.700	0.760	0.800	0.900	1.000	1.200	1.400	1.600	1.800	2.000	2.280	2.500
Shell	-	-	-	0.0757	0.1095	0.1393	0.1531	0.1683	0.1926	0.2049	0.2115	0.2266	0.2373	0.2498	0.2527	0.2470	0.2357	0.2235	0.2053	0.1914
Body	0.9840	0.9601	0.9540	0.9217	0.8878	0.8542	0.8385	0.8207	0.7884	0.7700	0.7583	0.7286	0.7007	0.6484	0.6011	0.3531	0.3057	0.2592	0.2148	0.1923

Figure 40: Absorbed fraction of electron energy for source located in the body.

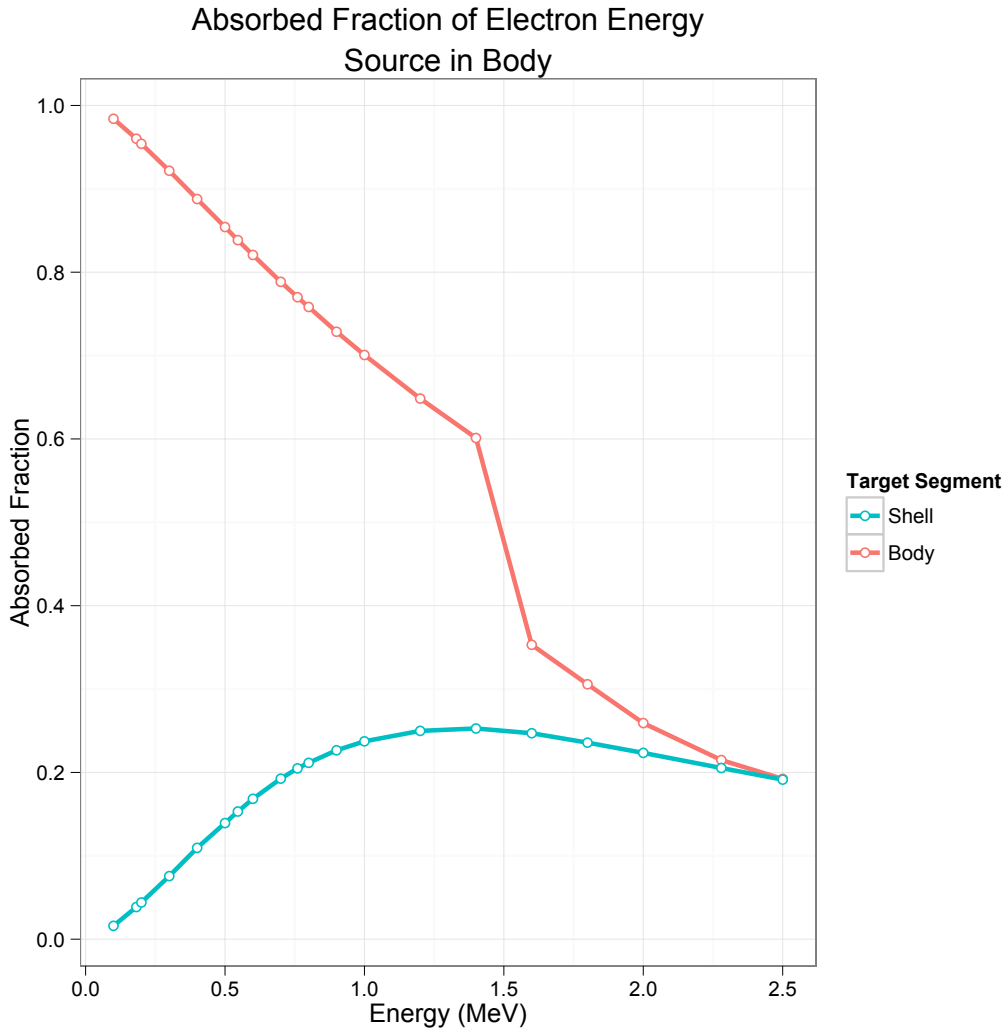

Figure 41: Absorbed fraction of electron energy for source located in the shell.

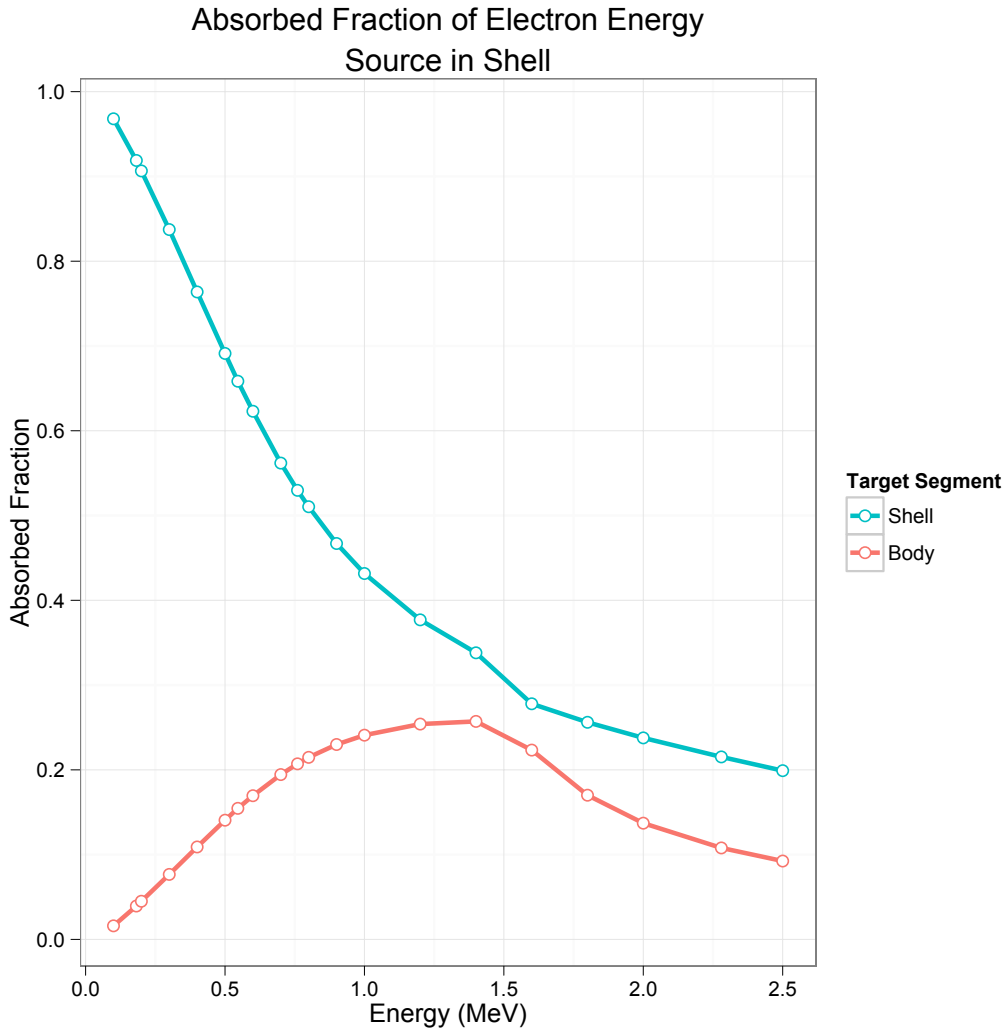

Table 31: Absorbed fractions of photon energy.

Source located in shell

Target	0.100	0.200	0.300	0.400	0.500	0.600	0.700	0.800	0.900	1.000	1.200	1.400	1.600	1.800	2.000	2.500
Energy (MeV)																
Shell	-	0.0127	0.0122	0.0115	0.0115	0.0110	0.0104	0.0099	0.0093	0.0087	0.0078	0.0070	0.0063	0.0056	0.0051	0.0036
Body	-	-	-	0.0087	0.0087	0.0087	0.0086	0.0085	0.0083	0.0082	0.0077	0.0073	0.0068	0.0060	0.0051	0.0041

Source located in body

Target	0.100	0.200	0.300	0.400	0.500	0.600	0.700	0.800	0.900	1.000	1.200	1.400	1.600	1.800	2.000	2.500
Energy (MeV)																
Shell	-	-	-	0.0094	0.0093	0.0092	0.0090	0.0088	0.0085	0.0083	0.0077	0.0072	0.0067	0.0059	0.0056	0.0045
Body	-	0.0148	0.0157	0.0159	0.0157	0.0153	0.0148	0.0143	0.0137	0.0132	0.0120	0.0109	0.0099	0.0088	0.0072	0.0050

Figure 42: Absorbed fraction of photon energy for source located in the body.

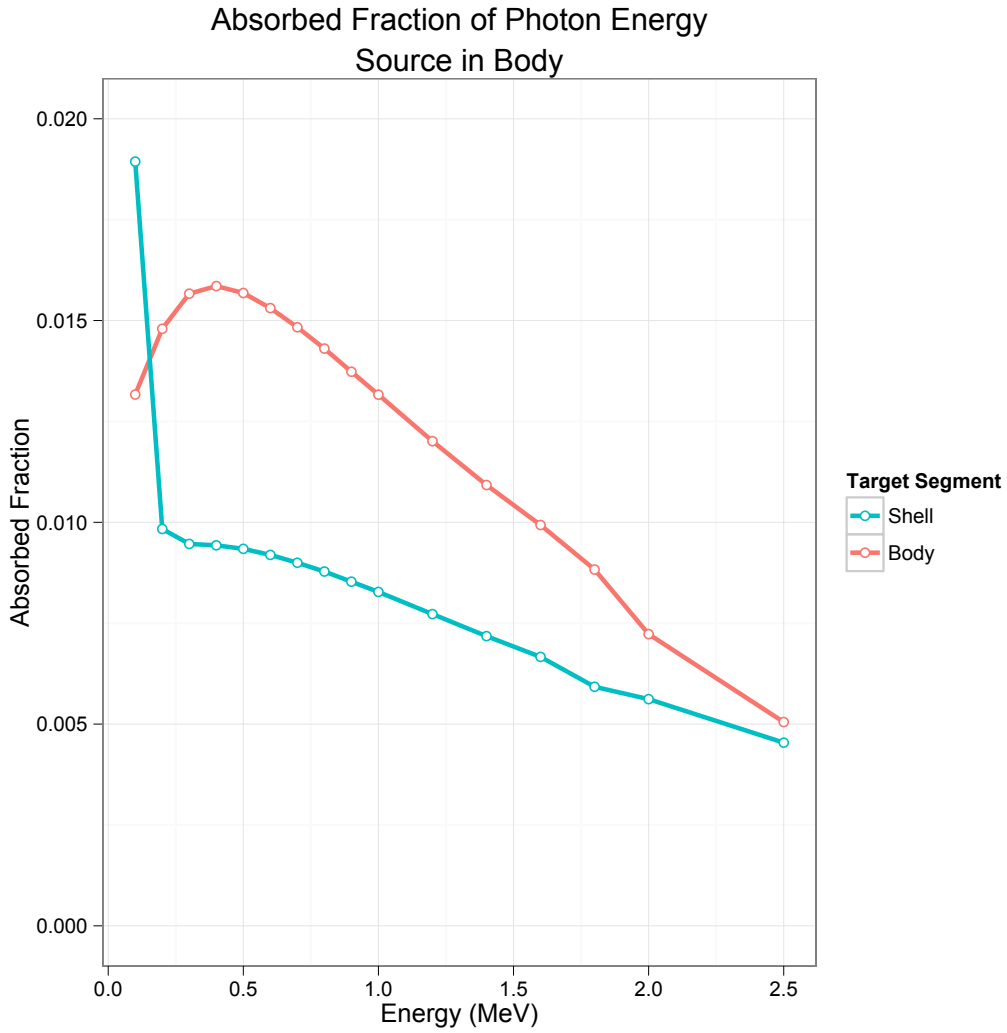

Figure 43: Absorbed fraction of photon energy for source located in the shell.

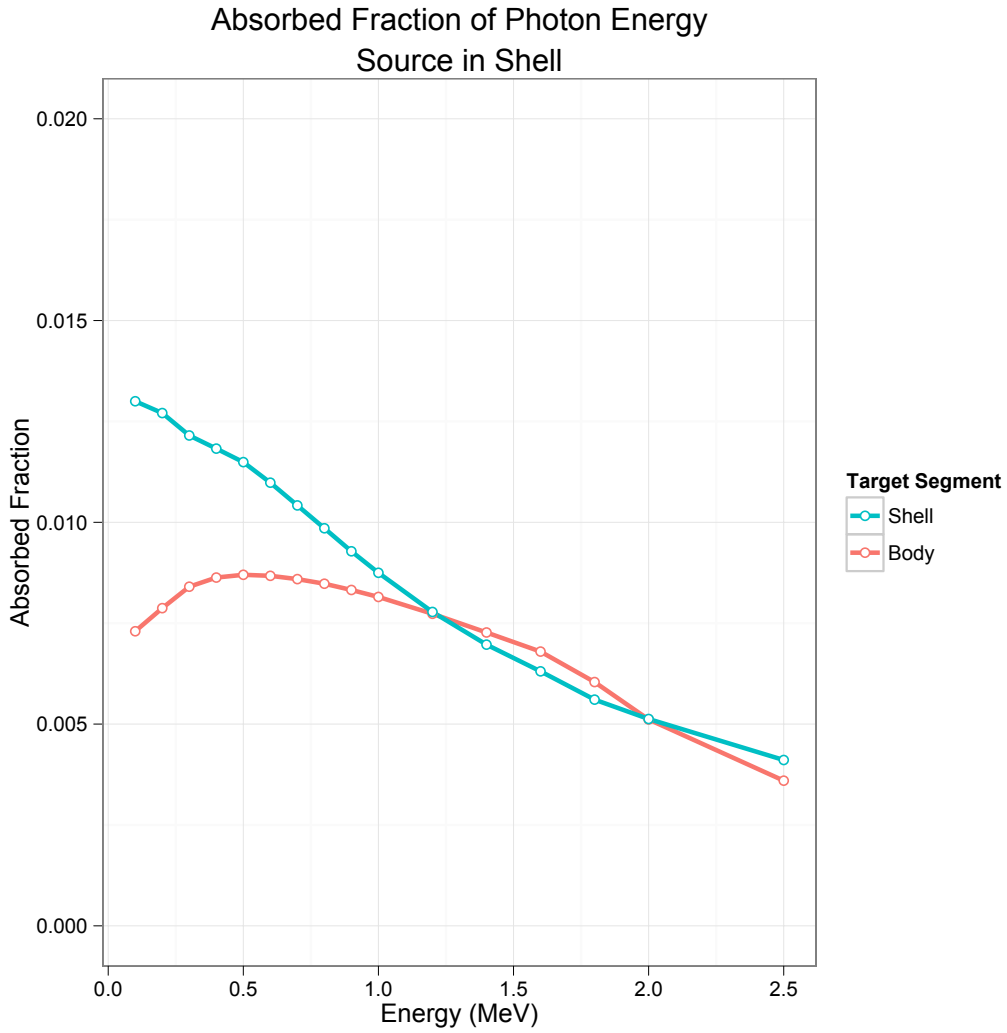

External sources were not successfully modeled. Despite large numbers of particle histories (five billion for photons and fifty million for electrons) the coefficients of variance remained in the 50-1000% range. However, those values with smaller (˜50%) variance give some indication that the absorbed fraction of energy in the soft tissues from an external source is <2% of the absorbed fraction for an internal electron source, and <0.2% of the absorbed fraction for an internal photon source. Thus it is possible to conclude that internal, not external, exposure drives dose-effects in *C. decisum,* likely due to the protection conferred by the snail's high-Z calciferous shell. This low absorbed fraction, combined with the fact that radiological analysis of soils was inconclusive and knowledge from previous studies that sediment concentrations of radionuclides are 100-1000 times less than those accumulated within the organism itself, led to the exclusion of the external component of dose rate from this study.

Tables 32-34 show dose conversion factors calculated from absorbed fraction data. The DCFs were calculated for those radionuclides found in snails samples from Chalk River Laboratories. DCFs for the voxelized model are separated into body and shell targets. As will be discussed, at the present time there is no generally accepted method of weighting segment doses to obtain a whole-body DCF.

Table 32: Strontium-90 DCFs

Source	Target	DCF $\left(\frac{\mu Gy}{d}\right)\left(\frac{Bq}{kg}\right)^{-1}$
shell	shell	2.39x10^{-3}
shell	body	1.03x10^{-3}
body	shell	1.00x10^{-3}
body	body	2.50x10^{-3}

Table 33: Yttrium-90 DCFs

Source	Target	DCF $\left(\frac{\mu Gy}{d}\right)\left(\frac{Bq}{kg}\right)^{-1}$
shell	shell	5.58x10^{-3}
shell	body	2.10x10^{-3}
body	shell	2.10x10^{-3}
body	body	8.10x10^{-3}

Table 34: Hydrogen-3 DCFs

Source	Target	DCF $\left(\frac{\mu Gy}{d}\right)\left(\frac{Bq}{kg}\right)^{-1}$
shell	shell	8.31x10^{-5}
shell	body	0
body	shell	0
body	body	8.31x10^{-5}

5.4.2 Range of Calculated Dose Rates

Dose rates for this study varied by location (Figure 44). Across the entire site the dose rates ranged from a mean of 0.02 μGy h^{-1} at Upper Bass (below the MDC, and so set to one half of the MDC, in accordance with statistical established protocol[40]) to 16.1μGy h^{-1}in Perch Lake. Mean values

for each of the study locations are reported below in table 35. The range of dose rates fits well with the dose rates considered to be controversial at this time. It is worth noting that these values are in good agreement (to a factor of three) with previously estimated dose rates, although due to differences in the dosimetric methodology, it seems probable that this similarity arises primarily due to happenstance.

Table 35: Mean shell dose rates for *C. decisum* at CRL, by location

Location	Calculated DR $\left(\frac{\mu Gy}{hr}\right)$
Lower Bass	1.51
Perch Creek	5.13
Perch Lake	16.1
Toussaint	0.29
Upper Bass	<MDA

*Upper Bass dose rates were below the average MDA of 0.09 μGy h^{-1}

Figure 44: Snail shell dose rate for individual snails, by location.

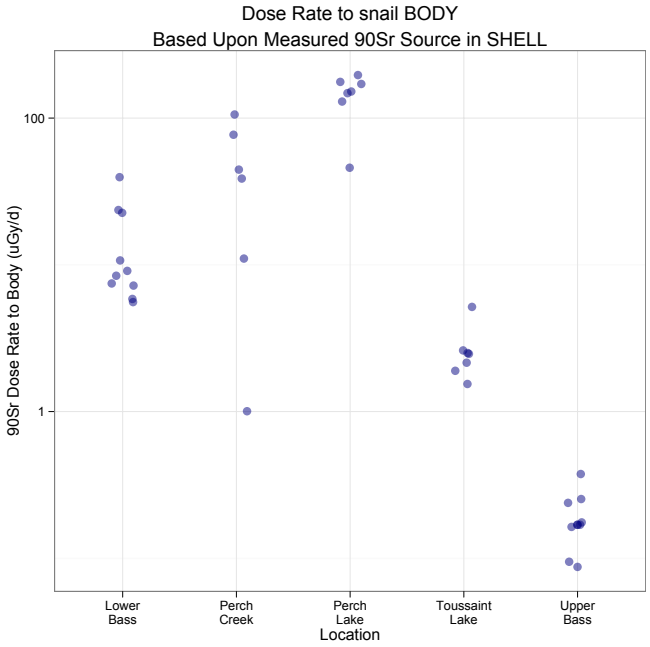

It should be noted that actual dose rates are slightly higher than those presented in table 35. Ambient dose rate was omitted from this study due to sediment concentrations of ^{90}Sr being below minimum detectable levels. However, this likely arose due to the small (1-2g) sample size used in the density

fractionation protocol; had samples been prepared by a more traditional ashing protocol (where larger masses are included for analysis), it likely would have been possible to detect a dosimetrically relevant concentration of ^{90}Sr. As such, this study has only established the minimum dose rate for snails, based upon internal tissue concentrations.

5.4.3 Estimation of Natural Background from ^{40}K

Natural background dose rate was estimated from the concentration of Potassium in snail tissues. Table 36, below, shows calculated DCFs for this isotope in snails:

Table 36: ^{40}K DCFs in units of μGy-kg (Bq-d)$^{-1}$ for snail tissues.

		Target	
		Shell	Body
Source	Shell	3.79×10^{-3}	6.62×10^{-4}
	Body	6.89×10^{-4}	4.76×10^{-3}

From these DCFs and ^{nat}K concentrations, the average dose rates to shell from ^{40}K were estimated for each study location. These are offered as a means of illustrating the internal "background" dose rate, and appear in table 37, below.

Table 37: Dose to snail shell from^{40}K located in shell.

Location	^{40}K Dose Rate μGy-hr^{-1}
Lower Bass	0.31
Perch Creek	0.24
Perch Lake	0.24
Toussaint	0.14
Upper Bass	0.15

6 Analysis

Data was analyzed for three different factors: first, regression analysis was used to determine the influence of environmental (explanatory) variables upon the mass of snails. Second, the same technique was used to determine the influence of environmental (explanatory) variables upon the number of snails captured at each location. Finally, concentration ratios were determined for the aquatic snail, and the influence of environmental (explanatory) variables on tissue-uptake of ^{90}Sr was explored.

6.1 Data parsing for regression analysis

Data analysis was complicated by the fact that only a subset of all captured snails were analyzed for ^{90}Sr content, principally because of the high cost per sample in terms of laboratory supplies. The subset that was analyzed was *not* randomly selected, a potential study-design flaw, but a necessary step to ensure that samples analyzed would be above limits of detection; the result was that larger individuals were selected for analysis. To quantify and provide a solution to the problem this presented regarding regression modeling, the following analysis was undertaken:

First, it was necessary to determine if snail mass varied by location for all collected snails. Linear regression was performed, and showed conclusive evidence of snail mass differing by location ($p<<0.001$). The mean mass by location, and number of individuals at each, is displayed below in table 38:

Table 38: Snail mass and replicates for entire data set, grouped by location. ANOVA showed convincing evidence of variation in shell mass by location ($p<<0.001$).

Location	Mean mass (mg)	Individuals Captured
Lower Bass	1341	23
Perch Creek	2898	47
Perch Lake	1367	20
Toussaint Lake	1320	92
Upper Bass	1486	30

However, among that subset of snails whose tissues were analyzed for ^{90}Sr content, there was no evidence of this same variation in shell mass by location ($p=0.31$), as shown in table 39, below. Additionally, it is evident that the mean masses in this subgroup differ from those in the complete population above.

Table 39: Snail shell mass and replicates for subgroup analyzed for ^{90}Sr content, grouped by location. ANOVA showed no evidence of variation in shell mass by location (p=0.31).

Location	Mean mass (mg, d.w.)	Individuals Captured
Lower Bass	783	9
Perch Creek	2139	6
Perch Lake	922	7
Toussaint Lake	1658	7
Upper Bass	1590	10

This creates a difficulty with regard to regression analysis: when analysis was first undertaken utilizing only the subpopulation data, no variables were significant ($p<0.1$) explainers of snail mass. However, since snail mass does not vary with respect to location, and many variables (e.g., water concentrations of macronutrients and contaminants) do vary with respect to location (as seen for dose rate in table 40, below, $p<0.001$ when regressed by location), it would in fact be impossible for any explanatory variables to have a significant relationship with snail mass.

Table 40: Shell dose rate and replicates for subgroup analyzed for ^{90}Sr content, grouped by location.

Location	Mean shell dose rate ($\mu Gy\text{-}d^{-1}$)	Replicates
Lower Bass	34	9
Perch Creek	123	6
Perch Lake	386	7
Toussaint Lake	6.9	7
Upper Bass	0.1	10

This was a significant setback in data analysis, and a significant (unintentional) flaw in the design of this study. To allow for regression analysis to proceed, the mean dose rate at a location was substituted for those individual snails upon whom tissue analysis had not been conducted. Those whose dose rates were known exactly were included in the model with the more detailed data intact. This substitution allowed regression analysis to be conducted upon all snails under study, instead of merely the subpopulation of those whose tissue concentrations of ^{90}Sr had been quantified. Despite its limitations, this approach is in some ways consistent with the desired outcome of this study: to relate the effect of dose rate with the distribution of snail mass. By associating a mean dose rate with the entire distribution of snails, it is possible to analyze the impact upon the entire population.

6.2 Multiple Linear Regression: Mass as a Response Variable

A least-squares linear fit was employed to determine which environmental variables were significant predictors of snail population health and to generate a dose-response curve. Data was analyzed using the statistical computing software R[7]. Within R's framework, the ggplot2[8] and companion to applied regression (car)[9] packages were utilized. All analysis software was both open-source and freeware.

6.2.1 Elimination of collinear variables

Codependence of model variables was of particular concern in this study, especially in the case of limnological data. Collinearity of variables will cause regression modeling to fail, as these variables are not independent of each other and violate the fourth regression model assumption (see section 6.4.1.). To assess collinearity, the variance inflation factor (VIF) of each model coefficient was monitored. The VIF is an index of the increase in a regression coefficient's variance due to collinearity with another variable. It is equal to the square of the increase (multiplicative) in the standard error of each model variable compared to a case where the variable is uncorrelated with another variable in the model. For example, a VIF of 6.12 would correspond to a 2.47-times increase in a coefficient's standard error in the dependent versus independent case.

Practically, VIF analysis means beginning with a simple model and gradually introducing additional variables. After each variable is introduced, the VIFs of regression coefficients are calculated: an increase in VIF between models indicates collinearity between the new variable and at least one existing variable. Since VIF analysis does not describe which variables are collinear, it is best to start with a simple model and introduce variables slowly, as opposed to beginning with a complex model and removing codependent variables. Kutner et al[53] have suggested that a VIF of less than ten is desirable; others have suggested cut-offs as low as four. Kutner's limit was used for this study, although few VIFs fell in the intermediate (4-10) range, with the majority VIFs either less than five or greater than two hundred.

In addition to environmental variables that were collinear, it was quickly determined that dose rates to snail body and snail shell were collinear (a reasonable outcome given the linear combinations by

[7] http://www.r-project.org/
[8] http://ggplot2.org/
[9] http://cran.r-project.org/web/packages/car/index.html

which dose is calculated in this situation). For this reason, dose rate to snail shell was chosen as a factor representative of radiation dose. This dose rate was chosen because it was the largest of all radiation-related factors and, due to the statistical uncertainty inherent in radiological counting, was therefore the factor known with the best accuracy.

6.2.2 Models run

Table 41 presents the variables included as a part of regression modeling.

Table 41: Regression model variable descriptions.

Variable Name	Variable Description	Variable Name	Variable Description
mass	wet mass of snail, mg [measured *in situ*]	water_ca	concentration of calcium in lake water, mg-L^{-1}
org_frac	mass fraction of organic material in soil	water_p	concentration of phosphorus in lake water, mg-L^{-1}
shell_dr	radiation dose rate to snail shell μGy-d^{-1}	snail_ca	concentration of calcium in snail shell, mg-kg^{-1} f.w.
water_temp	temperature of water at lure, ºC [measured *in situ*]	snail_p	concentration of phosphorus in snail shell, mg-kg^{-1} f.w.
light	ambient light incident on snail lure (lux) [measured *in situ*]	snail_mg	concentration of magnesium in snail shell, mg-kg^{-1} f.w.
snail_k	concentration of potassium in snail shell, mg-kg^{-1} f.w.	snail_na	concentration of sodium in snail shell, mg-kg^{-1} f.w.
snail_sr	concentration of ^{nat}strontium in snail shell, mg-kg^{-1} f.w.	water_ph	pH of collected lake water [measured *in situ*]
water_tds	total dissolved solids of collected lake water, ppm [measured *in situ*]	water_EC	electroconductivity of collected lake water, μS [measured *in situ*]
water_k	concentration of potassium in lake water, mg-L^{-1}	water_mg	concentration of magnesium in lake water, mg-L^{-1}
water_na	concentration of sodium in lake water, mg-L^{-1}	water_sr	concentration of ^{nat}strontium in lake water, ng-L^{-1}

VIF analysis requires that the initial model be as simple as possible. The variables included in this model were chosen subjectively, based upon their likelihood to be linearly independent of other

variables in the model. This first model regressed mass on several variables: mass˜org_frac + shell_dr + water_temp + light + water_ca + water_p + snail_ca + snail_p. It produced the following analysis of variance (ANOVA) table (Table 42):

Table 42: ANOVA table for first regression model.

```
Residuals:
    Min      1Q  Median      3Q     Max
-2782.1  -834.4  -188.0   572.7  5357.5

Coefficients:
              Estimate Std. Error t value Pr(>|t|)
(Intercept)  1.717e+03  1.595e+03   1.076   0.2828
org_frac    -1.568e+03  1.265e+03  -1.239   0.2164
shell_dr    -8.615e-01  8.277e-01  -1.041   0.2989
water_temp  -6.807e+01  6.028e+01  -1.129   0.2599
light        7.731e-03  3.125e-03   2.474   0.0140 *
water_ca     2.344e+02  4.678e+01   5.011 1.01e-06 ***
water_p      1.212e+03  3.798e+03   0.319   0.7499
snail_ca     3.460e-04  4.455e-04   0.777   0.4381
snail_p     -6.665e-02  3.895e-02  -1.711   0.0883 .
---
Residual standard error: 1279 on 256 degrees of freedom
Multiple R-squared: 0.1984,Adjusted R-squared: 0.1734
F-statistic: 7.922 on 8 and 256 DF,  p-value: 1.591e-09
```

And the following VIF table (Table 43):

Table 43: VIF table for first regression model.

```
org_frac   shell_dr   water_temp   light     water_ca
1.438326   1.447626    1.462104   1.310463   1.652048
water_p   snail_ca    snail_p
1.376094   1.097487   1.136033
```

These tables indicate that light and water_ca are significant predictors of snail mass, while other variables fail the significance test. The VIF table shows that there is no collinearity among the included variables, and so the analysis proceeded stepwise, with each model including a single new factor. If the VIF blew up, the factor was dropped from the model; if the VIF remained with acceptable levels, the factor was included and a new factor added until all the factors in table 35, above, had been tested. Tables 44 and 45, below, depict ANOVA and VIF tables for a model that showed a high degree of collinearity (mass˜org_frac + shell_dr + water_ temp + light + water_ca +

water_p + snail_ca + snail_p + snail_mg + snail_k + water_ph + water EC + water_tds).

Table 44: ANOVA table for a model that showed a high degree of covariance.

```
Residuals:
    Min      1Q  Median      3Q     Max
-2810.8  -834.1  -142.7   595.8  5350.6

Coefficients:
              Estimate Std. Error t value Pr(>|t|)
(Intercept)  1.997e+03  2.148e+03   0.929 0.353608
org_frac    -1.422e+03  1.356e+03  -1.049 0.295271
shell_dr    -3.966e-01  1.000e+00  -0.396 0.692089
water_temp  -5.388e+01  6.471e+01  -0.833 0.405849
light        8.942e-03  3.537e-03   2.528 0.012086 *
water_ca     2.804e+02  7.875e+01   3.560 0.000443 ***
water_p      1.895e+02  4.122e+03   0.046 0.963371
snail_ca     6.491e-04  7.506e-04   0.865 0.388003
snail_p      5.538e-04  7.197e-02   0.008 0.993866
snail_mg     8.238e-01  7.039e+00   0.117 0.906924
snail_k     -1.513e+00  1.279e+00  -1.182 0.238237
water_ph    -8.399e+01  1.986e+02  -0.423 0.672784
water_EC    -1.702e+01  6.083e+01  -0.280 0.779830
water_tds    2.775e+01  1.199e+02   0.231 0.817164
----
Residual standard error: 1287 on 251 degrees of freedom
Multiple R-squared: 0.2046,Adjusted R-squared: 0.1634
F-statistic: 4.967 on 13 and 251 DF,  p-value: 8.981e-08
```

Table 45: VIF table for a model that showed a high degree of covariance.

```
org_frac   shell_dr   water_temp   light    water_ca    water_p
1.631505   2.089234   1.664830   1.658837   4.627013   1.601753
snail_ca    snail_p   snail_mg    snail_k   water_ph   water_EC
3.078399   3.831622  4.257726   5.006839   1.479535 787.208559
water_tds
779.780193
```

6.2.3 Final variables

Twelve factors were included in the final model and six were omitted for collinearity; the results are tabulated in Table 46.

Table 46: Collinearity of regression model variables for snail mass model.

Variable Name	Collinear	Variable Name	Collinear
mass	N/A	water_ca	N
org_frac	N	water_p	N
shell_dr	N	snail_ca	N
water_temp	N	snail_p	Y
light	N	snail_mg	N
snail_k	N	snail_na	Y
snail_sr	Y	water_ph	N
water_tds	N	water_EC	Y
water_k	Y	water_mg	N
water_na	Y	water_sr	N

The output of this model is given in tables 47 and 48 below.

Table 47: ANOVA table for model inclusive of all linearly-independent factors.

```
Residuals:
    Min      1Q  Median      3Q     Max
-2729.6  -825.4  -115.2   596.3  5402.6

Coefficients:
              Estimate Std. Error t value Pr(>|t|)
(Intercept)  8.384e+02  2.396e+03   0.350  0.72674
org_frac    -1.793e+03  1.400e+03  -1.280  0.20158
shell_dr    -3.877e-01  9.980e-01  -0.389  0.69797
water_temp  -3.427e+01  6.575e+01  -0.521  0.60268
light        7.937e-03  3.549e-03   2.237  0.02619 *
water_ca     2.379e+02  8.814e+01   2.699  0.00743 **
water_p      2.657e+03  4.645e+03   0.572  0.56780
snail_ca     6.033e-04  7.442e-04   0.811  0.41831
snail_p     -6.745e-04  7.183e-02  -0.009  0.99252
snail_mg     1.077e+00  7.007e+00   0.154  0.87798
snail_k     -1.523e+00  1.273e+00  -1.197  0.23254
water_ph    -1.389e+02  2.018e+02  -0.688  0.49201
water_tds   -1.183e+01  1.088e+01  -1.087  0.27799
water_sr     1.147e+00  1.086e+00   1.056  0.29200
---
Residual standard error: 1284 on 251 degrees of freedom
Multiple R-squared: 0.2079,Adjusted R-squared: 0.1669
F-statistic: 5.068 on 13 and 251 DF,  p-value: 5.821e-08
```

Table 48: VIF table for model inclusive of all linearly-independent factors.

```
org_frac   shell_dr water_temp      light   water_ca   water_p
1.747627   2.088337   1.725972   1.676486   5.820071   2.043014
snail_mg    snail_k   water_ph  water_tds   water_sr  snail_ca    snail_p
4.237433   4.975045   1.533264   6.447317   7.185902  3.038024   3.832329
```

These results show that there is no (p>0.05 relationship) between snail mass and all variables except for light, which shows intriguing but inconclusive association (p=0.03), and water calcium, which shows convincing evidence (p=0.007) of being associated with snail mass. To test the significance of these variables independently of the unassociated factors, they were run as their own model with formula mass~light + water_ca (ANOVA, Table 49, VIF tabulated in Table 50).

Table 49: ANOVA table for the simplified model.

```
Residuals:
    Min      1Q  Median      3Q     Max
-2677.9  -891.0  -195.1   611.2  5447.0

Coefficients:
              Estimate Std. Error t value Pr(>|t|)
(Intercept) -3.834e+02  2.925e+02  -1.311   0.1911
light        4.647e-03  2.752e-03   1.689   0.0925 .
water_ca     2.620e+02  3.669e+01   7.142 9.09e-12 ***
---
Residual standard error: 1288 on 262 degrees of freedom
Multiple R-squared: 0.1679,Adjusted R-squared: 0.1616
F-statistic: 26.44 on 2 and 262 DF,  p-value: 3.466e-11
```

Table 50: VIF table for the simplified model.

```
 light    water_ca
1.001997  1.001997
```

This model also shows convincing evidence (p<0.001) for dissolved calcium's influence on snail mass. However, there was suggestive, but inconclusive, evidence (p=0.09) for the amount of light influencing snail mass.

Of the other eleven models tested, all showed convincing evidence (p<0.001) for dissolved calcium's impact upon snail mass, while all showed moderate (0.01<p<0.09) evidence for light's impact upon

the mass of snails. None of the models tested showed any evidence that snail mass distribution varied with dose rate ($p>0.1$).

6.2.4 Residual Plots

Residual plots were created for two separate models (mass~light and mass~water_ca) to examine the strength of the model fit, these are displayed as figures 45 and 46 below. The plots, especially the regression on light, show some minimal fanning, suggesting the model variance increases with the magnitude of light and water_ca. However, this fanning is minimal enough that it should not impact model validity, especially because each residual plot is independent of the other's effect upon the entire model. Other than some fanning, the residuals appear to be fairly randomly distributed around zero, suggesting that the regression model is a good fit of the data.

Figure 45: Jittered residual plot for mass˜water_ca

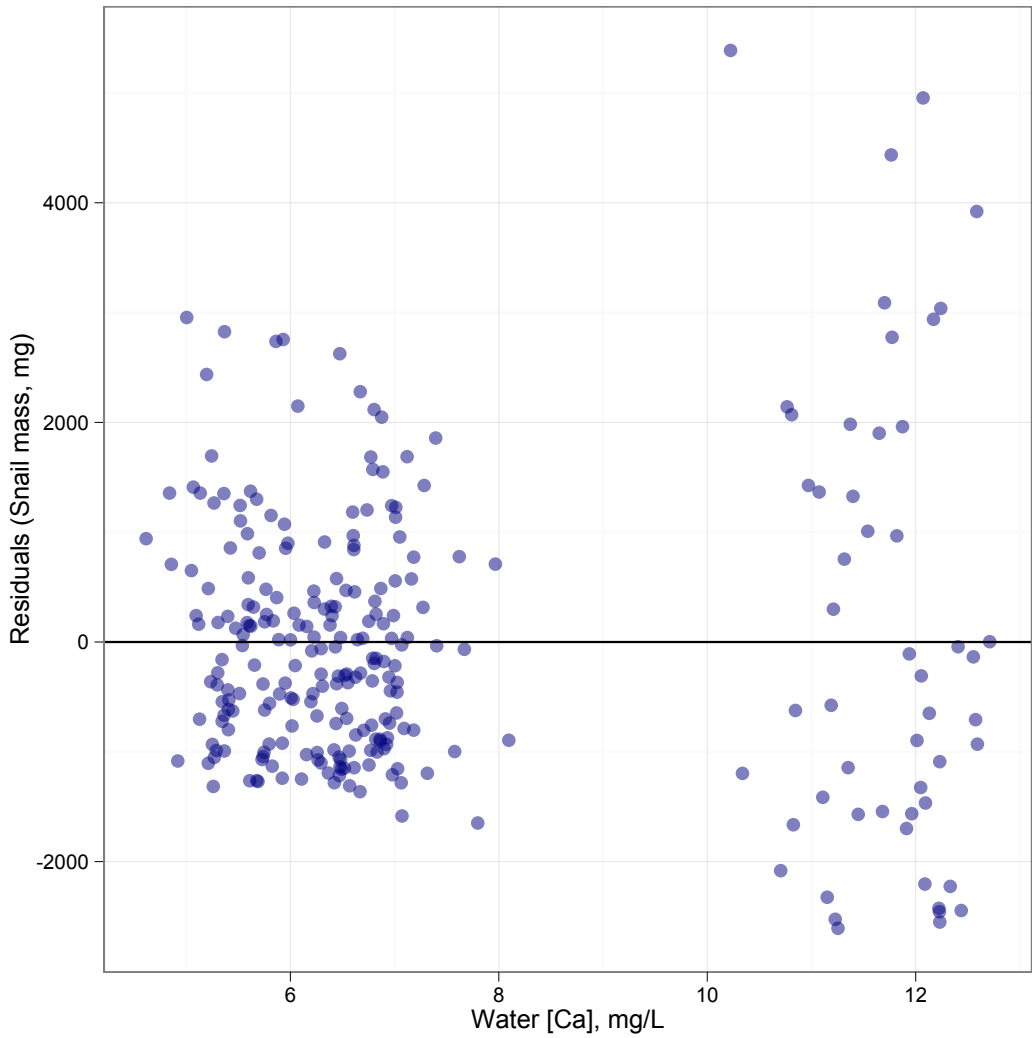

Figure 46: Jittered residual plot for mass~light

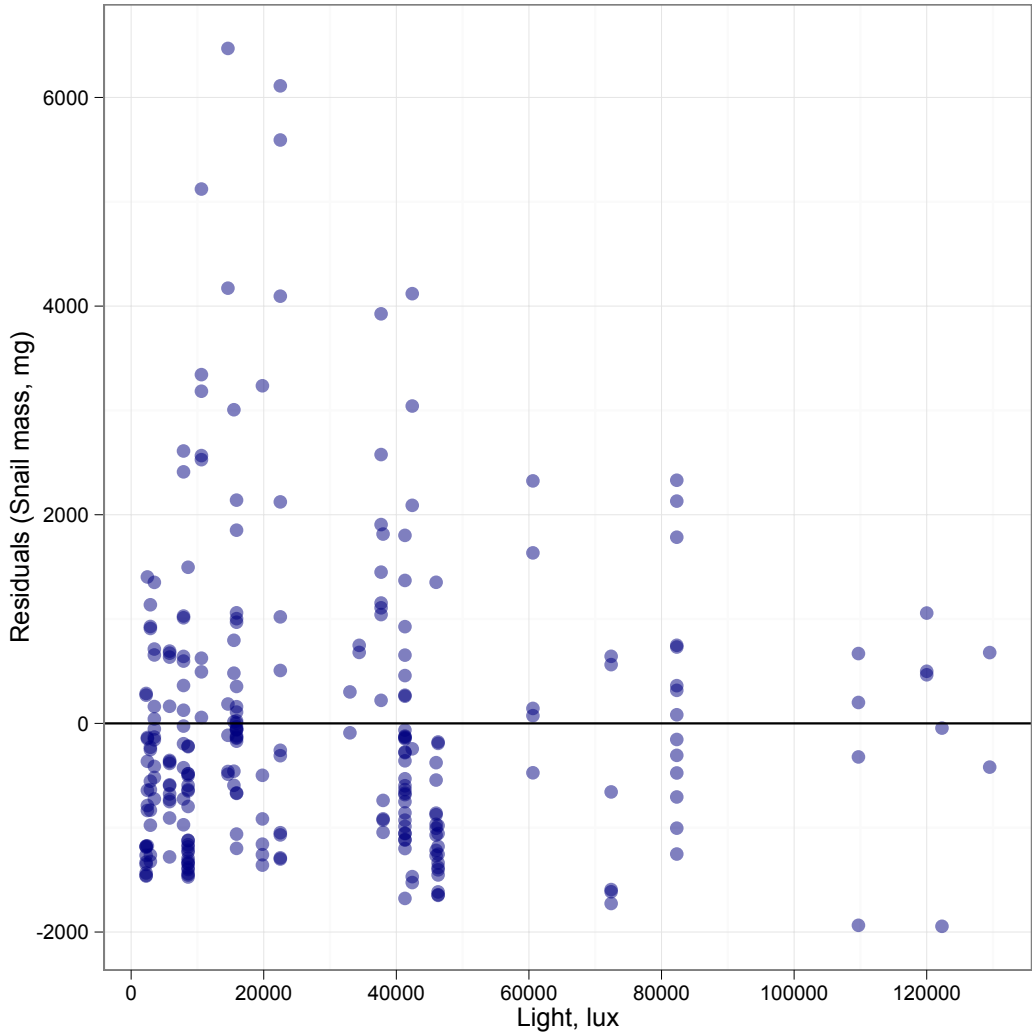

6.3 Speculation concerning unexplained variation in snail mass

A large fraction of the variation in snail mass remains unexplained by any of the environmental factors included in this study. There are three hypotheses for some of the variation; likely both of them contribute in some way. Firstly, predation was not well understood or included in this model. Minnow traps were used to conduct rudimentary surveys of species present in the water bodies sampled, but the results collected via this method should be considered only partially representative of predation stress. This is for two reasons: firstly, minnow traps were unable to capture larger fish

present, and the smaller fish are of a size that makes them unable to consume any but the smallest snails. That the distribution of fish of a size likely to consume snails is different from small fish is a possibility that cannot be discounted. Secondly, certain fish known to be present in CRL's lakes, and that rely upon snails as a food source (e.g., Yellow Perch)[59] went undiscovered by the minnow traps. A more robust survey of predatory fish would bring clarity to this issue, but was not feasible to attempt as a part of this study.

The second factor potentially explains the larger snail masses observed for individuals captured from Perch Creek, where snails were significantly larger than any other site sampled, despite little variance in environmental characteristics. This may arise due to the geography of Perch Creek, which is blocked with a weir. It is possibly that snails move out of Perch Lake and into Perch Creek, then downstream toward the weir where they accumulate. Allison[7] notes that *Campeloma* easily move both up and downstream, so some larger individuals certainly move back upstream toward Perch Lake, however, restricted volume of Perch Creek in the area adjacent to the weir area may provide partial protection from the medium and large-sized fish that prey on *Campeloma*. This in turn increases the average lifespan of snails near the weir and ultimately results in larger individuals.

The final hypothesis follows the multiple-stressors route. Some of the lakes under study have above-background (though generally not considered toxic)[38] levels of heavy metal contamination. It is conceivable that some fraction of snail mass variance is due to this extra environmental stressor. Undertaking this study would make for a fascinating and useful future study.

While the above three hypotheses likely do not explain all the variation in snail mass, they represent reasonable explanations based upon conditions that were anecdotally observed but not measured as a part of this study. However, there is at this time no concrete evidence for any particular hypothesis and that they remain speculative in nature.

6.4 Multiple Linear Regression: Number of Lured Snails as a Response Variable

In addition to the regression performed on snail mass, which has already been discussed, multiple regression was also applied to the number of snails retrieved per baited lure. This provides an understanding of which factors predict the greatest *number* of snails as opposed to the factors which

predict the *most robust* (massive) snails.

6.4.1 Data parsing for regression analysis

Many of the same explanatory variables utilized to regress on mass were also employed in the second regression model. The only difference was that there were fewer observations (due to the fact that there were more lured snails than traps) and that this time, the regression model looked at "num_snails", or the number of snails lured to each trap, as the response variable. Once again, lake-wide means for ion concentrations in water and mean snail shell dose rate were applied to all traps.

6.4.2 Elimination of collinear variables

See section 6.4.2, above, for a discussion of variance inflation factor and the exclusion of collinear variables from regression models.

6.4.3 Models run

The variables included in the initial model were the same as those presented in table 41, above, and were again chosen subjectively based upon their likelihood to be linearly independent of other variables in the model. This first model regressed mass on several variables: num_snails~ shell_dr + water_temp + light + water_ca + water_p + snail_ca. It produced the following analysis of variance (ANOVA) table (Table 51):

Table 51: ANOVA table for first regression model.

```
Residuals:
   Min     1Q Median     3Q    Max
-6.347 -2.289 -1.182  2.109 13.034

Coefficients:
              Estimate Std. Error t value Pr(>|t|)
(Intercept)  1.211e+01  5.109e+01   0.237   0.8135
shell_dr    -1.689e-03  4.393e-03  -0.384   0.7021
water_temp   1.801e-01  2.694e-01   0.668   0.5067
water_light -3.152e-05  1.631e-05  -1.933   0.0583 .
water_ca     1.393e+00  1.513e+00   0.921   0.3611
water_p      1.725e+02  3.905e+01   4.418 4.61e-05 ***
snail_ca    -8.933e-05  1.831e-04  -0.488   0.6276
---
Residual standard error: 3.952 on 56 degrees of freedom
Multiple R-squared: 0.4431,Adjusted R-squared: 0.3835
F-statistic: 7.427 on 6 and 56 DF,  p-value: 7.084e-06
```

And the following VIF table (Table 52):

Table 52: VIF table for first regression model.

shell_dr	water_temp	water_light	water_ca	water_p	snail_ca
2.022496	1.711901	1.181749	2.123449	1.797470	3.010737

As in section 6.4, variables were again included in the model after their linear independence had been established, until all variables had been tested and a final inclusive model had been reached.

6.4.4 Final variables

Seven factors were included in the final model and eleven were omitted for collinearity (summarized in Table 53), with a final model of: num_snails ˜ shell_dr + water_temp + water_light + water_ca + water_p + snail_k.

Table 53: Collinearity of regression model variables for number of snails model.

Variable Name	Collinear	Variable Name	Collinear
num_snails	N/A	water_ca	N
org_frac	N	water_p	N
shell_dr	N	snail_ca	N
water_temp	N	snail_p	Y
water_light	N	snail_mg	Y
snail_k	N	snail_na	Y
snail_sr	Y	water_ph	Y
water_tds	Y	water_EC	Y
water_k	Y	water_mg	Y
water_na	Y	water_sr	Y

Tables 54 and 55, below, show ANOVA and VIF tables for the final, linearly independent, model.

Table 54: ANOVA table for model inclusive of all linearly-independent factors.

```
Residuals:
   Min     1Q Median     3Q    Max
-6.347 -2.289 -1.182  2.109 13.034

Coefficients:
              Estimate Std. Error t value Pr(>|t|)
(Intercept) -4.100e+01  5.955e+01  -0.689   0.4940
shell_dr    -1.688e-03  4.393e-03  -0.384   0.7022
water_temp   1.801e-01  2.694e-01   0.668   0.5067
water_light -3.152e-05  1.631e-05  -1.933   0.0583 .
water_ca     1.393e+00  1.513e+00   0.921   0.3611
water_p      1.725e+02  3.908e+01   4.415 4.66e-05 ***
snail_k      5.577e-02  1.143e-01   0.488   0.6276
---
Residual standard error: 3.952 on 56 degrees of freedom
Multiple R-squared: 0.4431,Adjusted R-squared: 0.3835
F-statistic: 7.427 on 6 and 56 DF,  p-value: 7.084e-06
```

Table 55: VIF table for model inclusive of all linearly-independent factors.

```
shell_dr   water_temp water_light   water_ca     water_p     snail_k
2.022787    1.711901    1.181749    2.123357    1.800535    3.012104
```

These results show that there is no (p>0.05 relationship) between the number of snails lured and any variable except for the water concentration of phosphorus, for which there is convincing evidence

($p<0.001$) of an association. To test the significance of water phosphorus independently of the unassociated factors, it was run as its own model with formula num_snails~water_p (ANOVA data in Table 56).

Table 56: ANOVA table for the simplified model.

```
Residuals:
   Min     1Q Median     3Q    Max
-9.369 -2.301 -1.696  1.699 13.699

Coefficients:
            Estimate Std. Error t value Pr(>|t|)
(Intercept)   -6.767      1.698  -3.986 0.000182 ***
water_p      181.358     29.310   6.188 5.64e-08 ***
---
Residual standard error: 3.977 on 61 degrees of freedom
Multiple R-squared: 0.3856,Adjusted R-squared: 0.3755
F-statistic: 38.29 on 1 and 61 DF,  p-value: 5.641e-08
```

The VIF is not displayed here as multicollinearity is not possible in a model with only one explanatory variable.

This model shows convincing evidence ($p<0.001$) for phosphorus' influence on number of snails.

Of the other eleven models tested, all showed convincing evidence ($p<0.001$) for phosphorus' impact upon number of snails. None of the models tested showed any evidence that snail number varied with dose rate ($p>0.1$).

6.4.5 Residual Plot

A residual plot was created for the simplified phosphorus model (num_snails~water_p) to examine the strength of the model fit and is displayed as figure 47 below. The plots shows no evidence of fanning and values appear to be fairly randomly distributed around zero, suggesting that the regression model is a good fit of the data.

Figure 47: Jittered residual plot for num_snails~water_p

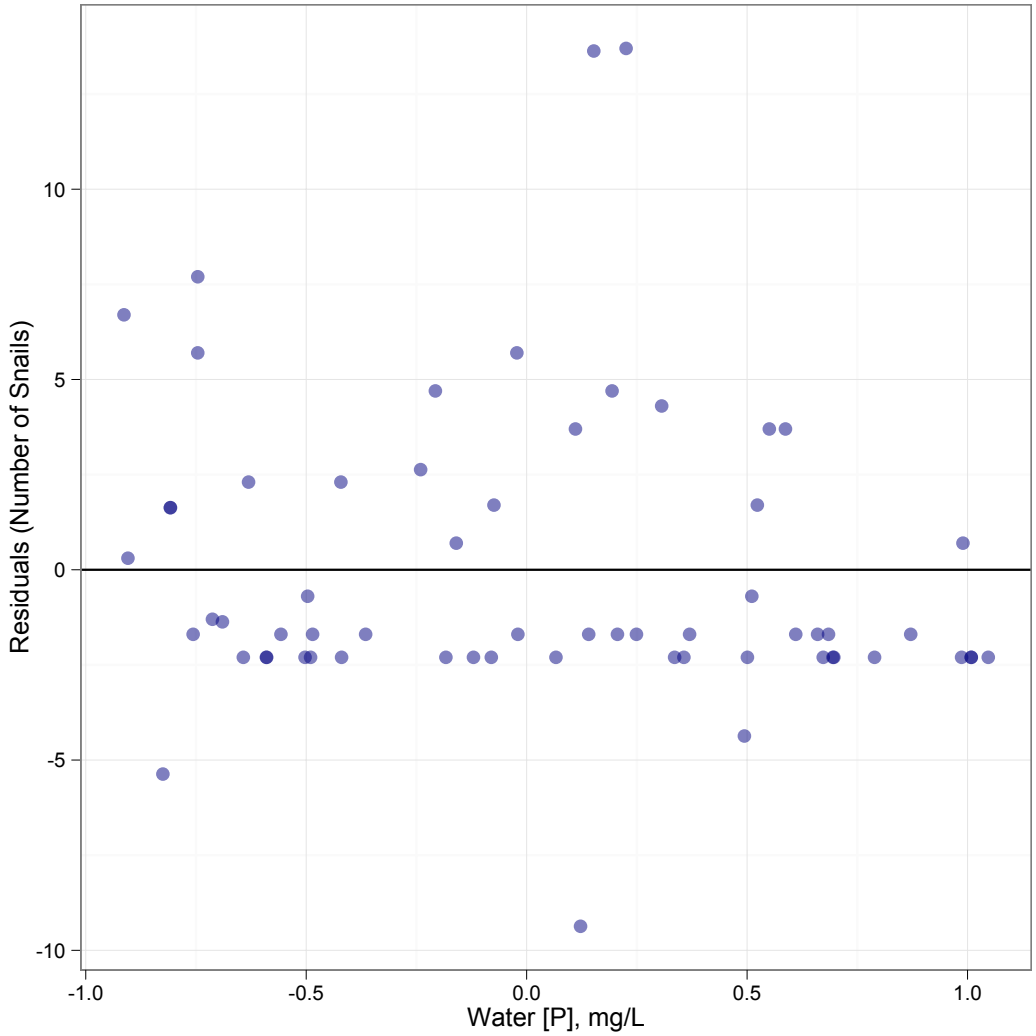

6.5 Derivation of environmental concentration ratios

Many dosimetric methodologies rely upon concentration ratios to estimate the body burden of radionuclides within biota. The concentration ratio relates the tissue concentration of a radionuclide to the concentration of that radionuclide within some environmental factor, e.g., water concentration, soil concentration, or concentration in an organism's food source. It is presented as:

$$CR = \frac{C_{tissue}}{C_{environment}} \tag{6.1}$$

Others[15, 75] have noted that it may be more appropriate to normalize this ratio by the amount of carbon present in the organism under investigation, following a method known as ecological stoichiometry. While we do not disagree with the stoichiometric approach (particularly in the case of a mollusk, where a mineral shell may increase body mass disproportionately to the total organism growth), total carbon was not measured as a part of this study, and so concentration ratios were used to relate environmental factors to tissue concentrations of radionuclides in *C. decisum*.

6.5.1 (^{90}Sr) Water concentration as an indicator of shell-tissue concentration

Three water-related concentrations were explored as a environmental indicators of ^{90}Sr concentration in shell tissue: concentration of ^{90}Sr, concentration of $^{\text{nat}}$Sr, and concentration of $^{\text{nat}}$Ca (Figures 48-50). Of these, the ratio of $\left(\frac{^{90}Sr}{^{nat}Ca}\right)_{shell}\left(\frac{^{90}Sr}{^{nat}Ca}\right)^{-1}_{water}$ appears to best predict the concentration of radionuclide within a snail's shell (R^2=0.7993, p<0.001). However, as will be discussed below in more detail in 6.6, regression modeling shows that water concentration of Ca is not a rigorous predictor of tissue concentration of ^{90}Sr, indicating that the most correct predictor is water concentration of ^{90}Sr alone. (R^2=0.5863, p<0.001).

Figure 48: Regression relating the ratio [^{90}Sr] to [^{nat}Sr] in tissues to the same ratio in environmental (water) samples. Grey area represents the 95% CI.

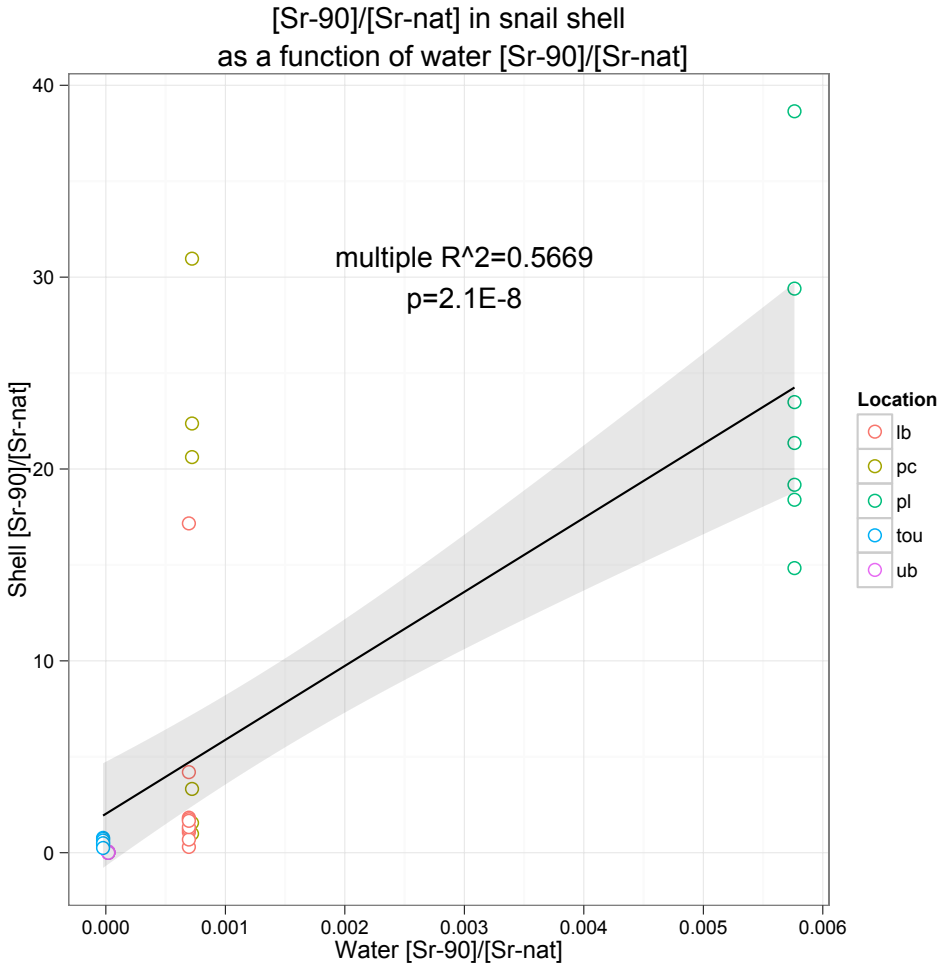

Figure 49: Regression relating tissue concentrations of ^{90}Sr to environmental concentrations (water) of the same species. Grey area represents the 95% CI.

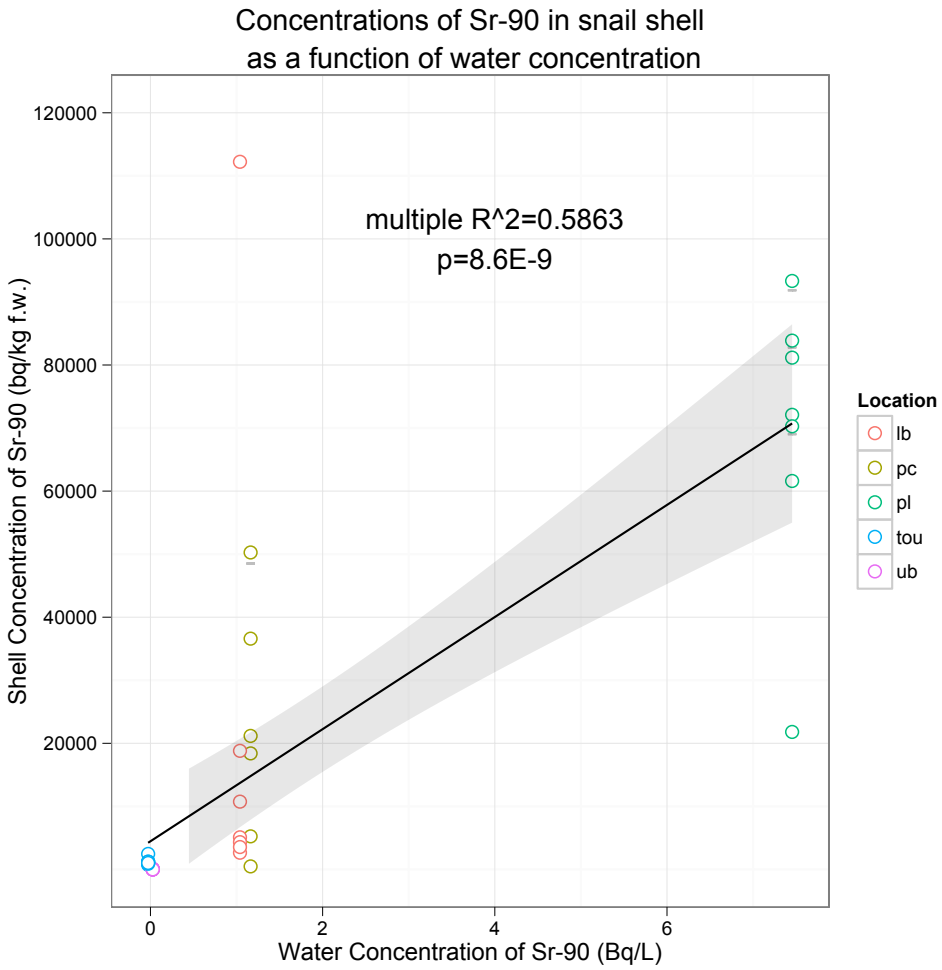

Figure 50: Regression relating the ratio [^{90}Sr] to [^{nat}Ca] in tissues to the same ratio in environmental (water) samples. Grey area represents the 95% CI.

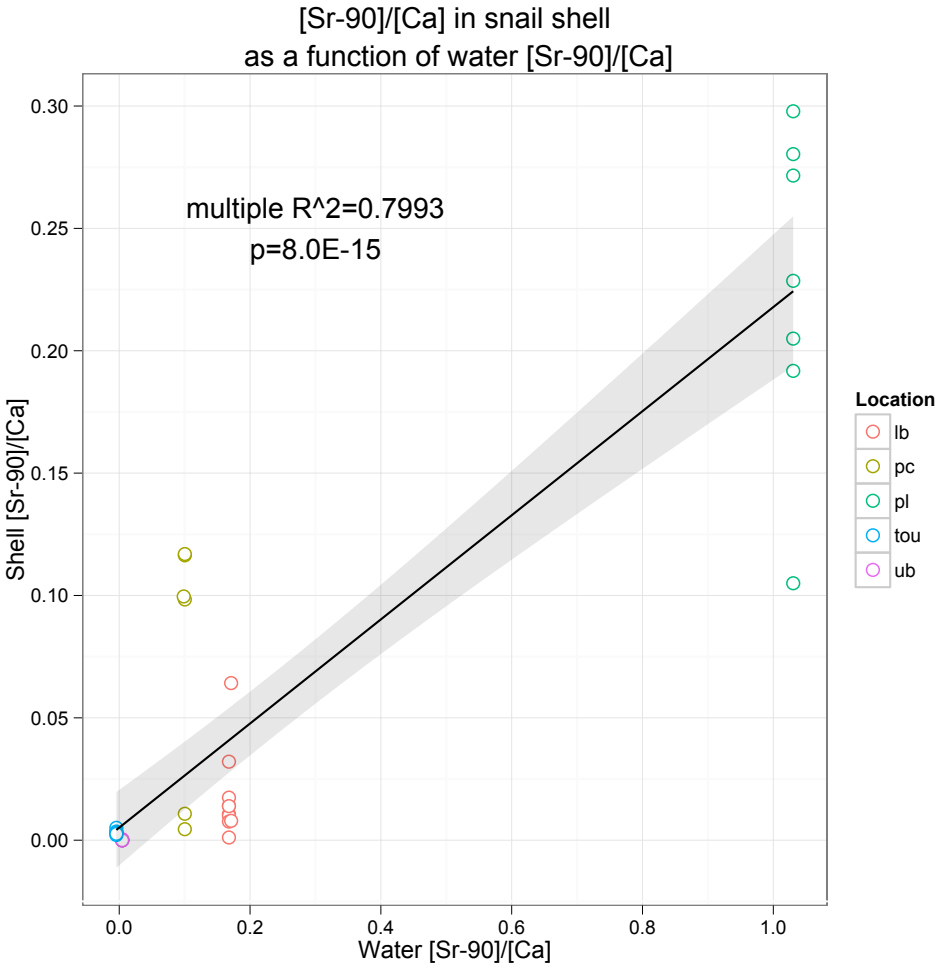

More than anything, the imperfect fits of these regression ratios underscore the difficulty of accurately predicting tissue concentrations based a simple ratio. Lake waters are well mixed, and snail tissue concentrations are decidedly more heterogeneous, making it difficult to model the statistical variation in tissue concentrations between individuals.

Mass-dependence of concentration ratios To test whether or not concentration ratios were a function of mass (a proxy for age) regression fits were made for CRs as a function of mass (Figure 51). There was no evidence ($p>0.1$) that CR was dependent upon snail mass. An example fit is

shown below, looking at the concentration of ^{90}Sr, normalized by Ca, for snail shell:water.

Figure 51: Shell:water concentration ratio (^{90}Sr/Ca) as a function of mass. Grey area represents the 95% CI.

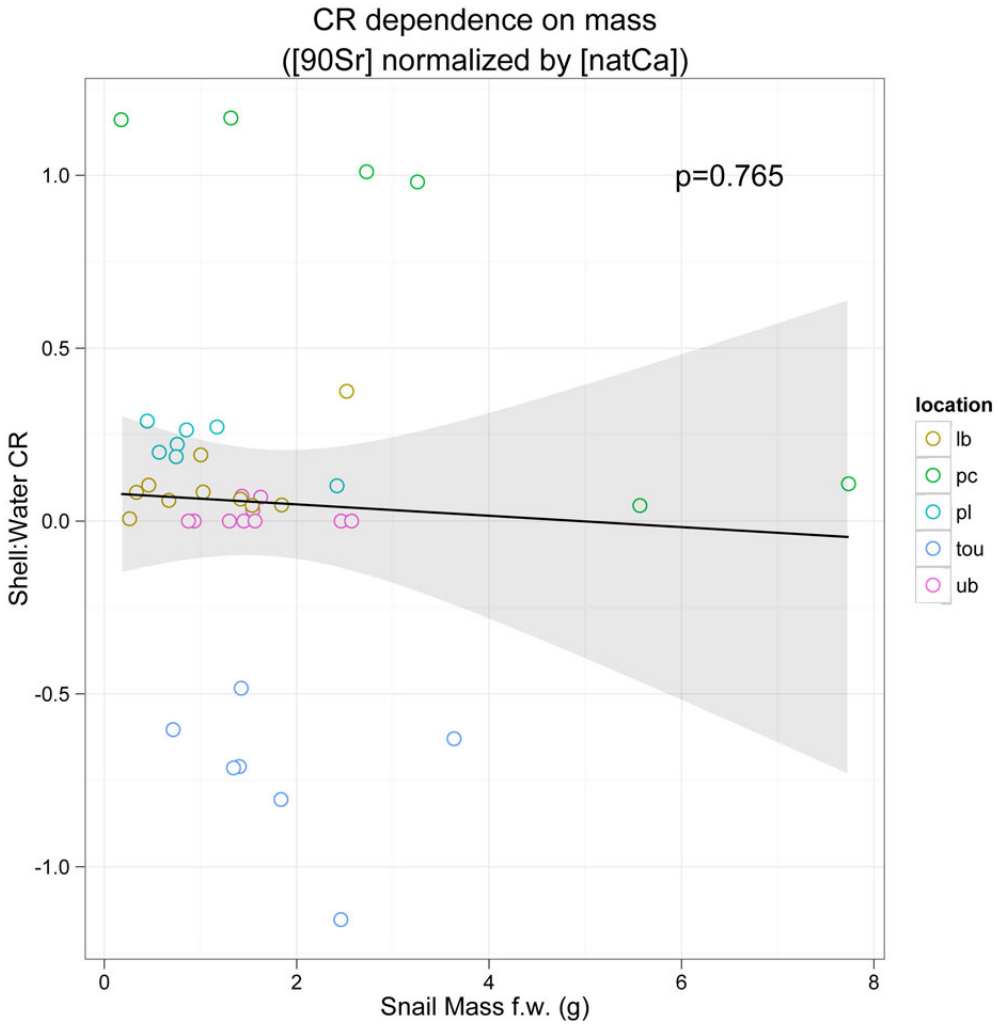

6.6 Environmental factors influencing ^{90}Sr concentration ratio

To determine which environmental factors influenced concentration ratio, a third regression model was run, this time regressing the tissue concentration of 90Sr on the variables described below in table 57.

Table 57: CR regression model variable descriptions.

Variable Name	Variable Description	Variable Name	Variable Description
water_conc_sr	concentration of ^{90}Sr in lake waters, in Bq-L^{-1}	water_ca	concentration of calcium in lake water, mg-L^{-1}
env_temp	temperature of water at lure, ºC [measured *in situ*]	water_p	concentration of phosphorus in lake water, mg-L^{-1}
env_light	ambient light incident on snail lure (lux) [measured *in situ*]	snail_ca	concentration of calcium in snail shell, mg-kg^{-1} f.w.
snail_k	concentration of potassium in snail shell, mg-kg^{-1} f.w.	snail_p	concentration of phosphorus in snail shell, mg-kg^{-1} f.w.
snail_sr	concentration of ^{nat}strontium in snail shell, mg-kg^{-1} f.w.	snail_mg	concentration of magnesium in snail shell, mg-kg^{-1} f.w.
env_tds	total dissolved solids of collected lake water, ppm [measured *in situ*]	snail_na	concentration of sodium in snail shell, mg-kg^{-1} f.w.
water_k	concentration of potassium in lake water, mg-L^{-1}	env_ph	pH of collected lake water [measured *in situ*]
water_na	concentration of sodium in lake water, mg-L^{-1}	env_EC	electroconductivity of collected lake water, µS [measured *in situ*]
water_sr	concentration of ^{nat}strontium in lake water, ng-L^{-1}	water_mg	concentration of magnesium in lake water, mg-L^{-1}
snail_conc_sr	concentration of ^{90}Sr in snail shell, Bq-kg^{-1} f.w.		

6.6.1 Data parsing for regression analysis

The data set for this analysis relied only upon those snails whose concentrations of ^{90}Sr had been quantified, and thus was a more prescripted data set than either of the two analyses. This was done increase confidence in the model.

6.6.2 Elimination of collinear variables

See section 6.4.2, above, for a discussion of variance inflation factor and the exclusion of collinear variables from regression models.

6.6.3 Models run

The variables included in the initial model were the same as those presented in table 36, above, and were again chosen subjectively based upon their likelihood to be linearly independent of other variables in the model. This first model regressed mass on several variables: snail_conc_sr ~ water_conc_sr + snail_ca + snail_sr, and proceeding to iterate through all variables until only the linearly independent variables remained in the model.

6.6.4 Final variables

Eleven explanatory variables were included in the final model and seven were omitted for collinearity, with a final model of: snail_conc_sr~ water_conc_sr + snail_ca + snail_sr + water_ca + water_sr + snail_mg + snail_p + env_temp + env_ph + env_light + water_p.

Table 58: Collinearity of regression model variables for number of snails model.

Variable Name	Collinear	Variable Name	Collinear
water_conc_sr	N	water_ca	N
env_temp	N	water_p	N
env_light	N	snail_ca	N
snail_k	Y	snail_p	N
snail_sr	N	snail_mg	N
env_tds	Y	snail_na	Y
water_k	Y	env_ph	N
water_na	Y	env_EC	Y
water_sr	N	water_mg	Y
snail_conc_sr	N/A		

Tables 59 and 60, below, show ANOVA and VIF tables for the final, linearly independent, model.

Table 59: ANOVA table for model inclusive of all linearly-independent factors.

```
Residuals:
   Min     1Q Median     3Q    Max
-41778  -7068   -415   7305  55436

Coefficients:
                Estimate Std. Error t value Pr(>|t|)
(Intercept)   -6.358e+04  9.437e+04  -0.674 0.505974
water_conc_sr  7.086e+03  1.831e+03   3.870 0.000595 ***
snail_ca       1.058e-02  1.408e-02   0.752 0.458478
snail_sr       2.821e+00  2.167e+00   1.302 0.203583
water_ca       5.737e+03  4.268e+03   1.344 0.189666
water_sr      -3.185e+01  5.022e+01  -0.634 0.531162
snail_mg      -9.448e+01  1.243e+02  -0.760 0.453357
snail_p       -5.317e-01  1.190e+00  -0.447 0.658389
env_temp       2.828e+03  2.831e+03   0.999 0.326429
env_ph         4.613e+02  8.333e+03   0.055 0.956239
env_light      2.206e-01  1.239e-01   1.780 0.085935 .
water_p       -1.672e+05  2.662e+05  -0.628 0.534895
---
Residual standard error: 18450 on 28 degrees of freedom
Multiple R-squared: 0.7548,Adjusted R-squared: 0.6584
F-statistic: 7.834 on 11 and 28 DF,  p-value: 5.387e-06
```

Table 60: VIF table for model inclusive of all linearly-independent factors.

water_conc_sr	snail_ca	snail_sr	water_ca	water_sr	snail_mg
2.821638	5.951043	4.451336	8.198924	6.947230	6.492113
snail_p	env_temp	env_ph	env_light	water_p	
5.124036	2.168624	2.167482	1.800688	3.731074	

These results show that there is no ($p>0.05$ relationship) between tissue concentration of ^{90}Sr and any variable except for the water concentration of ^{90}Sr, for which there is convincing evidence ($p<0.001$) of an association. To test the significance of water phosphorus independently of the unassociated factors, it was run as its own model with formula snail_conc_sr~water_conc_sr (the concentration ratio, in effect). ANOVA data is given in Table 61.

Table 61: ANOVA table for the simplified model.

```
Residuals:
   Min     1Q Median     3Q    Max
-48967  -8651  -4447    -38  98658

Coefficients:
              Estimate Std. Error t value Pr(>|t|)
(Intercept)       4296       3880   1.107    0.275
water_conc_sr     8919       1215   7.339 8.59e-09 ***
---
Residual standard error: 20570 on 38 degrees of freedom
Multiple R-squared: 0.5863,Adjusted R-squared: 0.5754
F-statistic: 53.86 on 1 and 38 DF,  p-value: 8.595e-09
```

The VIF is not displayed here as multicollinearity is not possible in a model with only one explanatory variable.

This model shows convincing evidence ($p<0.001$) for water concentration of ^{90}Sr influencing tissue concentration of ^{90}Sr.

Of the other nine linearly independent models tested, all showed convincing evidence ($p<0.001$) for a relationship between ^{90}Sr in the water and ^{90}Sr in tissues. It is important to keep the results of significance tests in mind when selecting the most appropriate concentration ratio for modeling organism uptake of radionuclides. While it may be tempting to include other variables (such as Ca concentration in this study) to improve the strength of fit (multiple R^2), it is important to recall that the inclusion of sufficient parameters will allow R^2 to approach unity regardless of the presence of any real association between between explanatory and dependent variables. It is important to include only those environmental variables whose relationship to the dependent variable bear up to statistical tests of significance in concentration ratio modeling.

6.6.5 Residual Plot

A residual plot was created for the simplified model (snail_conc_sr~water_conc_sr) to examine the strength of the model fit and is displayed as figure 51 below. The plot shows no evidence of fanning. The residuals appear to be fairly randomly distributed around zero, suggesting that the regression model is a good fit of the data.

Figure 52: Jittered residual plot for snail_conc_sr˜water_conc_sr

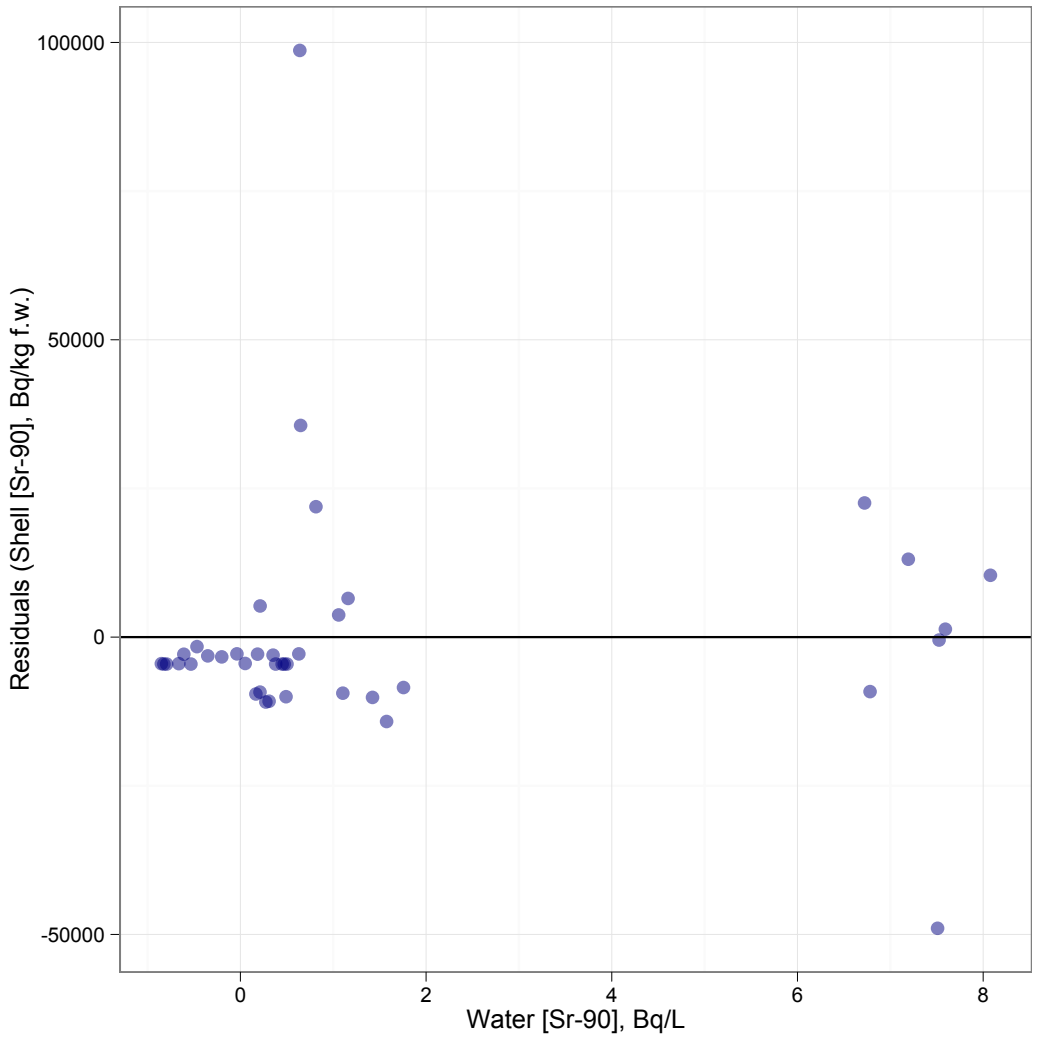

6.6.6 Improving R^2 by use of additional explanatory variables

Statisticians are very aware of the fact that the inclusion of additional variables will increase the fit of a model (as indicated by multiple R^2); additional explanatory variables may even cause R^2 to approach unity. For the model above, this tendency is illustrated in table 62, below, which shows the improvement in R^2 as each new linearly-independent explanatory variable is added, despite the fact that only one of these variables significantly ($p<0.05$) predicts the dependent variable (tissue concentration of ^{90}Sr). It is important to be aware of this tendency, and to exclude explanatory

variables based upon the statistical strength (p-value) of the relationship to the dependent variable in a regression model.

Table 62: Change in R^2 due to inclusion of additional explanatory variables in regression model.

# variables in model	Multiple R^2
3	0.6266
4	0.6655
5	0.6671
6	0.6918
7	0.6990
8	0.7255
9	0.7267
10	0.7513
11	0.7548

6.7 Importance of Substrate

All lures were placed in a location with a soft, muddy bottom. Due to the burrowing nature of the species under investigation, this is assumed to be the most important environmental factor for ensuring the capture of snails. This organism cannot survive on a rocky bottom, and would be highly vulnerable to predation in such an environment, even if it could survive.

7 Discussion

This study has several applications: firstly, it is the first time that voxelized dosimetry has been applied to field situations to estimate dose rates to NHB. Additionally, this advanced voxelized modeling can be applied to the determine of dose-effects relationships in situ. Finally, this data set can also be used to better understand the biogeochemical cycling of Sr in aquatic ecosystems at Chalk River Labs.

7.1 Comparison of voxelized Monte Carlo results with previous dosimetric modeling

In the past, models such as those employed by ICRP have had a significant advantage: they are relatively simple, requiring little processing power and providing estimates of dose-rates averaged across an entire organism. However, recent advancements in computing power and image processing software have afforded us the ability to calculate absorbed fractions (and therefore, DCFs) in a phantom constructed via a medical imaging modality (typically computed tomography or magnetic resonance imaging). These voxelized models can be employed to calculate organ-specific dose rates from heterogeneously distributed sources. Additionally, they are useful for the calculation of DCFs in cases of unusual geometry, such as that of a snail, where a high-Z calciferous shell encases a low-Z, soft bodied organism.

The snail study these data were derived for is part of an ongoing project conducted in collaboration with Chalk River Laboratories in Ontario, Canada. The principle radiological contaminants on site are ^{90}Sr and ^{3}H. Strontium, being homologous to Calcium, is expected to accumulate in snail shells where it may be sequestered for a number of years, resulting in a continuously high internal dose rate to these organisms. Several previous studies[5, 25, 79, 38] have relied upon the method of Blaylock[12] to estimate dose rates in benthic macro invertebrates. This method assumes a simplified (ellipsoidal) geometry and homogeneous distribution of internally deposited radionuclides and calculates dose via a point source methodology. Using these the dosimetry methodology described by Blaylock[12], which employs an ellipsoidal model, and radionuclide tissue concentrations data from snails harvested from the Chalk River Laboratories site, previous work[38] determined that burrowing aquatic snails experience, at a maximum, dose rates on the order of tens of milligrays daily, making the basis for a comparison of dose conversion factors as determined via simplistic versus

voxelized models. Environment Canada has recommended a threshold of 2Gy a^{-1} as the no-effects limit for macro-invertebrates[5]. As some sites at Chalk River Laboratories may exceed this limit, accurately determining dose in these invertebrates is of some importance.

7.1.1 Blaylock 1993

There is considerable difference between the absorbed fraction data as derived from a simplified model (e.g., Blaylock) and a voxelized model. Unsurprisingly, the resultant DCFs (Table 63) also differ by approximately an order of magnitude. It is difficult to know the exact magnitude of difference due to issues discussed in 6.1.2, relating to the combination of multiple tissue-dose rates into a single whole-body dose rate. Figures 53 and 54 depict the difference in AFs for simplified and voxelized models. The voxelized DCFs assume the source is perfectly partitioned into snail shell. Segment dose rates from the voxelized model were combined using different weighting schemes to produce a more appropriate comparison with the whole-body DCF generated via the simplified model.

Table 63: DCFs (μGy kg $Bq^{-1}d^{-1}$) for Strontium-90 (including Yttrium-90) for the simplified and voxelized models.

Simplified	Voxel - Body	Voxel - Shell	50/50 weighted	mass weighted	volume weighted
$1.43x10^{-2}$	$2.21x10^{-3}$	$7.97x10^{-3}$	$5.09x10^{-3}$	$4.53x10^{-3}$	$3.85x10^{-3}$

Figure 53: Comparison of segment-specific electron absorbed fractions for (a) source in shell and (b) source in body with whole-body absorbed fractions from Blaylock[12].

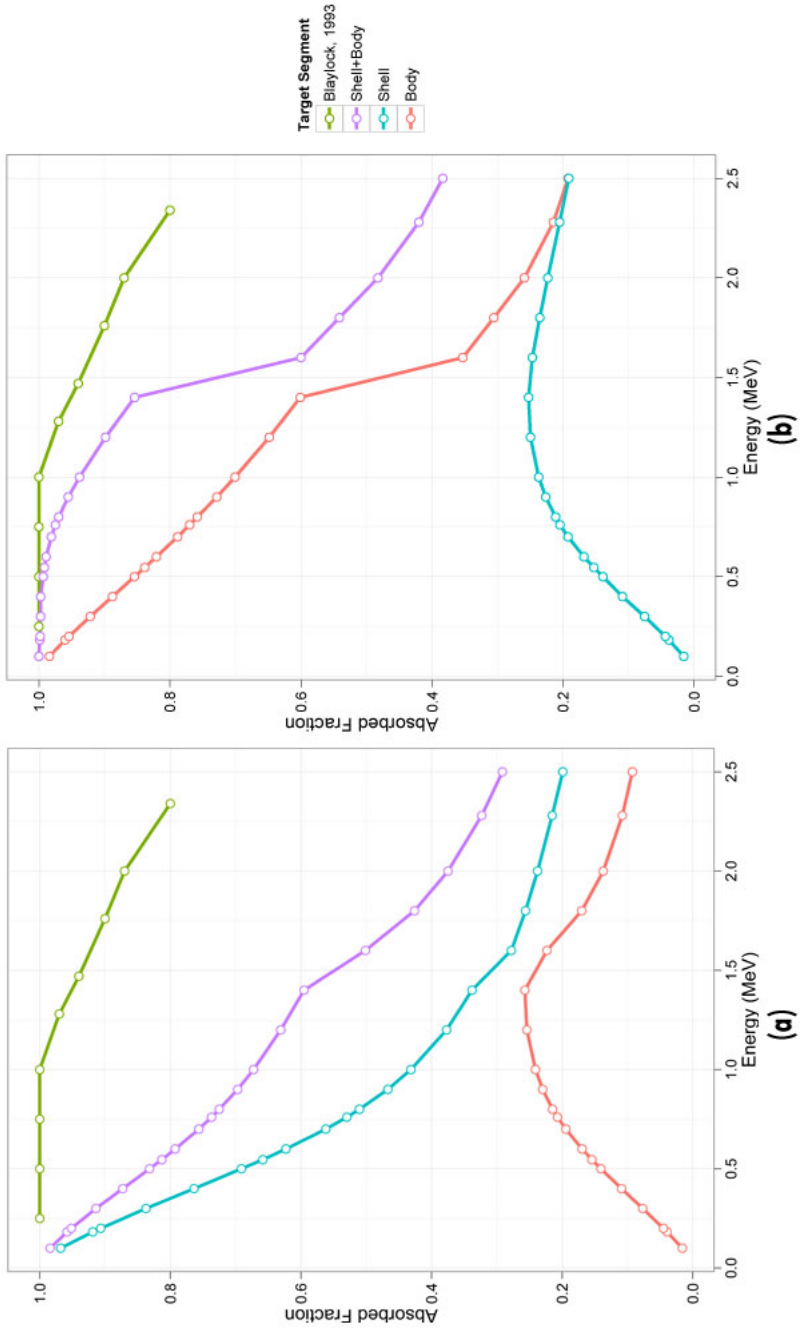

Figure 54: Comparison of segment-specific photon absorbed fractions for (a) source in shell and (b) source in body with whole-body absorbed fractions from Blaylock[12].

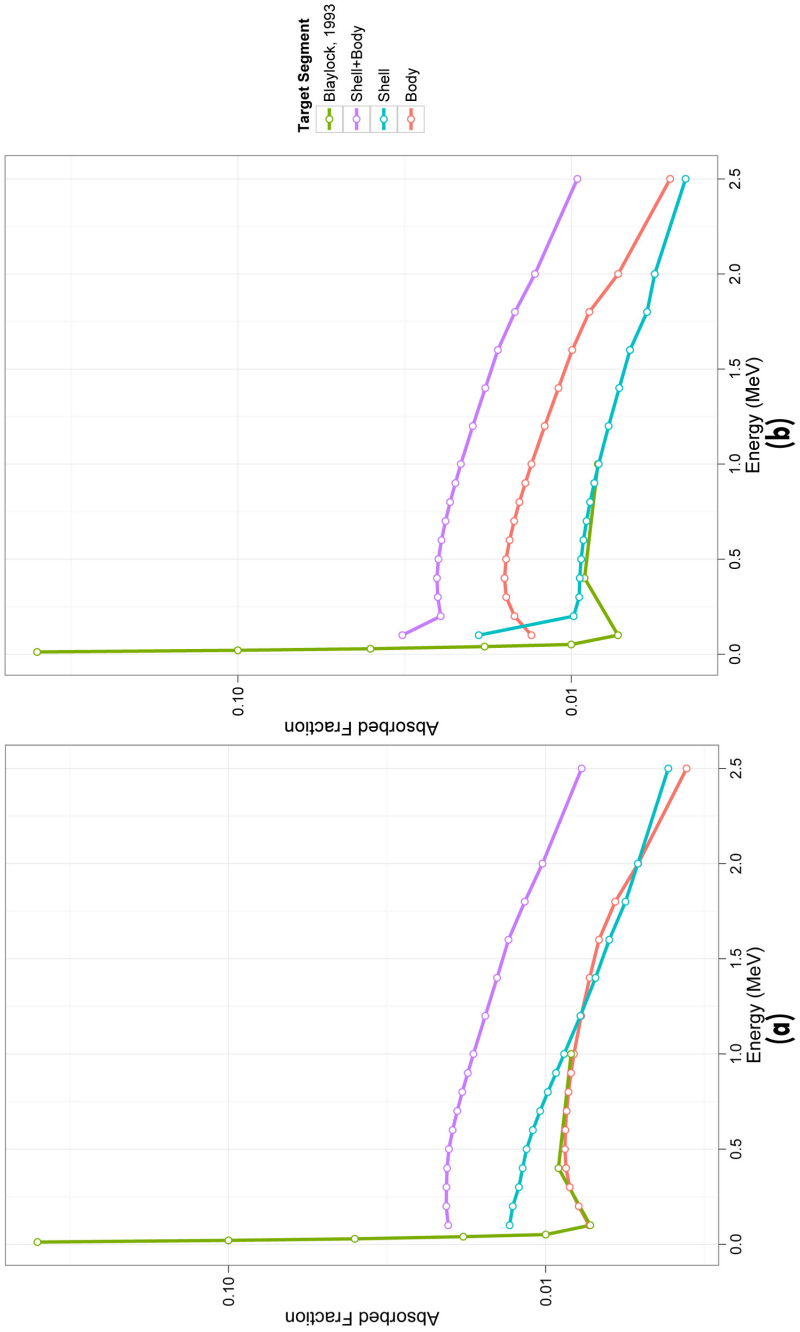

7.1.2 Voxel vs Simplified Modeling

Absorbed fractions calculated from the snail voxel model are consistently lower than absorbed fractions calculated from a simpler model. It is clear that the small size of the organism under study drastically affects energy deposition not only for low LET radiation such as photons, but also for higher LET electrons. Furthermore, the individual imaged in this study was selected due to its large body size; smaller specimens of the same species may receive even less energy deposition. These considerations indicate considerable conservatism in previous AF data for macro-invertebrates. While conservatism is often desirable, excess conservatism can result in the misallocation of resources. Our study site at Chalk River Laboratories is one such case: aquatic snail dose rates calculated via the simplistic model exceed threshold values at several sites, while those calculated utilizing voxel model results do not. Justification of risk and/or remediation of a site are expensive and time consuming; far better to improve dosimetric modeling to more accurately reflect the dose rate experienced by a population.

One potential drawback to the voxelized approach is the inability to sum individual organ dose rates into total body dose rates, as occurs routinely in the human dosimetric paradigm. The lack of tissue weighting factors for RAPs is somewhat vexing, but the creation of such parameters may be superfluous: in some aspects it makes more sense to consider individual organ dose rates when the goal is protection of non-human biota. The goal of NHB protection is the maintenance of populations, not individuals. Under this paradigm protection standards exist to prevent deterministic effects, particularly those that would impact population levels (e.g., reproductive effects). High organ doses rates caused by a well-partitioned radionuclide could result in reduced functionality of anatomic systems. This reduction or loss of functionality, in turn, impacts overall health status of individuals, and in the sum, population health. This ties back to the conservatism requirement: there is less need to be conservative if you are able to more accurately estimate organ doses, and therefore potential deterministic effects.This analysis bears particular consideration for the aquatic snails at Chalk River Laboratories, given that the principle contaminant, Strontium-90, tends to be highly partitioned into the animal's shell. The situation in no way resembles the homogeneous distribution assumed by the simplified model, and further emphasizes the need for voxelized models, at least for those radionuclides that tend to be highly partitioned.

7.2 Comparison with studies at Chernobyl

The dose-rate ranges in this study are comparable with those found in the work of Møller and Mousseau, who have extensively studied[55, 54, 57, 56, 58] the wildlife in and around the Chernobyl exclusion zone. These authors have reported a strong, negative relationship between radiation dose rate and population sizes for a variety of organisms (insects, birds, and some species of higher plant) at dose rates very comparable to those under investigation in this study. As this study found no evidence of such a relationship in snails, it represents an important piece of work and a significant contribution to the on-going discussion concerning the ecological effects of radiation exposure.

7.3 ANOVA Results

The ANOVA results from this study reveal interesting trends and patterns among those environmental variables which appear to impact snail populations, quantified as either the mass of individuals or the number of snails lured. Firstly, it is important to note that no relationship was found between radiation exposure and either measure of population health (snail size or number of snails lured). This is especially well illustrated by figure 55, which depicts snail mass as essentially unchanging ($p=0.70$) over the range of dose rates studied as a part of this study (and encompassing four orders of magnitude).

Figure 55: Snail mass as a function of snail shell dose rate.

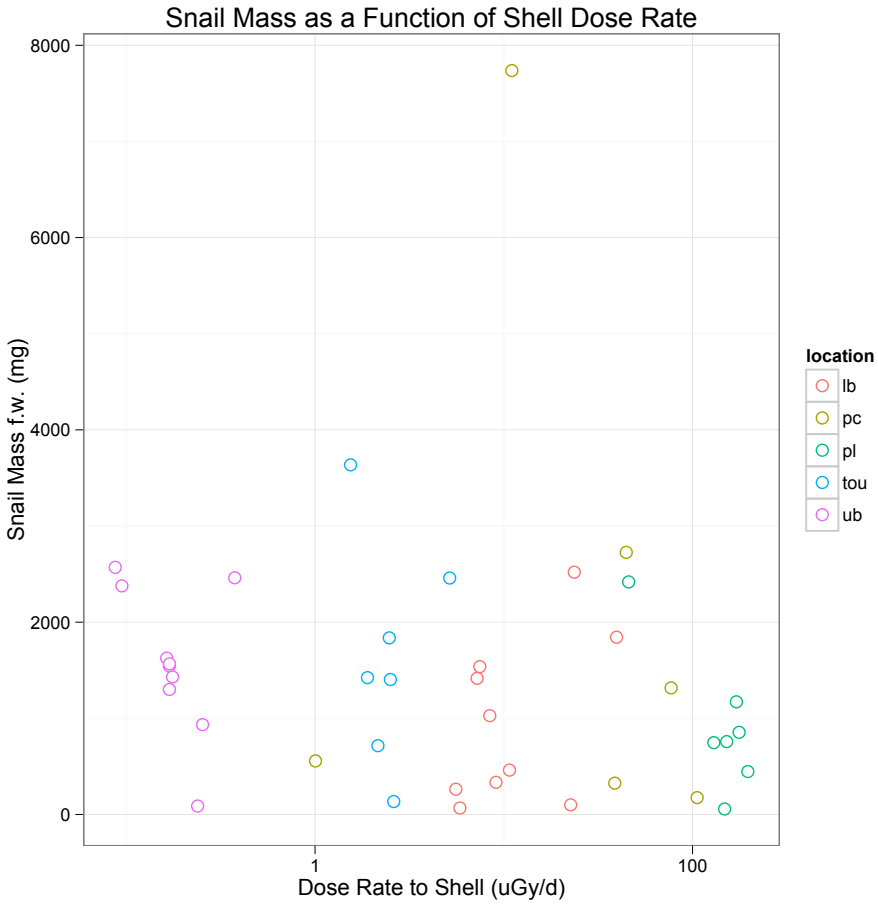

However, it is equally of note that this study was able to confirm previously understood biogeochemical influences upon the health status of snails. The correlations of snail mass and snail number with environmental Ca and P, respectively, is of note. That these relationships were statistically confirmed by this study lends credibility to the effectiveness of both the environmental endpoints and the methodologies utilized, as well as overall study design and implementation.

8 Conclusion

Environmental radiation protection is an important area of research: the determination of action-levels for cleanup will determine the fate of billions, perhaps trillions, of dollars. Remediation is expensive, and money earmarked for such purposes should be spent in such a way that it has the maximum protective effect. Determining where these clean-up limits ought to be set for radiologically contaminated sites remains controversial: it is an emotional subject, and a dearth of data concerning the field effects of radiation on NHB have made it difficult to set such action limits with a high degree of confidence.

This study has been successful inasmuch as it has demonstrated a field methodology for the evaluation of radiation dose-effects relationships in non-human biota. This type of study brings key improvements to previous dosimetric methodologies, and also underscores the importance of a biogeochemical methodology in radioecological studies. Furthermore, this study has informed the debate concerning "no effects" levels of contamination: there was no evidence that radiation dose rate affected either the number or mass of snails found at ^{90}Sr shell dose rates up to c.a., 20 μGy-hr^{-1} and ^{90}Sr body dose rates up to c.a., 5 μGy-hr^{-1}. Finally, it has contributed useful concentration ratio data, which will be utilized to improve existing NHB impact models such as the ERICA[17] tool.

The type of robust field study conducted here has the potential to inform and transform the way radioecological field studies are conducted, and will hopefully serve others well for informing the discussion concerning the transfer and impact of radionuclides upon the environment.

APPENDICES

A Technical Theory

Following is a description of the theoretical basis for techniques used in this dissertation.

A.1 Gamma Spectroscopy

Gamma spectroscopy is a technique used for the detection of ionizing photons (very roughly in the range of 10keV to 10MeV). Most commonly, gamma spectroscopy is used to detect those photons emitted by radioisotopes, and less commonly for quantifying machine-produced ionizing radiation. As a spectroscopic technique, energy discrimination is employed to produce a spectrum of counts, binned together by energy, that is characteristic of the materials or mechanical techniques producing gamma radiation. Figure 55 shows a sample gamma spectrum.

Figure 56: Gamma spectrum, without energy calibration

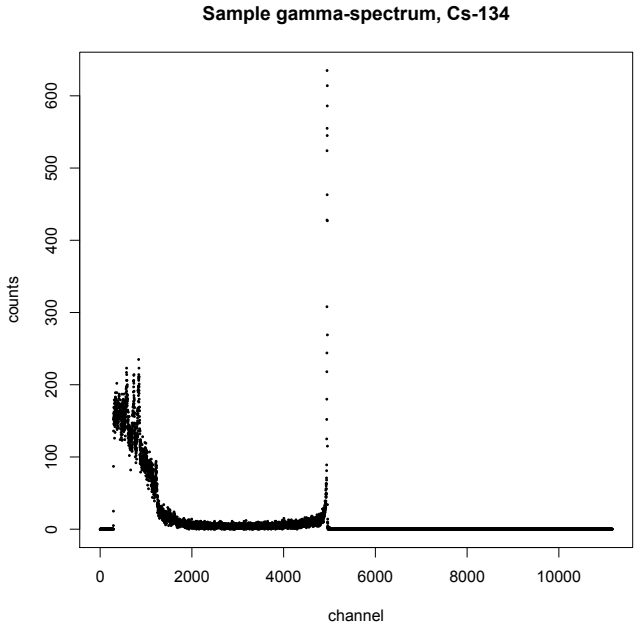

There are many materials used to construct detectors of gamma-wavelength photons, ranging from semiconductors to crystals to plastic scintillators; all of these operate according to roughly the sample principles - the idea being to capture the gamma photon and emit, eventually, an electron which can be counted - with some variation in their physics. This study relied upon high-purity germanium

detectors (HPGe) for all gamma spectroscopy and so the theory of this particular kind of detector is detailed here.

A germanium detector is a semiconductor detector in which radiation is measured by the number of charge carriers set free within the detector volume by an incident photon. Charge is liberated via the promotion of an electron from the valence band to the conduction band (0.7eV in the case of an HPGe detector); thus the number of electron-hole pairs is proportional to the energy deposited by the incident photon. The small band-gap results in excellent energy resolution for incident photons, however, thermal movement at room temperature is capable of promoting an electron to the conduction band, and thus, to avoid noise, such detectors must be cooled to liquid nitrogen temperatures (77K).

The electrical signal out of the detector is passed through an preamp and amplifier before being proceeding into a multichannel analyzer (MCA), which uses binning by pulse height to produce a discrete spectrum that very closely approximates the true continuous distribution of photons incident on the detector. The output of the MCA can be displayed graphically through software such as Gamma Vision or exported as a tally of counts per channel (or energy bin, if the detector has been calibrated to display in energy units).

A.2 Liquid Scintillation Counting (LSC)

Liquid scintillation counting is typically employed for counting low-energy beta or alpha particles. These particles tend to be difficult to count through traditional means due to both self absorption and attenuation in both air and the boundaries of the detection medium (for example, the steel plate around NaI detectors intended to protect the hygroscopic crystals used for detection). In liquid scintillation counting (LSC), the source is dissolved in a liquid, photolumiscent medium ("scintillation cocktail"). This eliminates the self-absorption problem and reduces the attenuation problem.

The scintillation cocktails used in LSC have historically been based on toluene or other organic

solvents with high capacity for stimulated luminescence. Incident radiations (beta and alpha) from the sample stimulate molecular electrons into higher orbitals; when these electrons decay to ground state they emit light in the visible portion of the spectrum. *Quench* is a measure of the efficiency of the collection of the visible-spectrum photons. *Color quench* is an interference that arises due to the optical properties of the sample solution (color in the solution is caused by absorption of a specific range of photon wavelengths) that results in a reduced collection efficiency of the scintillation photons. *Chemical quench* is process in which the sample solution (which is often acidic) interferes with the efficiency of the scintillation cocktail itself, often by decomposing the delicate organic molecules that luminesce in response to incident radiation. All forms of quench must be corrected for to produce a quantitative estimate of the activity present within a sample.

LSC relies on photomultiplier (PM) tubes to detect the scintillation photons emitted by the LSC cocktail. The counting must be done in darkness so that ambient light does not interfere with the collected signal. PM tubes function by converting incident photons to electrons through the use of a photoscintillator. These electrons are amplified through a series of stages ("dynodes") so that each incident photons corresponds to a pulse of current output from the PM tube. As in HPGe counting, above, this signal is typically sent through a multichannel analyzer (MCA), which uses pulse-height binning to produce a spectrum which mimics the distribution of energies of photons incident on the detector. In LSC this spectrum is shifted toward lower-energies than the true energies of the incident photons due to energy transfer inefficiency between the incident radiation and scintillation cocktail.

A.3 Inductively Coupled Plasma Mass Spectrometry (ICP-MS)

Mass spectrometry is a four-step process depicted in Figure 56: (1) atomization of a sample, (2) ionization of a substantial portion of the atoms formed in (1), (3) separation of the ions based on their mass-to-charge ratio ($^{m}/_{z}$), and finally (4) detection and counting of the ions for each unique $^{m}/_{z}$ ratio[72]. The process for each of these four steps is outlined here for the ICP-MS (inductively coupled plasma mass spectroscopy) technique used in this study[72].

1. Atomization and ionization are accomplished simultaneously using an Argon plasma torch following sample introduction with a nebulizer. This torch vaporizes the water matrix and strips the ionic constituents of their electrons.

2. See step (1) above.

3. The positively charged ion stream is focused, then passed into a quadrupole magnet that separates the postively-charged atomic ions by their mass-to-charge ratio, manipulating the trajectory of each unique $^{m}/_{z}$as it passes through the magnetic field.

4. The outgoing cations are collected in an electron multiplier that has been calibrated such that the location of each incident particle of determined $^{m}/_{z}$ is known. This current is amplified, processed and read out through a computer interface.

Figure 57: Conceptual diagram depicting each step of an ICP mass spectrometer.

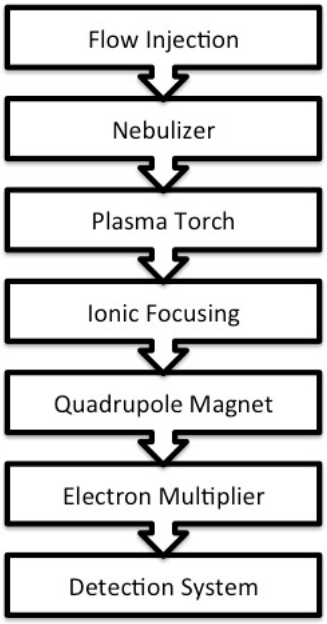

A.4 Inductively Coupled Plasma Atomic Emission Spectrometry (ICP-AES)

Sample introduction in ICP-AES relies upon the same plasma torch and nebulizer setup as ICP-MS (see A.4). Introduction to the plasma causes atomic ionization, followed by recombination. The ionization process results in characteristic light being emitted from the sample, the intensity of which is proportional to the amount of a given element within the atomized sample; the light is measured using a PMT and the signal sent through a standard spectrophotometric processing system (MCA, etc) before final output as an energy-binned spectrum on a computer.

A.5 Column Chromatography

Column chromatography is a chemical procedure that relies upon the sorption properties of a particular chemical species on a particular surface. The sorption properties may be determined by the size of the species to be sorbed, its chemical state, its electrical charge, or other properties. *Cation exchange column chromatography* will be the focus of this section, as it was the type of chromatography utilized as a part of this dissertation.

Ion exchange column chromatography relies upon the sorption of ions onto a resin bed that has been specially treated to create a chemiselective surface, either for a specific size or specific charge state of species (or both). For this dissertation, a Sr specific resin was procured from Eichrom (Lisle, IL). Eichrom prepares their resin by binding a crown ether (4,4'(5')-di-t-butylcyclohexano 18-crown-6) to resin beads[66]. This crown ether is size-specific for Sr extraction (allowing good separation from homologous Ca) and also provides a source of donor electrons that increase the bond strength of the composite species via electromagnetic interactions. On a molecular scale: the resin (specifically, the crown ethers bound to the resin) when treated with acidic media become protonated. As Sr passes through the column, it displaces the protons by sorbing more strongly (more energetically favorably) to the crown ether. When the resin is washed with a neutral pH media (e.g., water), the bound Sr washes out as a hydration product.

Cations other than Sr and H (such as Sr's daughter product, Y) are not bound to the resin due to size and/or charge exclusion principles; thus after passing the sample solution through the column, only Sr remains bound to the column. During the elution step, a purified solution of Sr in water is produced, which is an excellent preparation for liquid scintillation counting.

A.6 Monte Carlo Modeling

Monte Carlo is a computational science that relies upon random sampling to obtain numerical results. It is a category of modeling that is distinct from deterministic methods, where a transport equation is analytically solved for the average particle behavior. Thus, Monte Carlo methods are most powerful when being utilized to provide solutions to problems where it is impossible to derived a closed form expression for the behavior under investigation. These transport methods simulate particle transport by sequentially modeling each interaction of a subatomic particle (e.g., electron models consider collisional energy losses, coulombic scattering, Bremsstrahlung, knock-on and Auger electrons, and secondary production of x-rays). The computational algorithm then records some "characteristic of interest" that is a part of the typical particle behavior in a user-specified "tally". As the number of particles simulated increases, these results converge upon a normal distribution whose average value is the numerical representation of the characteristic of interest (this is mathematically provable via the central limit theorem). Since the precision of the measured characteristic is proportional to the number of particles measured, uncertainty in the calculated parameter may also be estimated.

The name "Monte Carlo" is a reference to the statistical sampling process itself, which is analogous to rolling dice and gives rise to realistic and complete particle histories through the random sampling of probability distributions (e.g., chance of particle scatter or absorption). Each run models the complete history (from particle "birth" until "death") for a user-specified number of particles based upon probabilities (transport data) and rules (physics!). This provides a complete and realistic model of the behavior of subatomic particles within the modeled system.

A.7 Least-Squares Regression Modeling

Least-squares regression is one of the oldest statistical methods, first described in 1805, although it had been in use since 1795[30]. The earliest uses of regression modeling were *linear* models, which explain a single variable as a function of another single variable. For this study, *multiple regression* was employed, wherein a single variable is expressed in terms of several explanatory variables. Both these methodologies rely upon the same mathematical concepts, which provide the foundation for nearly all regression and analysis of variance procedures in statistical computing. This section will examine the theory of regression modeling utilizing linear regression; statistical computing packages take much of the work out of the analogous situation in multiple regression. It will loosely follow the derivations of Ramsey and Schafer[30].

The goal of regression is to produce a linear function in the form of eqn A.1, below.

$$fit_i = \hat{\mu}\{Y|X\} = \hat{\beta}_o + \hat{\beta}_1 X \tag{A.1}$$

Where the carat (ˆ) symbol indicates the estimate of the parameter under the hat. So in this case, μ, the estimated mean (or *predicted value*) of the function Y regressed upon X is explained by two variables, $\hat{\beta}_o$ and $\hat{\beta}_1$. The residual ($\mathrm{res_i}$, eqn A.2 below) is an indicator of the quality of the fit, and measures the difference between the observed data, $\mathrm{Y_i}$ at some $\mathrm{X_i}$ and the regression model's predicted value at that same $\mathrm{X_i}$:

$$res_i = Y_i - fit_i \tag{A.2}$$

The magnitude of the difference for a single point does not represent the fit of the entire model, and so instead, the residuals are summed and squared to give an estimate of quality-of-fit known as the residual sum of squares. By minimizing the parameter $\mathrm{res_i}$ via differentiation, it is possible to derive expressions for $\hat{\beta}_o$ and $\hat{\beta}_1$ (eqns A.3 and A.4, below) such that the residual sum of squares is minimized, hence *least squares analysis*.

$$\hat{\beta}_1 = \frac{\Sigma_{i=1}^{n}(X_i - \bar{X})(Y_i - \bar{Y})}{\Sigma_{i=1}^{n}(X_i - \bar{X})^2} \tag{A.3}$$

$$\hat{\beta}_o = \bar{Y} - \hat{\beta}_1 \bar{X} \tag{A.4}$$

Another useful parameter for regression analysis is the number of degrees of freedom (DF), which is given by the number of observations minus the number of parameters in the model.
The parameters $\hat{\beta}_o$ and $\hat{\beta}_1$ are themselves distributions with a representative variance, $\hat{\sigma}$, which can be related to the residuals and number of degrees of freedom by equation A.5, below:

$$\hat{\sigma} = \sqrt{\frac{\sum_{i=1}^{n} res_i^2}{DF}} \tag{A.5}$$

The variance can further be related to the standard error of the spread for both $\hat{\beta}_o$ and $\hat{\beta}_1$, for n degrees of freedom, by equations A.6 and A.7, below.

$$SE(\hat{\beta}_1) = \sigma\sqrt{\frac{1}{(n-1)s_X^2}} \tag{A.6}$$

$$SE(\hat{\beta}_o) = \sigma\sqrt{\frac{1}{n} + \frac{\bar{X}^2}{(n-1)s_X^2}} \tag{A.7}$$

Where s_X^2 is the sample variance for all X values. These equations provide a means for the calculation of 95% (2σ) confidence intervals for the regression fit.

Combined, these mathematical relationships provide a powerful tool for describing relationships between empirically derived data such as the regression models run as a part of chapter 6.

A.8 Assumptions underlying least squares regression

Regression modeling relies upon four major assumptions[30]. Following is a discussion of each assumption and how the data in this study meet (or do not meet) them.

1. *There is a normally distributed subpopulation of responses for each value of the explanatory variable;*

   Normality is met fairly well by the data in this study. Even without log transformation, it is clear from the strip-charts presented in chapter 5 that the data are roughly normally distributed. Given that regression modeling and the F-test (below, A.9) are fairly resistant to deviations from normality[30], it is safe to conclude that this assumption will not influence the outcome of the modeling efforts conducted as a part of this study.

2. *The mean of all the subpopulations fall on a straight line function of the explanatory variable;*

Again, by examining the strip charts in chapter 5, it is reasonable to conclude that the mean of subpopulations are linearly correlated with the explanatory variable.

3. *The subpopulation standard deviations are all equal (to σ);*
   Change in variance is of most concern for sets of data whose predictor variables vary over a wide scale (e.g., orders of magnitude difference in the numerical value of a variable). In practice for this model, the only variable that shows large variation in magnitude is the light reaching the snail trap. Fanning in a residuals plots is another method of determining whether or not subpopulations have equal variance[30]. In the case of the model run for this study, there is some minimal fanning of both water calcium at light, but neither is severe enough to invalidate the model (see section 6.4.5).

4. *The selection of an observation from any of the subpopulations is independent of the selection of any other observation.*
   There are two parts of this assumption: multicollinearity and the independence of measurements. To eliminate the first, multicollinearity was tested for and collinear variables eliminated utilizing the variance inflation factor (see section 6.4.2). But, more generally, statistical inference relies upon the principle that each response variable sampled is independent of all the other response variables sampled, and associated with uniquely measured explanatory variables. This is violated a number of times throughout my protocols: firstly, each snail is not lured by its own unique trap; many snails are attracted to each trap. This means that, within the model, some snails share common characteristics (such as water temperature at a trap, or the light recorded at the trap). More generally, snails of the same lake are in the same water environment (in terms of dissolved ion concentration), and also in terms of dose rate for those snails whose radionuclide tissue concentrations were not measured directly. These variables were measured multiple times (but not independently for each snail) average values were applied across the board to snail mass data, as though they had been measured independently. While this is not considered rigorous by statisticians, ecological sampling is fraught with such simplifications by its very nature.

The calculation of internal dose, as shown above in section 4.5, is mathematically nothing more than the permutation of tissue concentrations resulting in the creation of several linearly dependent dose rates. Because of this, inclusion of multiple tissue dose rates in the regression model will result in multicollinearity between those variables, violating requirement number four, above. Because of this,

it is not only unnecessary but actually impossible to include multiple tissue dose rates as explanatory variables in a population regression analysis. It is worthwhile to note that this mathematical reality does not reflect the biological reality, in which the tissue experiencing the highest dose rate may not be the limiting structure in terms of organism survival, or another endpoint. Therefore, regression analysis should be regarded with caution: it is important to understand the biology of the organism(s) under study so that mechanistically appropriate explanatory variables may be included in the regression model.

Finally, it is of note that this study was observational, not experimental in nature. Thus, all conclusions about environmental factors that influence snails' population and/or size are correlative, not causative. While it is possible to propose that a causative relationship exists, it is not statistically possible to establish this relationship with randomization of treatment groups. As treatment groups were already established for this study (by pre-existing contamination on-site) it was not possible to perform this randomization. However, the location and concentration of contamination is semi-random since the original point of geospheric infiltration could be considered to be randomly selected (radionuclide contamination does follow ground-water dispersal patterns into lakes and water bodies at CRL).

A.9 Analysis of Variance and the F-test

Regression modeling can provide a t-ratio by which it is possible to examine the significance of a variable within a linear model. The t-ratio is defined by equation A.8[30]:

$$t - ratio = \frac{\hat{\beta}_j - \beta_j}{SE(\hat{\beta}_j)} \tag{A.8}$$

Where β_j is the j^{th} regression coefficient and the standard errors are given for a simple regression model in equations A.6 and A.7, above. This ratio leads directly to the ability to test the significance of each regression coefficient on a t-distribution by associating a probability that the regression association is due to random chance and data distribution rather than actual effect.

The F-test is a method for testing the overall significance of a regression by examining the extra sum-of-squares produced by the inclusion of extra variables within a linear model. This method compares a "full" model with all variables included to a "reduced" model which includes only significant

variables. The F-statistic is determined according to equation A.9:

$$F - statistic = \frac{\left(\frac{\text{Extra sum of squares}}{\#\text{of}\beta\text{s tested}}\right)}{\hat{\sigma}^2(\text{full model})} \tag{A.9}$$

Where the extra sum of squares is the difference between the residual sum of squares for the full and reduced models. When the reduced model - that is, the model with non-significant variables excluded - is correct and all model assumptions (see section 6.4.1) hold, the F-statistic is distributed along an F-distribution, allowing for the estimation of an associated p-value that is characteristic of the strength of the model.

B Protocols and Procedures

Following are step-wise procedures of interest to any person replicating the work conducted as a part of this dissertation.

B.1 Snail lure placement

1. Shallow, mucky areas are preferable for finding the burrowing Campeloma. Limited rocky presence and limited amounts of vegetation make for the easiest sites for snail recovery.
2. Before placing lure:
   (a) Measure water pH
   (b) Measure water temp
   (c) Measure water TDS (ppm KCl scale)
   (d) Measure light in the area where you'll be placing the trap (note weather conditions: e.g., sunny or cloudy)
   (e) Photograph the site
   (f) Take a water sample (nalgene bottle)
   (g) Take a sediment sample (Ziploc baggy)
   (h) Note dominant substrate if other than silty/muddy sediment.
3. Lures are made by placing an approximately 1oz (30 mL) scoop of chicken dung in the center of a piece of cheesecloth. The corners are tied together to make a pouch, and then tied to a wooden stake. The pouch should be placed such that it is resting on or slightly buried in the mud. Attach a piece of flagging tape to the stake to make it easy to spot.
4. Note GPS coordinates of the lure.
5. Lures should be checked approximately 10d after being placed.

6. Soil samples can be placed in the freezer, water samples should be acidified w/ 3mL of pure nitric acid and left on the counter.

B.2 Snail lure retrieval

1. Place the square metal quadrat so that it is centered on the lure itself – not the stake the lure is attached to. Push the quadrat into the mud.
2. Pull up the lure. Remove any snails on it to a sample cup with water (keep the snails alive, please!).
3. Using the sieves and trowels, gently excavate the top 6" of mud that are within the quadrat and check for snails. Remove any snails to the sample cup.
4. For each snail:

    (a) Measure/record mass (jeweler's scale – please note the mass of the 10g calibration weight each time you use the scale).

    (b) Measure/record max shell length (digital calipers).

    (c) Mark with nail polish (if not already marked) and record if snail has been marked previously.

    (d) Note and record total number of snails, as well as number of each species (most common in the lakes and streams seem to be Campeloma and Physella).

5. Pick 1/3 of the lured snails for harvesting. Remove these to a separate Ziploc bag. When you return to the lab, transfer them to clean water to flush the GI tract.
6. Release remaining snails back into the water.
7. Place a new lure at a minimum of 10m away from where the old lure was set.

B.3 Snail preparation

1. Live snails are euthanized by freezing at -23^{o}C for a minimum of 24h.
2. Snails are warmed to room temperature in a water bath to ensure that tissues are pliable.
3. The snail is washed in tap water and dried. A wet mass is recorded.
4. The snail is separated into shell and body portions.
5. The snail is dried at 60^{o}C for a minimum of 48h.
6. The dry mass of the shell and body portions are recorded separately.

B.4 Water sample processing (AES)

1. Acidify solution with 3mL of 67% environmental grade nitric acid per 250mL of water upon returning to the lab.
2. Filter 60mL of water through a Whatman 0.45μm cellulose nitrate membrane filter using a syringe.
3. Deliver 50mL centrifuge tube of filtered water to the chemistry division for AEMS.

B.5 Water sample processing (^{90}Sr analysis)

1. Add 1L of water (as measured with a volumetric flask) to a glass beaker or (preferably) a polyethylene jar. The water has previously been acidified at a ratio of 3mL 67% HP nitric acid / 250 mL water (12mL total). A stir bar is also placed in each sample jar.

2. Sample jar is placed on a stirring plate. 1mL of Sr standard ($1.0^{\text{mg}}/_{\text{mL}}$ stable Sr) is added to each sample. (w/ continuous stirring)

3. Remove 1mL of water from sample jar; send for analysis of Sr concentration by ICP-MS.

4. 2mL of $Ca(NO_3)_2$ solution is added to each sample ($40\ ^{\text{mg Ca2+}}/_{\text{mL}}$). (w/ continuous stirring) Prep for this standard:

5. 1mL of concentrated phosphoric acid (H_3PO_4) is added to each sample. (w/ continuous stirring)

6. Adjust the pH (check w/ pH paper) using concentrated ammonium hydroxide until the solution reaches above 9. This should take 3-20 mL of NH_4OH (varies with water source). Calcium phosphate precipitate will form once the solution turns basic. (w/ continuous stirring)

7. Half of the sample is placed in a 500mL centrifuge tube.

8. Centrifuge at 3500rpm for 3minutes. Discard the supernatant. Add the second 500mL aliquot and centrifuge again for 3 min at 3500rpm. Discard the supernatant. Rinse sample jar with 3 aliquots of ddH_2O. Add these to the centrifuge tube and centrifuge again for 3 min at 3500rpm. NOTE: If precipitate does not settle, centrifuge again at 1000 rpm for 3min, then decant.

9. Wash the precipitate with 150mL of ddH_2O; agitate the tube to loosen the precipitate button.

10. Centrifuge sample at 3500 rpm for 3 minutes. Discard the supernatant. NOTE: If precipitate does not settle, centrifuge again at 1000 rpm for 3min, then decant.

11. Add 10mL of concentrated HNO_3 and transfer solution to a 50mL centrifuge tube. Add up to 10 mL of ddH_2O. Sample is now ready for column chromatography.

B.6 Snail shell digestion

1. The shell is dissolved in 8mL of neat nitric acid overnight in a 50mL centrifuge tube. Note: some of these digestions were a little too vigorous; samples that had noticeable precipitate outside of the container were discarded.

2. After ca. 24h, 2mL of 70% H_2O_2 is added, and the samples are again allowed to sit overnight to digest any organic material.

3. Next, 1mL of cold strontium ($1^{mg}/_{mL}$ Sr2+ in 2% HNO_3) standard is added to each digestion, followed by 6mL of ddH_2O. 1mL of this mixture is diluted in 49mL of 1% HNO_3 and sent for ICP-MS (Ca+Sr).

B.7 Snail body digestion

Before and between samples, digestion vials are washed by microwaving 6mL of high purity 67% nitric acid at 500W for 10 minutes. The acid wash is discarded and vial components are rinsed twice in ddH_2O. This wash is also discarded.

The mass of the sample to be digested is recorded. For safety, each digestion must contain < 0.500g of sample. All samples were sufficiently small to be digested whole. Samples are digested in 6mL of high purity 67% nitric acid + 1mL of high purity 30% H_2O_2. The protocol used for digestion is given in Table 64.

Table 64: Microwave digestion protocol

Time (min)	Power (watt)
1	250
1	0
5	250
5	400
5	650

Samples are allowed to cool for 1h before being removed from the microwave. The digestate is poured into a 20mL glass bottle, along with two ddH_2O rinses of the digestion vial. The digestate is capped and set aside. The digestion vials are then cleaned, as noted above, and reused.

B.8 Sediment Density Fractionation

Sediments were processed into a heavy fraction (HF) and light fraction (LF) utilizing sodium polytungstate density fractionation.

Drying of sediments

1. Mass out between 2.0 and 2.5g of soil. Record exact wet mass.
2. Dry overnight at 100^{o}C. Record dry mass.

Sodium polytungstate (SPT) solution

1. Add the required volume (table B.2) of deionized water in a 1L container.
2. Add the SPT mass corresponding to water volume (table B.2). Aim for the solution to be too heavy, not too light.
3. Agitate the solution.
4. Check the density with a 5mL volumetric flask.
5. Let solution sit overnight to homogenize.
6. Adjust the solution density to +/- 0.02 g cm^{-3} of target density.

Table 65: Mixing table for SPT solutions (makes 1L).

Density	SPT(g)	Water(mL)
1.00	0	1000
1.10	121	979
1.20	264	936
1.30	379	921
1.40	504	896
1.50	615	885
1.60	741	856
1.70	867	833
1.80	990	810
1.90	1125	775
2.00	1250	750
2.30	1662	637
2.40	1803	595
2.50	1930	570
2.60	2052	545
2.70	2175	527
2.80	2297	504
2.90	2420	478
3.00	2552	450

Fractionation and aspiration

Figure 57 illustrates terminology/jargon used below.

Figure 58: Density fractionation diagram.

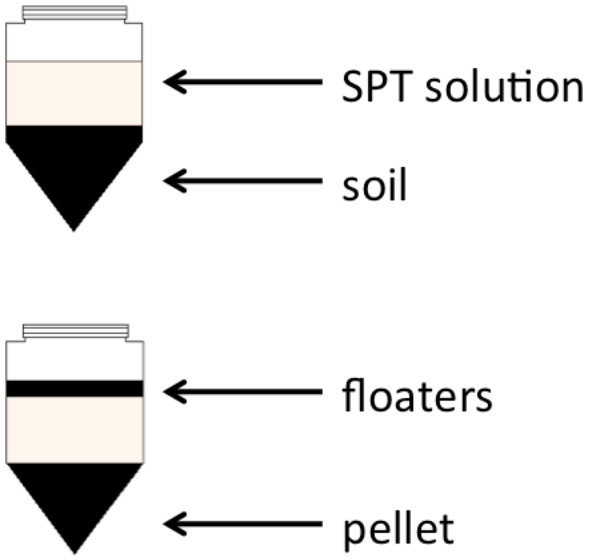

1. Add soil to a centrifuge tube & record mass.

2. Add excess SPT solution at the correct density. Seal CF tube tightly.

3. Shake 2h on low speed.

4. Centrifuge at 3000 rpm for 10 minutes (Figure 58 shows a sample after centrifugation).

Figure 59: Test tube after centrifugation.

5. Check and record density by pipetting under the floaters using a 5mL volumetric flask.

6. If adjusting density, shake up 10 minutes and centrifuge again. Repeat until you obtain the correct density (+/- 0.02 g cm^{-3}).

7. Shake 10 minutes and re-spin before aspiration.

8. Aspirate floaters and set aside.

Rinsing

1. Pour aspirate into a centrifuge tube, being sure to rinse & retain residual.
2. Fill CF tube with deionized water & spin in centrifuge 3000 rpm for 10 minutes.
3. Pour or aspirate liquid off and save for recycling.
4. Repeat this operation at least 3 times or until the density after spinning is less than 1.01 g cm^{-3}.

Vacuum Filtration

1. Pour water and contents of test tube into vacuum funnel with pre-weighed filter paper. Figure 59 depicts the vacuum filtration set-up.

Figure 60: Vacuum filtration apparatus.

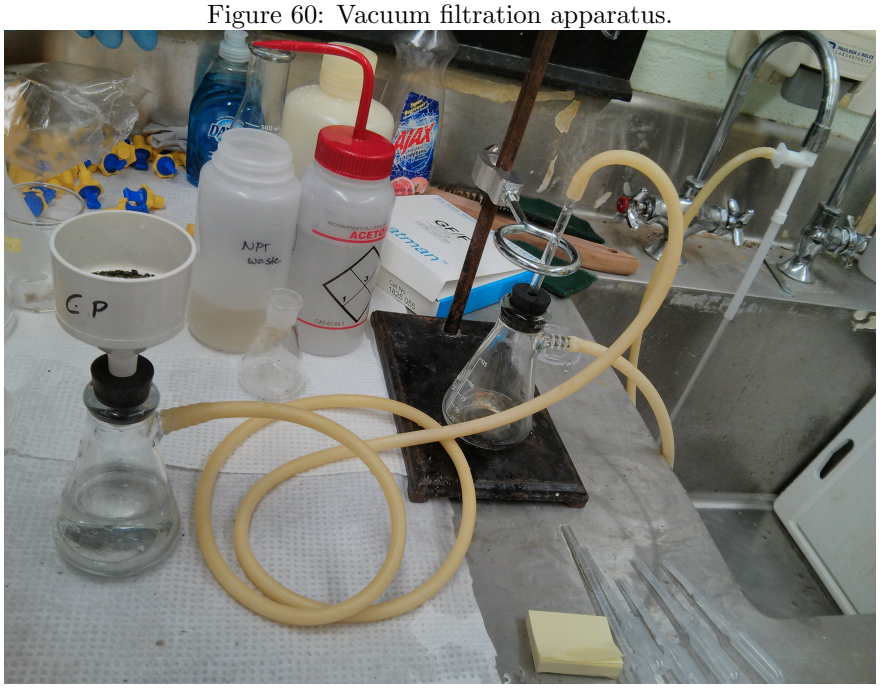

2. Vacuum line will pull off water, and begin drying of sediments.

3. Dry sediment fractions at 40 to 50^{o}C for 2 days. Figure 60 depicts samples after filtration but prior to drying.

Figure 61: Sediment fractions and filter paper masses, ready for drying.

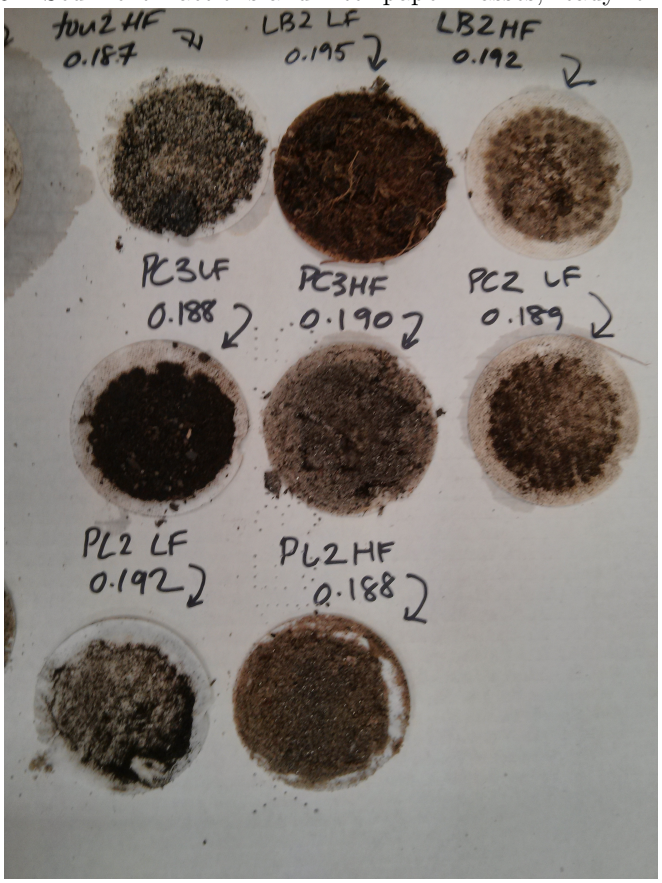

B.9 Sediment leeching

Sediment fractions were leeched in 8mL of 8M HNO_3 for 72h.

B.10 Column chromatography

Note: To use this procedure, samples must be in < 20mL of 8M HNO_3. You should also have added 1mL of mg mL^{-1} cold Sr tracer. An aliquot of this should be sent off for ICP-MS to quantify the exact concentration of cold Sr in the sample.

B.10.1 Assembling the Box

1. Place 50 mL centrifuge tubes in the vacuum box rack. Replace the lid and adjust for proper fit.
2. Place yellow outer tips (12) into the holes in the top of the vacuum box lid. Place white inner tips (12) inside the outer tips.
3. For each sample, fit a pre-labelled (usually with sample identifier) Eichrom Sr resin cartridge into the inner (white) tip.
4. Connect a 50mL syringe to the cartridge.
5. Plug any unused tips using the yellow Eichrom plugs.
6. Attach vacuum pump to the vacuum box.
7. You should also prep a second rack at this point – one that is set up for LS vials. Place 12 vials into the rack – each vial should be pre-weighed with the mass noted on the vial cap.

B.10.2 Column Conditioning

1. Add ca. 10mL of ddH_2O to each syringe.
2. Adjust the vacuum pressure to zero, then turn on the vacuum. Slowly raise the vacuum until you are pulling about 3 $^{mL}/_{min}$ through the cartridge. Note: when you first begin to draw vacuum you may need to press down (gently) on the top of the vacuum box to get a good seal.

3. Once reservoir is drained, turn off vacuum. Discard the eluate that has collected in the centrifuge tubes; return tubes to the vacuum box rack. Replace the vacuum box top.

4. Add ca. 10mL of 8M HNO_3 into the syringe. Turn on the vacuum and adjust to a flow rate of about $3^{mL}/_{min}$.

5. Once reservoir is drained, turn off vacuum. Discard the eluate that has collected in the centrifuge tubes in the acid waste.

B.10.3 Separation of Sr

1. Replace the centrifuge tubes used above with labelled centrifuge tubes corresponding to the label on the Eichrom resin (usually the sample identifier). Replace vacuum box top.

2. Add the sample solution to the syringe – verify that the centrifuge tube catching the eluate, as well as the Sr-resin cartridge, all carry the same sample identifier as the sample solution.

3. Start the vacuum – flow rate no greater than 1 $^{mL}/_{min}$.

4. Rinse the centrifuge tube with 3-5mL of 8M HNO_3. Set aside, and add to syringe when it is nearly empty.

5. Rinse the centrifuge tube a second time with 3-5mL of 8M HNO_3. Set aside, and add to syringe when it is nearly empty.

6. Add 10mL of 8M HNO_3 once the syringe is nearly empty to wash the column.

7. Once the cartridge drains, note the time, then turn off the vacuum. Remove and cap centrifuge tube; retain this in case something goes wrong with the separation.

8. Replace all inner (yellow) and white (inner) tips associated with the vacuum box (unless these tips were plugged and not in use during the separation).

9. Label your LS vials to correspond with the sample identifier they will be receiving eluate from. Place the LS rack inside the vacuum box.

10. Remove the syringe and replace with a 20mL syringe. Pipette 6mL of ddH_2O into this syringe.
11. Restart the vacuum and allow the water to pass through at a flow rate no greater than $1^{mL}/_{min}$.
12. Stop the vacuum, remove the LS vials. Discard the yellow (outer) and white (inner) tips. Remove Sr cartridges and retain in case something goes awry.
13. Weigh the LS vial with the collected eluate and record the total weight.
14. Add 14mL of scintillation cocktail and count. Note: You want to begin counting samples as soon as possible after separation. I used a 30min count for my samples.

B.10.4 ICP-MS Analysis

1. Pipette 0.2mL of eluate into a pre-weighed 50mL centrifuge tube. Record the exact mass transferred.
2. Fill tube with 0.1M HNO_3; record total mass.
3. Label sample and send for ICP-MS.

B.11 Sample MCNP card

This MCNP card shown here has been modified from the runnable version. Thirty-plus pages of geometry information ("Lattice Unit Cell") has been removed; some has been left as an illustrative placeholder. The geometry information would need to be replaced with the Voxelizer output geometry to produce a fully-functional MCNP card. However, the input shown here gives the structure used to build the snail voxelized phantom.

```
c This input file was made with the MCNP Lattice Tool
c originally created by Erick Daniel Cardenas-Mendez (a.k.a. Ace Wave)
c for the Human Monitoring Laboratory of Health Canada
c
c Input file originally created on:
c Fri Feb 8 2013
c
c Empty space universe: 4
c compression factor: 3
c
c
c
c ++++++++++++++++++++++++++++++++++++++++++++++++++++++++
c
c     Cells
c
c ++++++++++++++++++++++++++++++++++++++++++++++++++++++++
c
   999  0 999                imp:p 0 imp:e 0    $ Outside universe
   998  0          -999  5   imp:p 1 imp:e 1    $ Vacuum outer
c
c Filling Universes
    1     1  -0.966  -7  u = 1  imp:p 1 imp:e 1 $body
    10    0           7  u = 1  imp:p 0 imp:e 0
    2     2  -1.632  -7  u = 2  imp:p 1 imp:e 1 $shell
    20    0           7  u = 2  imp:p 0 imp:e 0
    3     0          -7  u = 3  imp:p 1 imp:e 1 $Exterior (Vacuum)
    30    0           7  u = 3  imp:p 0 imp:e 0
    4     0          -7  u = 4  imp:p 1 imp:e 1 $Default Surround(Vacuum)
    40    0           7  u = 4  imp:p 0 imp:e 0
c
c Lattice Unit Cell
c
    996    0   -6    lat = 1 u = 996 imp:p 1 imp:e 1
                  fill = 0:127 0:127 0:30
     4 695r 3 14r 4 106r 3 26r 4 96r 3 34r 4 90r 3 38r 4 85r 3 44r 4
     79r 3 50r 4 74r 3 54r 4 70r 3 58r 4 67r 3 60r 4 64r 3 64r 4
     61r 3 66r 4 58r 3 70r 4 55r 3 72r 4 52r 3 76r 4 49r 3 78r 4
```

```
     47r 3 80r 4 45r 3 82r 4 43r 3 84r 4 41r 3 86r 4 39r 3 88r 4

c
c Cell Containing Lattice
c
    997  0  -5  fill = 996 imp:p 1 imp:e 1
c

c ++++++++++++++++++++++++++++++++++++++++++++++++++++++++
c
c     Surfaces
c
c ++++++++++++++++++++++++++++++++++++++++++++++++++++++++
c
  999 so  10     $10cm universe
c
c Box for Filling Universes
c
  5  rpp   0.000  3.2130  0.000  3.2130  0.000  3.098698
  6  rpp   0.000  0.0251056  0.000  0.0251056  0.000  0.099958
  7  rpp   -0.001  0.0252 -0.001 0.0252 -0.001   0.1010
c

c ++++++++++++++++++++++++++++++++++++++++++++++++++++++++
c
c     Materials
c
c ++++++++++++++++++++++++++++++++++++++++++++++++++++++++
c
c body
m1
               1000    0.6241397 $body
               8000    0.2196971
               6000    0.1426367
               7000    0.0106519
               15000   0.0016644
               16000   0.0001997
               11000   0.0002996
               19000   0.0002829
               17000   0.0002164
               12000   0.0000666
               14000   0.0000666
               26000   0.0000433
               30000   0.0000350
c
c shell
m2
               20000    0.2      $shell
```

```
               12000    0.2
               8000     0.6
c Air
m7
               7000    -0.755
               8000    -0.232
              18000    -0.013
c
c +++++++++++++++++++++++++++++++++++++++++++++++++++++++
c
c        Source
c
c
c +++++++++++++++++++++++++++++++++++++++++++++++++++++++
c
mode p e
sdef erg=0.1 par=3 eff=0.001 X=d1 Y=d2 Z=d3 cel=d4
si1 0.0001 0.02509
sp1 0 1
si2 0.0001 0.02509
sp2 0 1
si3 0.0001 0.09989
sp3 0 1
si4 L u=(1<996<997)
sp4 1
*f8:e u=(1)   $body
*f18:e u=(2)  $shell
*f28:e u=(3)  $void spaces-internal
*f38:e u=(4)  $external source
*f48:e u=(1 2 3 4)  $entire snail
e8 0 0.001 2i 1.5
e18 0 0.001 2i 1.5
e28 0 0.001 2i 1.5
e38 0 0.001 2i 1.5
e48 0 0.001 2i 1.5
nps 1000000
```

References

[1] Scientific research helps the war effort. National Research Council Canada.

[2] Handbook of parameter values for the prediction of radionuclide transfer in temperate environments. Technical report, International Atomic Energy Association, 1994.

[3] Effects of radiation on the environment. Technical report, United Nations Scientific Committee on the Effects of Atomic Radiation, 1996.

[4] Guidance for the calculation of derived release limits for radionuclides in airborne and liquid effluents from ontario power generation nuclear facilities. Technical Report N-REP-03482-10000, Ontario Power Generation (OPG), 2002.

[5] *Proceedings of the Third International Symposium on the Protection of the Environment from Ioinsing Radiation (SPEIR 3)*, Vienna, Austria, 2002. International Atomic Energy Agency.

[6] 2nd International Symposium on Ionizing Radiation. *Analysis of Riverbed Sediments Near the Chalk River Laboratories*, 2003.

[7] Leonard N. Allison. Trapping snails of the genus campeloma. *Science*, 95(2457):131–132, 1942.

[8] V Arena. *Ionizing Radiation and Life*. CV Mosby, St. Louis, 1971.

[9] ZM Bacq and P Alexander. *Fundamentals of Radiobiology*. Pergamon Press, New York, Oxford, 2nd edition, 1961.

[10] NA Beresford, A Hosseini, JE Brown, C Cailes, K Beaugelin-Seiller, CL Barnett, and D Copplestone. Assessment of risk to wildlife from ionising radiation: can initial screening tiers be used with a high level of confidence? *Journal of Radiological Protection*, 30(2):265, 2010.

[11] JP Beumer and GJ Bacher. Species of anguilla as indicators of mercury in the coastal rivers and lakes of victoria, australia. *Journal of Fish Biology*, 2:87–94, 1982.

[12] BG Blaylock, ML Frank, and BR O'Neal. Methodology for estimating radiation dose rates to freshwater biota exposed to radionuclides in the environment. Technical Report ES/ER/TM–78, United States Department of Energy, Washington, DC, 1993.

[13] Richard V. Bovbjerg. Ecological aspects of dispersal of the snail campeloma decisum. *Ecology*, 33(2):pp. 169–176, 1952.

[14] CR Boyden. Trace element content and body size in molluscs. *Nature*, pages 311–314, 1974.

[15] Clare Bradshaw, Ulrik Kautsky, and Linda Kumblad. Ecological stoichiometry and multi-element transfer in a coastal ecosystem. *Ecosystems*, 15(4):591–603, 2012.

[16] F Bréchignac, G Polikarpov, DH Oughton, G Hunter, R Alexakhin, YG Zhu, J Hilton, and P Strand. Protection of the environment in the 21st century: radiation protection of the biosphere including humankind (statement of the international union of radioecology). *J Environ Radioact*, 70(3):155–159, 2003.

[17] JE Brown, B Alfonso, R Avila, NA Beresford, D Copplestone, G Pröhl, and A Ulanovsky. The erica tool. *Journal of Environmental Radioactivity*, 99(9):1371 – 1383, 2008.

[18] G P Brownless. Issues around radiological protection of the environment and its integration with protection of humans: promoting debate on the way forward. *Journal of Radiological Protection*, 27(4):391, 2007.

[19] Environment Canada. Investigation results. 2001.

[20] AP Casarett. *Radiation Biology*. Prentice-Hall, Englewood Cliffs, New Jersey, 1968.

[21] EL Cooper and JO McHugh. Migration of radiocontaminants in a forested wetland on the canadian shield: Nuclide speciation and arboreal uptake. *Science of The Total Environment*, 28(3):215 – 230, 1983.

[22] EL Cooper and MM Rahman. A study of cycling 90sr in a natural forest on the canadian shield. *Science of The Total Environment*, 157:107–113, 1994.

[23] Roger Cox, Hans-Georg Menzel, and Julian Preston. Internal dosimetry and tritium—the icrp position. *Journal of Radiological Protection*, 28(2):131, 2008.

[24] X Dai, Y Cui, and S Kramer-Tremblay. A rapid method of determining strontium-90 in urine samples. published this year.

[25] Damon Delistraty. Radioprotection of nonhuman biota. *Journal of Environmental Radioactivity*, 99(12):1863 – 1869, 2008.

[26] GM Dolinar, JH Rowat, AT Jeffs, RWD Killey, and TA Niel. The waste management areas at chalk river laboratories: Conceptual decomissioning plan rc-2193 (rev. 2). Technical Report RC-2193, AECL Chalk River Laboratories, 2000.

[27] Doyle. Unpublished. Master's thesis, Royal Roads University, 2001.

[28] RW Killey et al. Waste management area f: Arsenic, radium and uranium distribution 14 years after emplacement. Technical Report RC-1129, AECL Chalk River Laboratories, 1993.

[29] Sample et al. Development and validation of bioaccumulation models for small mammals. Technical Report ES/ER/TM-219, Lockheed Martin Energy Systems Inc, 1998.

[30] Ramsey FL and Schafer DW. *The Statistical Sleuth*. Brooks/Cole, Boston, MA, 3rd edition, 2013.

[31] DA Fraser. Ecological studies of forest trees at chalk river, ontario, canada. 1: Tree species in relation to soil moisture sites. *Ecology*, 35(3):406–414, 1954.

[32] J Garnier-Laplace, S Geras'kin, C Della-Vedova, K Beaugelin-Seiller, TG Hinton, A Real, and A Oudalova. Are radiosensitivity data derived from natural field conditions consistent with data from controlled exposures? a case study of chernobyl wildlife chronically exposed to low dose rates. *Journal of Environmental Radioactivity*, 121(12-21), 2013.

[33] et. al. GH Kramer. Tools for creating and manipulating voxel phantoms. *Health Physics*, 98(3):542–548, 2010.

[34] Gore and Storrie. An environmental baseline study for waste management area "b" and "c" at aecl chalk river laboratories. Technical report, CH2M Hill, Prepared for Atomic Energy of Canada Limited, Environmental Technologies Branch, Chalk River Laboratories, Chalk River, Canada, 1997.

[35] WED Halliday and AWA Brown. The distribution of some important forest trees in canada. *Ecology*, 24(3):353–373, 1943.

[36] SP Hamburg, RD Yanai, MA Arthur, JD Blum, and TG Siccama. Biotic control of calcium cycling in northern hardwood forests: Acid rain and aging forests. *Ecosystems*, 6:399–406, 2003.

[37] F Hare. Climate and zonal divisions of the boreal forest formation in eastern canada. *Geographical Review*, 40:615, 1950.

[38] D Hart and P McKee. Ecological effects of chalk river laboratories. Technical report, AECL Chalk River Laboratories, 2005.

[39] K Higley, D Bytwerk, and L Houser. Transparency in the selection of biosphere parameters for geological disposal systems. In *Waste Management Proceedings*, 2011.

[40] KA Higley. Estimating transfer parameters in the absence of data. *Radiation and Environmental Biophysics*, 49(4):645–656, 2010.

[41] CH2M Hill. Summary tables. 2002.

[42] GA Hills. A decimal system for the classification and mapping of ontario soils. *Journal of Agricultural Science*, 25:253, 1945.

[43] 2008 ICRP. Environmental protection: the concepts and use of reference animals and plants. icrp publication 108. *Ann. ICRP*, 38(4-6), 2008.

[44] M Ingram. *Biological effects of ionizing radiation. An annotated bibliography covering the years 1898-1957*. TID-3097, 1966.

[45] Carr J. Map of chalk river laboratories water bodies. Personal Communication, August 2012.

[46] J.H. Steinmetz J.W. Arthur, B.J. Halligan. Life cycle of the freshwater snail campeloma decisum (viviparidae) in the laboratory. *The Nautilus*, 95(2):84–88, 1981.

[47] RWD Killey. Strontium-90 contamination of the swamp west of waste area b. Technical Memorandum, October 1988.

[48] RWD Killey, RR Rao, and S Eyvindson. Radiocarbon speciation and distribution in an aquifer plume and groundwater discharge area, chalk river, ontario. *Applied Geochemistry*, 13(1):3 – 16, 1998.

[49] Glenn Knoll. *Radiation Detection and Measurement*. John Wiley and Sons, Inc., 2000.

[50] Lounsbury and Adams. A safety and hazards analysis of the chalk river laboratories waste management areas. Technical Report AECL-MISC-306 PROTECTED, AECL Chalk River Laboratories, 1999.

[51] CR MacDonald and MJ Laverock. Ingestion rates and radionuclide transfer in birds and mammals on the canadian shield. Technical Report TR-722, AECL Chalk River Laboratories, 1998.

[52] Z Mastala, KV Balogh, and J Salanki. Reliability of heavy metal pollution monitoring utilizing aquatic animals versus statistical evaluation methods. *Archives of Environmental Contamination and Toxicology*, 23:476–483, 1992. 10.1007/BF00203813.

[53] Kutner MH, Nachtsheim CJ, and Neter J. *Applied Linear Regression Models*. McGraw-Hill Irwin, 2004.

[54] AP Møller, J Erritzée, F Karadas, and TA Mousseau. Historical mutation rates predict susceptibility to radiation in chernobyl birds. *Journal of Evolutionary Biology*, 23(10):2132–2142, 2010.

[55] AP Møller and TA Mousseau. Species richness and abundance of forest birds in relation to radiation at chernobyl. *Biology Letters*, 3(5):483–486, 2007.

[56] AP Møller and TA Mousseau. Conservation consequences of chernobyl and other nuclear accidents. *Biological Conservation*, 144(12):2787 – 2798, 2011.

[57] AP Møller and TA Mousseau. Efficiency of bio-indicators for low-level radiation under field conditions. *Ecological Indicators*, 11(2):424 – 430, 2011.

[58] TA Mousseau and AP Møller. Landscape portrait: A look at the impacts of radioactive contaminants on chernobyl's wildlife. *Bulletin of the Atomic Scientists*, 67(2):38–46, March/April 2011.

[59] Martinez ND. Artifacts or attributes? effects of resolution on the little rock lake food web. *Ecological Monographs*, (61):367–392, 1991.

[60] TA Niemi and KJ Ross. 2001 annual report for radiological monitoring results for chalk river and whiteshell laboratories sites volume 3 - environmental monitoring. Technical Report AECL-MISC-362-01, AECL Chalk River Laboratories, 2001.

[61] TA Niemi and KJ Ross. 2001 annual report of radiological monitoring results from the chalk river and whiteshell laboratories sites volume 3 - environmental monitoring. Technical Report AECL-MISC-362-01, AECL Chalk River Laboratories, 2002.

[62] TA Niemi and NM Soonwala. 1998 annual report on radiological monitoring results for the chalk river and whiteshell laboratories, volume 2 - effluent monitoring. Technical Report AECL-MISC-362-98, AECL Chalk River Laboratories, 1999.

[63] Deborah Oughton. Protection of the environment from ionising radiation: ethical issues. *Journal of Environmental Radioactivity*, 66(1–2):3 – 18, 2003.

[64] A Perera, D Euler, and I Thompson. *Ecology of a Managed Terrestrial Landscape*. UBC Press, 2001.

[65] A Perlowagora-Szumlewicz. Effects of ionizing radiation on the population kinetics of the snail australorbis glabratus: Age at exposure and the effects of radiation on reproduction. *Radiation Research*, 23(3):392, 1964.

[66] E. Philip Horwitz, Renato Chiarizia, and Mark L. Dietz. A novel strontium-selective extraction chromatographic resin. *Solvent Extraction and Ion Exchange*, 10(2):313–336, 1992.

[67] CM Pierce. *The effects of radiation and radioisotopes on the life processes, an annotated bibliography*. TID-3098, 1963.

[68] K.S.B. Rose. Lower limits of radiosensitivity in organisms, excluding man. *Journal of Environmental Radioactivity*, 15(2):113 – 133, 1991.

[69] KSB Rose. Lower limits of radiosensitivity in organisms, excluding man. *Journal of Environmental Radioactivity*, 15(2):113–133, 1991.

[70] Second International Symposium on Ionizing Radiation: Environmental Protection Approaches for Nuclear Facilities. *Are Conditions and Health of Fish Populations Influence by Exposure to Radioactive Contaminants?*, Ottawa, Ontario, May 2001.

[71] JK Shultis and RE Faw. An mcnp primer. Technical report, Dept of Mechanical and Nuclear Engineering, Kansas State University, Manhattan, KS 66506, 2004-2006.

[72] Nieman T. Skoog D., Holler F. J. *Principles of Intrumental Analysis*. Thomson Learning Inc., 1998.

[73] K Smith, D Jackson, and MD Wood. Demonstrating compliance with protection objectives for non-human biota with post-closure safety cases for radioactive waste respositories. Technical report, BIOPROTA, 2012.

[74] AH Sparrow, AG Underbrink, and RC Sparrow. Chromosomes and cellular radiosensitivity: I. the relationship of d0 to chromosome volume and complexity in seventy-nine different organisms. *Radiation Research*, 32(4):915–945, 1967.

[75] R Sterner and J Elser. *Ecological Stoichiometry: The Biology of Elements from Molecules to the Biosphere*. Princton University Press, 41 William Street, Princeton, NJ 08540, 10 edition, 2002.

[76] Janet Swim, Susan Clayton, Thomas Doherty, Robert Gifford, George Howard, Joseph Reser, Paul Stern, and Elke Weber. Psychology and global climate change: Addressing a multi-faceted phenomenon and set of challenges. Technical report, American Psychological Association, http://www.apa.org/science/about/publications/climate-change.aspx, 2010.

[77] Recommendations of the international commission on radiation protection publication 26. *Annals of the International Commission on Radiation Protection*, 1(3), 1977.

[78] X-5 Monte Carlo Team. *MCNP - A General Monte Carlo N-Particle Transport Code, Version 5*. Los Alamos National Laboratory, la-ur-03-1987 edition, April 2003.

[79] Patricia Thomas and Karsten Liber. An estimation of radiation doses to benthic invertebrates from sediments collected near a canadian uranium mine. *Environment International*, 27(4):341 – 353, 2001.

[80] CC Travis and AD Arms. Bioconcentration of organics in beef, milk, and vegetation. *Environmental Science and Technology*, 22(3):271–274, 1988.

[81] CW Turner. Non-radiological liquid effluent monitoring at crl: The results for 2000. Technical Report AECL-MISC-421-00, AECL Chalk River Laboratories, 2001.

[82] J Valentin. A framework for assessing the impact of ionising radiation on non-human species: Publication 91. *Annals of the International Commission on Radiation Protection*, 33(3):201–270, 2003.

[83] JE Weaver and FE Clements. *Plant Ecology*. McGraw Hill Book Co, New York, 2nd edition, 1938.

[84] Elke U. Weber. What shapes perceptions of climate change? *Wiley Interdisciplinary Reviews: Climate Change*, 1(3):332–342, 2010.

[85] M White, M Chejlava, B Fried, and J Sherma. The concentration of calcium carbonate in shells of freshwater snails. *American Malacological Bulletin*, 22(1):139–142, 2007.

[86] TL Yankovich and D Killey. Radionuclide transfer through sediment pathway in perch lake. Technical Memorandum, 2002.

[87] TL Yankovich, KJ King, RWD Killey, R Collins, and GM Dolinar. Ecological risk assessment for perch lake at aecl's chalk river laboratories - present conditions. Technical report, AECL Chalk River Laboratories, 2003.